The roles of vegetation, sediment transport, and humans in the evolution of low-lying coastal landforms: Modeling and GIS investigations

by

Rebecca Lauzon

Earth and Ocean Sciences
Duke University

Date:_____

Approved:

_____
Allen Murray, Supervisor

_____
Marco Marani

_____
James Heffernan

_____
Joel Rowland

Dissertation submitted in partial fulfillment of
the requirements for the degree of Doctor
of Philosophy in Earth and Ocean Sciences in the Graduate School
of Duke University

2018

ABSTRACT

The roles of vegetation, sediment transport, and humans in the evolution of low-lying coastal landforms: Modeling and GIS investigations

by

Rebecca Lauzon

Earth and Ocean Sciences
Duke University

Date:_____

Approved:

_____
Allen Murray, Supervisor

_____
Marco Marani

_____
James Heffernan

_____
Joel Rowland

An abstract of a dissertation submitted in partial fulfillment of the requirements for the degree of Doctor of Philosophy in Earth and Ocean Sciences in the Graduate School of Duke University

2018

Abstract

Low-lying coastal landforms such as barrier islands and river deltas are attractive sites for human habitation and infrastructure. They are also highly vulnerable to both climate change impacts such as rising sea levels or increases in storm intensity and anthropogenic impacts such as changes in sediment supply. In this dissertation I aim to improve understanding of some of the primary drivers of the evolution of low-lying coastal landforms over varying space (1-100s km) and time (decadal to millennial) scales. I focus in Chapter 2 on the influence of shoreline curvature and resulting gradients in alongshore sediment transport on shoreline change; in Chapter 3 on the influence of wave-edge erosion on back-barrier marsh resilience; and in Chapters 4 and 5 on the cohesive effects of vegetation on river deltas.

Sandy coastlines, often associated with low-lying barrier islands that are highly vulnerable to sea level rise and storms, can experience high rates of shoreline change. However, they also attract human habitation, recreation, and infrastructure. Previous research to understand and quantify contributions to shoreline erosion has considered factors such as grain size, underlying geology, regional geography, sea level rise, and anthropogenic modifications. Shoreline curvature is often not considered in such analyses, but subtle shoreline curvature (and associated alongshore variation in relative offshore wave angles) can result in gradients in net alongshore transport which can cause significant erosion or accretion. In Chapter 2, we conducted a spatially extensive analysis

of the correlation between shoreline curvature and shoreline change rates for the sandy shorelines of the US East and Gulf coasts. For wave-dominated, sandy coasts where nourishment and shoreline stabilization do not dominate the shoreline change signal, we find a significant negative correlation between shoreline curvature and shoreline change rates over decadal to centurial and 1-5 km temporal and spatial scales. This indicates that some of the coastal erosion observed in these areas can be explained by the smoothing of subtle shoreline curvature by gradients in alongshore transport. In other settings, this signal can be obscured by tidal, anthropogenic, or geologic processes which also influence shoreline erosion. While limited in practical application to long, sandy shorelines with limited human stabilization, these results have widespread implications for the inclusion of shoreline curvature as an important variable in modelling and risk assessment of long-term coastal erosion on sandy, wave-dominated coastlines.

The marshes and bays in the back-barrier environment between barrier islands and the mainland can also experience wave-driven erosion, and their dynamics are coupled to those of barrier islands. Previous results show that overwash provides an important sediment source to back-barrier marshes, sustaining a narrow marsh state under conditions in which marsh drowning would otherwise occur. In Chapter 3, I expand the coupled barrier island-marsh evolution model GEOMBEST+ to explore the effects of wind waves on back-barrier marshes. I find that the addition of marsh-edge erosion leads to wider, more resilient marshes and that horizontal erosion of the marsh edge is a more efficient sediment source than vertical erosion of the marsh surface as it drowns. Where

marshes and bays are vertically keeping up with sea level, and the net rate of sediment imported to (or exported from) the basin is known, the rate of marsh-edge erosion or progradation can be predicted knowing only the present basin geometry, sea-level rise rate, and the net rate of sediment input (without considering the erosion or progradation mechanisms). If the rate of sediment input/export is known, this relationship applies whether sediment exchange with the open ocean is negligible (as in basins dominated by riverine sediment input), or is significant (including the loss of sediment remobilized by waves in the bay). Analysis of these results reveals that geometry and stratigraphy can exert a first order control on back-barrier marsh evolution and on the marsh-barrier island system as a whole, and provides new insights into the resilience of back-barrier marshes and on the interconnectedness of the barrier-marsh system.

Coastal wetlands such as marshes are also an important component of river deltas. Like barrier islands, these low-lying landscapes are both attractive to human settlement (providing fertile farmland, fisheries, hydrocarbon reserves, and many other services) and prone to hazards such as flooding and land loss. Delta evolution is governed by complex interactions between coastal, marine, and fluvial processes, many of which are still not well understood. In Chapters 4 and 5, I use the delta-building model DeltaRCM to explore the effects of vegetation, specifically its ability to introduce cohesion, on delta morphology and the dynamics of delta distributary networks. The use of this rule-based model allows me to simplify vegetation dynamics and effects in order to enhance the

clarity of potential insights into which processes or interactions may be most important in the context of vegetation as a cohesive agent.

Cohesive sediment exerts a significant influence on delta evolution, increasing shoreline rugosity and decreasing channel mobility. Vegetation has been assumed to play a similar role in delta evolution, but its cohesive effects have not been explicitly studied. In Chapter 4, I use DeltaRCM to directly explore two cohesive effects of vegetation: decreasing lateral transport and increasing flow resistance. I find that vegetation and cohesive sediment do alter delta morphology and channel dynamics in similar ways (e.g. more rugose shorelines, deeper, narrower, less mobile channels), but that vegetation may have additional implications for deltaic sediment retention and stratigraphy, by confining flow and sand in channels. My results suggest that sediment composition is a first-order control on delta morphology but vegetation has a stronger influence on channel mobility timescales. To fully understand the cohesive influences acting on a delta, the influence of vegetation should be considered in addition to fine sediment.

In Chapter 5, I explore the cohesive effects of vegetation on delta evolution under different environmental conditions. The dynamics and evolution of deltas and their channel networks are controlled by interactions between a number of factors, including water and sediment discharge, cohesion from fine sediment and vegetation, and sea level rise rates. Vegetation's influence on the delta is likely to be significantly impacted by other environmental factors. For example, increasing sea level or sediment discharge increases aggradation rates on the delta, and may result in sediment transport processes

such as deposition and erosion, both of which can kill vegetation, happening more rapidly than vegetation growth. I conduct two sets of experiments; in the first, I explore the interactions between vegetation and sea level rise rate, and in the second, between vegetation and rate of sediment and water discharge. As expected, I find that sea level rise decreases vegetation's ability to stabilize channels but that vegetation can still exert a strong influence on the delta at low rates of sea level rise. This limit appears to be higher for channel dynamics than delta morphology, supporting the findings of Chapter 4. In addition, I propose two new insights into delta evolution under different discharge conditions with and without vegetation. First, without vegetation, I observe a shift in avulsion dynamics with increasing water discharge: from a few active channels supplemented by overbank flow and undergoing episodic avulsion (with low discharge) to many active channels experiencing frequent local and partial avulsions (with high discharge). Second, with vegetation, increased sediment discharge and associated aggradation results in more frequent switching of the dominant channels, but also prevents vegetation from establishing in non-dominant channels, resulting in more frequent channel reoccupation and therefore in channel network planform stability. These insights have important implications for understanding the distribution of water, sediment, and nutrients on deltas in the face of future changes in climate, human modifications of fluxes of sediment and water to the coast, and especially for restored or engineered deltas with controlled water or sediment discharges.

Contents

Abstract iv

Contents ix

List of Tables xiii

List of Figures xiv

Acknowledgements xvii

1. Introduction 1

1.1 Barrier islands and salt marshes 1

1.2 River deltas 4

2. Shoreline curvature influences shoreline change on sandy, wave-dominated coasts: Observations from the U.S. East and Gulf Coasts 7

2.1 Introduction 7

2.2 Methods 17

2.3 Results & Interpretations 26

2.3.1 Texas 26

2.3.2 North Carolina 29

2.3.2.1 New Analysis 29

2.3.2.2 Comparison to Previous Analysis 31

2.3.3 Additional Analysis 33

2.3.3.1 Mid-Atlantic (New York to Virginia) 34

2.3.3.2 Virginia 36

2.3.3.3 Florida 37

2.4. Discussion 38

2.4.1 Variability in Wave Climate and Effective Diffusivity 38

2.4.2 Space and Time Scales of Relevance 40

2.4.3 Nourishment and Other Injected Signals 42

2.5 Implications 45

2.6 Acknowledgements 46

3. Effects of marsh edge erosion in coupled barrier island-marsh systems and geometric constraints on marsh evolution 47

3.1 Introduction 47

3.2 Model Description: GEOMBEST and GEOMBEST+ 53

3.3 Methods 61

3.4 Results 68

3.5 Discussion 70

3.5.1 Geometry and conservation of mass constraints 70

3.5.2 Stratigraphy and composition constraints 77

3.5.3 Limitations 79

3.5.4 Implications 83

3.6 Conclusions 88

3.7 Acknowledgements 89

4. Comparing the Cohesive Effects of Mud and Vegetation on Delta Evolution 90

4.1 Introduction 90

4.2 Model Description and Vegetation Rules 92

4.3 Delta Morphology 96

4.4 Channel dynamics 101

4.5. Comparison of cohesive effects of vegetation and cohesive sediment 103

4.6. Implications 105

4.7 Acknowledgements 107

5. Vegetation influence on delta evolution and dynamics under varying environmental conditions 108

5.1 Introduction 108

5.2 Methods 111

5.2.1 Model Description 111

5.2.2 Experimental Set-up 113

5.2.3 Data Analysis 116

5.3 Results and Discussion 118

5.4.1 Sea Level Rise 118

5.3.2 Sediment and Water Discharge 123

5.4 Potential for Future Work 131

5.5 Summary and Implications 133

5.6 Acknowledgements 135

6. Conclusions 136

6.1 Barrier islands and salt marshes 136

6.2 River deltas 138

References 141

Biography 156

List of Tables

Table 2.1: Correlation coefficient data for all space and time scales for all shoreline sections. 24

Table 2.2: Comparison of results from Lazarus and Murray (2007) and this study. 33

Table 3.1: Definitions of variables and abbreviations. 59

Table 5.1: Experimental setup. 115

List of Figures

Figure 2.1: Schematic of gradients in alongshore currents 10

Figure 2.2: Correlation between shoreline curvature and shoreline change 12

Figure 2.3: The extent of the shorelines considered in our study..... 16

Figure 2.4: A) A satellite image of the shoreline overlaid with the shoreline from the Coastline Extractor, B) the shape of the shoreline after it is smoothed at 1, 3, and 5 km scales, C) shoreline curvature and D) shoreline change data for Texas 8. 20

Figure 2.5: Comparison of three possible 1 km smoothing windows on a hypothetical 2 km long shoreline section. 21

Figure 2.6: Illustration of the sign conventions used in this analysis. 23

Figure 2.7: Map showing the significant correlation coefficients between shoreline curvature and shoreline change found for the Texas Gulf Coast. 27

Figure 2.8: Map showing the significant correlation coefficients between shoreline curvature and shoreline change found for the North and South Carolina coasts. 30

Figure 2.9: Map showing the significant correlation coefficients between shoreline curvature and shoreline change found for the Mid-Atlantic Coast..... 35

Figure 2.10: Map showing the significant correlation coefficients between shoreline curvature and shoreline change found for the Atlantic Coast of Florida. 38

Figure 3.1: Illustrative examples of two narrow back-barrier marshes on the East Coast of the United States. 51

Figure 3.2: Initial condition (A) and model output after 1 m of total RSLR (B) for a GEOMBEST+ simulation of an initially narrow marsh without wave edge erosion (e.g. from Walters et al. (2014)). Initial condition (C) and model output after 1 m of total RSLR (D) from GEOMBEST++ (including wave edge erosion). 55

Figure 3.3: Phase diagram showing the distribution of back-barrier marsh widths after 1 m of total RSLR..... 68

Figure 3.4: A) Evolution of marsh widths over 2m of total RSLR..... 70

Figure 3.5: Evolution of an initially full marsh over 1 m of total RSLR. 72

Figure 3.6: Schematic of a case where the marsh and bay are keeping up with sea level and so the only way the basin can empty and fill with sediment is by moving the location of the marsh boundary. 77

Figure 3.7: Difference in efficiency as a sediment source between lateral erosion and vertical erosion of the marsh platform. 79

Figure 4.1: a) Shoreline roughness, measured as shoreline length divided by the square root of delta area, and averaged over the second half of each run. b) Average width to depth ratio for channels along the arc of a semi-circle with an area 2/3 that of the delta, measured at the last timestep. c) Decay constant obtained from fitting an exponential decay function to the remaining unreworked fluvial surface, using a varying time lag encompassing the second half of the model run. d) The fraction of the fluvial surface remaining at the final timestep which has not been reworked 97

Figure 4.2: a) Cumulative frequency and b) probability density of subaerial (> -0.5 m) delta elevations 99

Figure 4.3: Vertically-averaged sand fractions 101

Figure 4.4: Plots of the fraction of time each channel cell spends as a channel 102

Figure 5.1: a) Delta area through time for no SLR with and without vegetation and for 5, 10, 25, and 50 mm/yr with vegetation. b) probability density function for subaerial (> -0.5 m) elevations for 0, 5, 10, 25, and 50 mm/yr of SLR with vegetation 118

Figure 5.2: Maps of the fraction of time any cell which is part of the channel network during the second half of the run remains part of the channel network 120

Figure 5.3: a) Drainage density, b) the fraction of the delta surface which has not been reworked by the channel network by the end of the model run (1- fR), c) P_c (the ratio of the number of channel cells which are channels for more than 50% of the time over less than 50% of the time), d) R (the rate of decay in remaining delta surface unreworked by the channel network), and e) shoreline roughness 121

Figure 5.4: a) R (the rate of decay in remaining delta surface unreworked by the channel network), b) drainage density, c) M (the rate of decay in channel planform overlap), d) P_c (the ratio of the number of channel cells which are channels for more than 50% of the time over less than 50% of the time) and e) shoreline roughness 125

Figure 5.5: Maps of the fraction of time any cell which is part of the channel network during the second half of the run remains part of the channel network. 126

Figure 5.6: Time series of maximum discharge values 128

Figure 5.7: Vertically-averaged sand fractions at the end of a model run. 130

Acknowledgements

I would like to thank my advisor, Brad Murray, for his seemingly endless patience and support. I would also like to thank those who have served on my committee at various stages, for their support and guidance: Marco Marani, Jim Heffernan, Joel Rowland, Laura Moore, and Brain McGlynn. I would like to thank my lab mates, Katherine Ratliff, Evan Goldstein, and Kenny Ells, for their company and many conversations. I would also like to thank Chelsea Clifford and Fateme Yousefi, for their emotional support and for always sharing their snacks. I would like to thank Beatriz Martin, Danielle Wiggins, Debbie Gooch, and Nicholas School IT for logistical support. I would also like to thank Anastasia Piliouras, for an opportunity that reminded me what I was capable of, and Rick Murray and Rachel Scudder, as without their early and since unfailing encouragement I would never have made it here. Lastly I would like to thank my family, for never doubting I could achieve anything, and Nick James, for always believing in me and for standing by me even at my crankiest.

1. Introduction

1.1 Barrier islands and salt marshes

Barrier islands and low-lying, sandy coastlines are highly vulnerable to sea level rise and storms and can experience high rates of shoreline change. They also attract human habitation, recreation, and infrastructure, making sources of and trends in this shoreline change an important area of research (e.g. Morton et al., 2005; Morton et al., 2004; Morton and Miller, 2005; Hapke et al., 2011; Gornitz et al., 1994; Gibbs and Richmond, 2015; Ruggiero et al., 2013; Fletcher et al., 2012; Hapke and Reid, 2007; Hapke et al., 2006; Hapke et al., 2013; Shaw et al.; 1998; Nicholls and Vega-Leinert, 2008, Coelho et al., 2006). Barriers tend to migrate landward in response to sea level rise (SLR) and to maintain elevation relative to sea level (Brunn, 1988). As storms erode the beach and nearshore seabed, overwash deposits that sand on the top and back of the island, raising its elevation and moving the system (including the shoreline) landward. The rate of this migration can be controlled by a number of factors (e.g. Moore et al., Wolinsky and Murray, 2009; Brenner et al., 2015), and previous attempts to understand and quantify contributions to shoreline erosion has considered factors such as sediment composition, underlying geology, regional geography, sea level rise, and anthropogenic modifications (e.g. Gutierrez et al., 2011; Yates and Cozannet, 2012; Vitousek et al., 2017; Ruggiero et al., 2010; Plant et al., 2016 ; Hapke et al., 2013).

Significant erosion or accretion can also result from subtle shoreline curvature and associated alongshore variation in relative offshore wave angles (e.g. Lazarus and

Murray, 2007; Lazarus et al., 2011; Lazarus and Murray, 2011; Valvo et al., 2006, Cowell et al., 1995; Dean and Yoo, 1992). Though these gradients in alongshore transport can result in significant cumulative shoreline change on time scales of years to centuries (Ashton and Murray, 2006a,b; Lazarus and Murray, 2007, Cowell et al, 1995), shoreline curvature is often not included in analyses of shoreline change rates. In Chapter 2, I present the results of a wide-ranging analysis of the correlation between shoreline change and shoreline curvature for the barrier shorelines of the U.S. East and Gulf coasts, suggesting that shoreline curvature should be included in future analyses of shoreline change.

On the landward side of the island, the barrier island is typically backed by a salt marsh or bay (together termed the "back-barrier") and so experiences different shoreline dynamics. Like barriers, salt marshes tend to maintain their elevation relative to sea level (in this case through deposition of inorganic sediment and production of organic matter; e.g. Reed, 1995; Friedrichs and Perry, 2001; Fitzgerald et al., 2008; Kirwan and Megonigal, 2013; D'Alpaos, 2011) and can experience significant wave-driven erosion (e.g. Schwimmer, 2001; Nyman et al., 2006; Marani et al., 2011; Mariotti and Fagherazzi, 2013; Fagherazzi et al., 2013). As waves erode the marsh edge, basin width (and therefore fetch and wave size) increases, enhancing erosion. On the other hand, if sediment concentrations are high enough for the marsh edge to prograde, basin (and wave) size decreases and progradation is enhanced. As a result of these feedbacks, a marsh edge is

always moving towards filling the basin or eroding away completely; a partially filled basin is an unstable state.

Interactions between salt marshes and adjacent barrier islands can play an important role in the evolution of the marsh-barrier system as a whole (e.g. Fitzgerald et al., 2008; Walters et al., 2014; Brenner et al., 2015; Walters and Kirwan, 2016). For example, when a barrier migrates over a marsh less sand is required to achieve the same island elevation than if the barrier were prograding into a bay, resulting in a slower island migration rate (Wolinsky and Murray, 2009; Walters et al., 2014; Brenner et al., 2015). If the island is migrating faster than the marsh is prograding, this can result in a loss of marsh (e.g. Deaton et al., 2016). On the other hand, overwash from barriers provides an important sediment source to back-barrier marshes (e.g. Walters et al., 2014; Walters and Kirwan, 2016) potentially resulting in an overwash-supported, long-lasting "narrow marsh" which would otherwise be unable to maintain its elevation (Walters et al., 2014). This narrow marsh state has been identified in distributions of satellite observations of marsh widths and in model results (Walters et al., 2014). However, the model used by Walters et al. (2014) did not consider wave erosion of marsh edges, which can be a significant source of marsh loss. In Chapter 3 I present the results of the addition of wave edge erosion to the model framework of Walters et al. (2014). The results suggest that the narrow marsh state persists with the addition of wave edge erosion. The results also highlight the constraints of geometry and conservation of mass on the evolution of back-barrier systems, and expand on our understanding of how wave edge erosion can actually increase marsh resilience (e.g. Mariotti and Carr, 2014).

1.2 River deltas

Coastal wetlands such as marshes are also an important component of river deltas. Like barrier islands, these low-lying landscapes are both attractive to human settlement (providing fertile farmland, fisheries, hydrocarbon reserves, and many other services) and prone to hazards such as flooding and land loss. Delta evolution is governed by complex interactions between coastal, marine, and fluvial processes (e.g. Galloway, 1975; Nienhuis et al., 2015; Geleynse et al., 2011; Leonardi et al., 2015) and environmental factors such as water and sediment discharge (Powell et al., 2009; Hoyal and Sheets, 2009; Orton and Reading, 1993; Edmonds et al., 2010), fraction of cohesive sediment (Caldwell and Edmonds, 2014; Hoyal and Sheets, 2009; Straub et al., 2013; Edmonds and Slingerland, 2009, Liang et al., 2015a; Tejedor et al., 2016) or the presence of vegetation (Nardin and Edmonds, 2014; Nardin et al., 2016, Lorenzo-Trueba et al., 2012), base level rise (Jerolmack, 2009; Liang et al., 2016a; Martin et al., 2009), and many others. In addition to the influence these factors have in shaping delta morphology, recent research has focused on the role of they play in determining autogenic timescales—timescales at which deltas undergo cycles of channelization, channel extension and aggradation, avulsion and incision of a new channel (e.g. Hoyal and Sheets, 2009; van Dijk et al., 2009; Kim et al., 2006).

Of particular interest in recent research is the effect of cohesion on the evolution of deltas and deltaic channel networks. Muddy, cohesive sediment increases the stability of channel bars and banks, deepening and elongating channels, decreasing channel

mobility, increasing autogenic timescales, and increasing shoreline rugosity (Edmonds and Slingerland, 2009; Hoyal and Sheets, 2009; Liang et al., 2015a; Caldwell and Edmonds, 2014; Straub et al., 2015). Vegetation also introduces cohesion; in rivers, vegetation can be instrumental in the transition from braiding to single channel flow (e.g. Gran and Paola, 2001; Murray and Paola, 2003; Tal et al., 2004; Tal and Paola, 2010) and in river and marsh environments it can concentrate flow into channels (e.g. Temmerman et al., 2005; 2007) and decrease bank erosion through root stabilization (e.g. Gran and Paola 2001; Tal et al., 2004; Millar, 2000; Schwarz et al., 2013; Ameen et al., 2017). While it has been hypothesized to play a role in delta evolution similar to that of cohesive sediment (e.g. Edmonds and Slingerland, 2009; Straub et al., 2015; Hoyal and Sheets, 2009), the cohesive effects of vegetation have not been extensively studied in deltaic systems. However, vegetation's cohesive influence on delta morphology and evolution could differ from that of cohesive sediment in important ways as vegetation may be sensitive to environmental conditions in ways that cohesive sediment is not. Increased SLR rates or sediment discharge would tend to increase deposition rates and may result in vegetation mortality if sediment transport processes act on timescales faster than those for vegetation growth (e.g. Murray and Paola, 2003; Pasquale et al., 2013; Perona et al., 2012), reducing vegetation's influence on the delta.

In Chapters 4 and 5 I seek to first (Chapter 4) assess the similarities and differences in cohesion introduced by vegetation or cohesive sediment and second (Chapter 5) to investigate the effects of SLR and sediment and water discharge on

vegetation's ability to influence delta morphology and evolution. These results suggest that cohesive sediment does not capture all the same cohesive effects as vegetation, and that both should be considered in order to fully understand cohesive influences on deltas; that vegetation is sensitive to environmental conditions; and that interactions between vegetation and factors such as sediment discharge can result in changes in channel dynamics which are different from those resulting just from cohesive sediment.

2. Shoreline curvature influences shoreline change on sandy, wave-dominated coasts: Observations from the U.S. East and Gulf Coasts

Rebecca Lauzon, Dr. A. Brad Murray, Scarlet Cheng, Jiahong Liu, and Dr. Eli Lazarus

2.1 Introduction

Understanding and predicting shoreline change on barrier islands can be difficult because a variety of processes acting on a variety of spatial and temporal scales govern rates of shoreline change. Despite these low-lying mobile landforms' high level of vulnerability to changes in sea level rise (SLR) and storm intensities, they are also popular places to live and vacation and as such are often heavily developed. In just the United States, coastal erosion can cost hundreds of millions in U.S. dollars yearly in damage (The Heinz Center Report, 2000), and estimates of the protection provided by beaches are similarly high; for just two beaches in Texas, it is estimated that replicating the level of protection afforded by beaches using shoreline stabilization would cost 141 million U.S. dollars (Taylor et al., 2015). As a result, many attempts have been made to quantify and analyze historical and current rates of shoreline change and assess erosion risk. One such example is the United States Geological Survey (USGS)'s National Assessment of Shoreline Change Project (Morton et al., 2005); this and other projects exist for diverse regions of the United States (Morton et al., 2004; Morton and Miller, 2005; Hapke et al., 2011; Gornitz et al., 1994; Gibbs and Richmond, 2015; Ruggiero et al., 2013; Fletcher et al., 2012; Hapke and Reid, 2007; Hapke et al., 2006; Hapke et al., 2013)

and beyond (e.g. Shaw et al.; 1998; Nicholls and Vega-Leinert, 2008, Coelho et al., 2006). Similarly, a diverse body of literature describes attempts to explain past and predict future trends in shoreline behavior by modeling the effects of a variety of processes and environmental conditions (Gutierrez et al., 2011; Yates and Cozannet, 2012; Vitousek et al., 2017; Ruggiero et al., 2010; Plant et al., 2016 ; Hapke et al., 2013). While these models perform well in some geomorphic settings, modelled and observed shoreline change often has poor agreement on sandy beaches (including barrier islands; e.g. Gutierrez et al., 2011; Yates and Cozannet, 2012).

It is difficult to determine the relative contributions of the morphological characteristics and processes that can affect shoreline change rates. These factors can include grain size distribution, wave climate, storms, tidal range, relative sea-level-rise (SLR) rates, underlying geology, regional geography (e.g. barrier vs. headland), anthropogenic influence, as well as others. Nearshore processes affect shoreline behavior over different scales, ranging from meters to tens of kilometers and timescales from days to centuries. In addition, which factors and processes are most important in causing long-term erosion can vary from one location to another, making it challenging to decide which to include in risk assessments or models of shoreline change.

Though there are some exceptions, much of the literature assessing shoreline vulnerability to erosion has focused on shoreline transgression due to SLR (e.g. Hinkel and Klein, 2009; Gornitz et al., 1994; FitzGerald et al., 2008; Gutierrez et al., 2011; Shaw et

al., 2008; Plant et al., 2016). While coastline transgression due to SLR can be a major cause of long-term coastal erosion (e.g. Leatherman et al., 2000; Pilkey and Cooper 2004; Moore et al., 2010; Vitousek et al., 2017), shorelines also experience erosion or accretion due to gradients in net alongshore transport resulting from subtle shoreline curvature (e.g. Lazarus and Murray, 2007; Lazarus et al., 2011; Lazarus and Murray, 2011; Valvo et al., 2006, Cowell et al., 1995; Dean and Yoo, 1992). Storms—another source of erosion on which previous research has focused—can result in temporary erosion as cross-shore currents move sand offshore. However, often calm-weather waves move that sediment back onshore, resulting in little or no net change in shoreline location over timescales greater than a few months (Morton et al., 1994; List and Farris, 1999; List et al., 2006; Zhang et al., 2002). In contrast to the temporary erosion often associated with most storms, gradients in alongshore transport can result in cumulative shoreline change on time scales of years to centuries (Ashton and Murray, 2006a,b; Lazarus and Murray, 2007, Cowell et al, 1995)

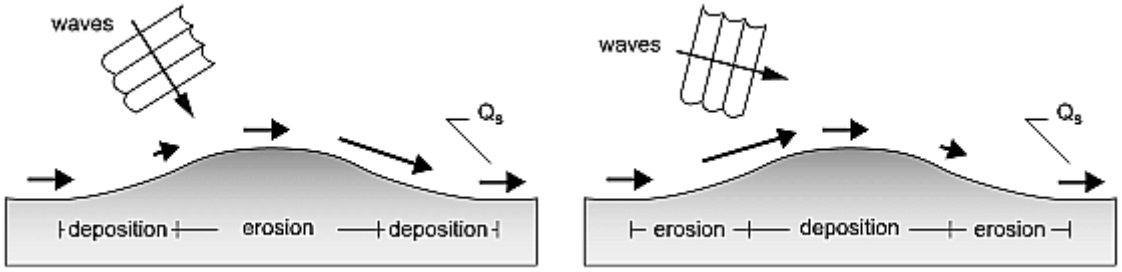

Figure 2.1: Schematic of gradients in alongshore currents created by curvature and high and low angle waves, and their implications for erosion and deposition. From Ashton and Murray (2006a).

Subtle coastline curvature, either concave seaward or convex, can cause gradients in alongshore transport as the difference in the angle between the offshore waves and the shoreline changes along the coast (Figure 2.1). (In this context, 'offshore' refers to a location seaward of the zone of approximately shore-parallel bathymetric contours typical of the inner continental shelf, or 'shoreface'.) The magnitude of alongshore transport at any point along the shoreline can be related to the incident offshore wave angle (as well as the wave height), and is maximized at an offshore wave angle of approximately 45 degrees (Falques, 2003; Ashton and Murray, 2006a). When waves approach from 'high angles' (angles between offshore wave crests and the shoreline > approximately 45 degrees), gradients in alongshore transport tend to converge on convex seaward shoreline features (causing accretion) and diverge on concave seaward ones (causing erosion; Ashton et al, 2001; Falques, 2003). When the offshore wave climate is dominated by high angle waves (i.e. most of the gross alongshore sediment flux results from high-angle waves), large-scale coastline curvature

tends to increase over time, and emergent coastline features can develop (e.g. Ashton et al, 2001; Falques, 2003; Ashton and Murray, 2006a). In contrast, when the offshore wave climate is dominated by low-angle waves (< 45 degrees), gradients in alongshore transport tend to smooth the shoreline, eroding convex seaward areas and accreting concave seaward ones. Though these gradients are higher (therefore moving sediment faster) in areas of high curvature, even subtle curvature can cause shoreline erosion or accretion (Valvo et al., 2006; Lazarus and Murray, 2007). When coastline curvature is subtle (involving a small range of shoreline angles), coastline evolution can be described with a diffusion equation, with a positive diffusivity corresponding to coastline smoothing (low-angle-dominated wave climates), and a negative diffusivity corresponding to coastline roughening (high-angle-dominated wave climates). The magnitude as well as the sign of the long-term 'effective diffusivity' depends on the relative influences on alongshore transport from high- and low-angle waves (e.g. Ashton and Murray, 2006b) affecting a particular coastline.

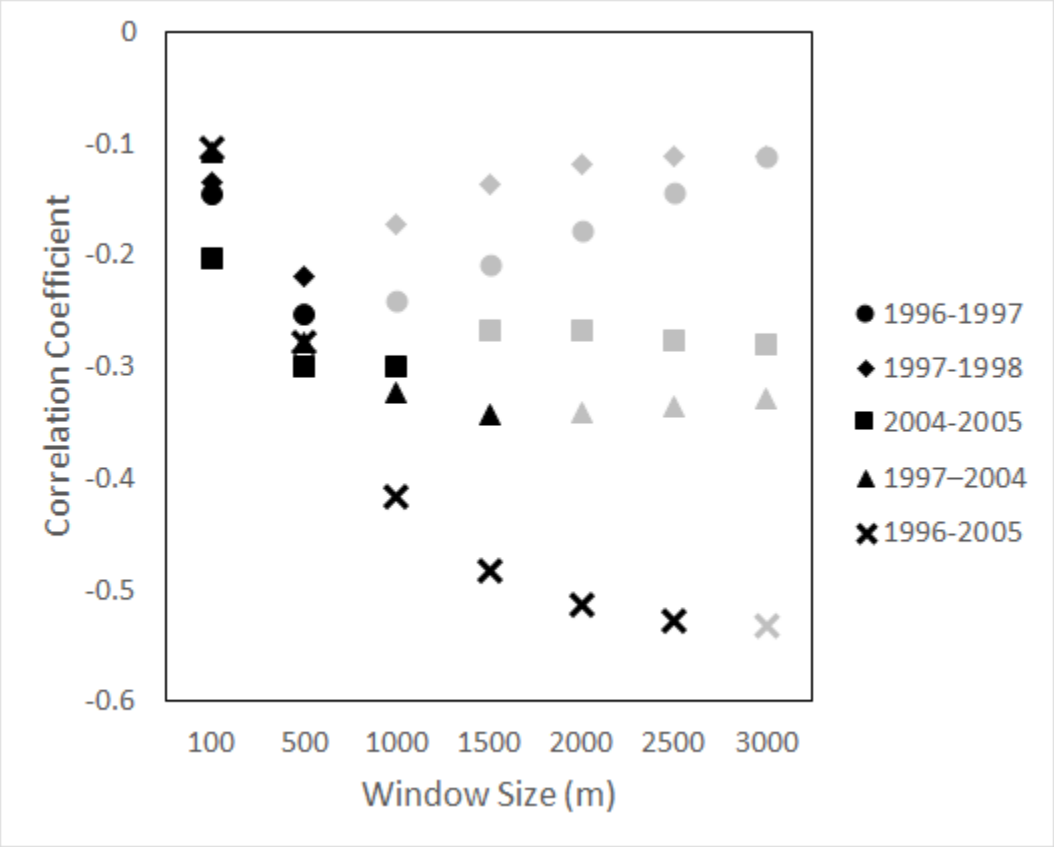

Figure 2.2: Correlation between shoreline curvature and shoreline change for the northern North Carolina coast on annual to decadal timescales found by Lazarus and Murray (2007). Data ploted in black are significant at a 95% confidence interval.

Previous research has identified the signal of coastline curvature in patterns of erosion and accretion along one stretch of coastline coast (Lazarus and Murray, 2007). Lazarus and Murray (2007) found that, on multi-annual timescales and 100m to km spatial scales, there is a significant correlation between shoreline curvature and shoreline change rates (Figure 2.2) on the Northern Outer Banks of North Carolina, USA. Using the convention that seaward convex curvature is positive and that landward shoreline

change (erosion) is negative, Lazarus and Murray (2007) found a negative correlation, suggesting the overall smoothing of the shoreline (Lazarus and Murray, 2007).

We would expect this smoothing signal, characteristic of a low-angle wave climate, to dominate almost everywhere. In locations where regional wave climates are dominated by high-angle waves (relative to the regional coastline trend), large emergent coastline features create locally low-angle wave climates, through both wave-shadowing effects and local shoreline reorientation (Ashton and Murray, 2006a,b). Therefore, though high-angle wave climates can cause very long term (up to millennial scale) coastline roughening on the spatial scale of the largest emergent structures (up to 100 km), we would still expect a diffusional smoothing signal on smaller scales almost everywhere along such a coastline (Ashton and Murray, 2006a,b).

On shorter timescales (years or less), this smoothing signal can be overwhelmed by temporary fluctuations in wave climate, such as a particular storm or set of storms delivering a high proportion of high-angle wave influence. Lazarus et al. (2011) found a short-term, positive (roughening) correlation between shoreline change and shoreline curvature for one area in North Carolina exhibiting a longer term negative, smoothing signal. The roughening signal corresponded with hurricanes in 1998 and 1999 that featured an atypically high proportion of influence on alongshore sediment transport from high-angle waves.

Storms that are severe enough to remove sediment from the beach and nearshore seabed and transport it landward of the beach, depositing it on a barrier (the 'overwash' process) or in the bay behind (during 'innundation' events) also tend to cause cumulative shoreline change. Sea-level rise tends to increase the long-term rate of such landward deposition (e.g. Bruun, 1962; Murray and Moore, 2018), causing the component of shoreline erosion that many studies focus on. Even when SLR causes significant erosion on a regional scale, gradients in alongshore transport can dominate local shoreline change rates (Cowell et al., 1995).

Additional evidence for the importance of shoreline curvature and gradients in alongshore transport in understanding patterns of shoreline change comes from the predictive power of models which include alongshore processes in addition to cross-shore ones – for example Vitousek et al. (2017), in which the authors reproduced signals of shoreline change on sandy beaches in California - and in the limitations identified in studies which do not. An analysis of the primary factors influencing decadal scale shoreline evolution of European coasts found that the variables they included in their study were insufficient for determining erosive behavior, and identified coastal structures, shoreline orientation, alongshore transport, sediment budgets, and human impacts as additional variables of interest in determining shoreline change rates (Yates and Cozannet, 2012). Similarly, in the United States, Gutierrez et al. (2011) identified engineering structures, tidal inlets, and beach width as additional factors which could

improve predictions of shoreline change rates on sandy shores. Many of these variables directly or indirectly affect or are affected by gradients in alongshore transport and shoreline curvature.

While Lazarus and Murray (2007) found a significant relationship between shoreline curvature and shoreline change in one area of North Carolina, much of the other available evidence comes from coastline evolution models. Lazarus and Murray's (2007; 2011) observational studies only looked at one location and at a limited range of timescales (years to decades). As the wave climate and effective diffusivity of the coastline varies from place to place, the relationship between shoreline curvature and shoreline change should vary as well. The length scale at which changes related to the initial condition (here, coastline shape) are apparent increases with the square root of time for diffusional systems; diffusion of large-scale features occurs more slowly than for small scale ones. As a result, we would expect that to see the effect of larger scale coastline curvature, we may need to consider longer-term shoreline change.

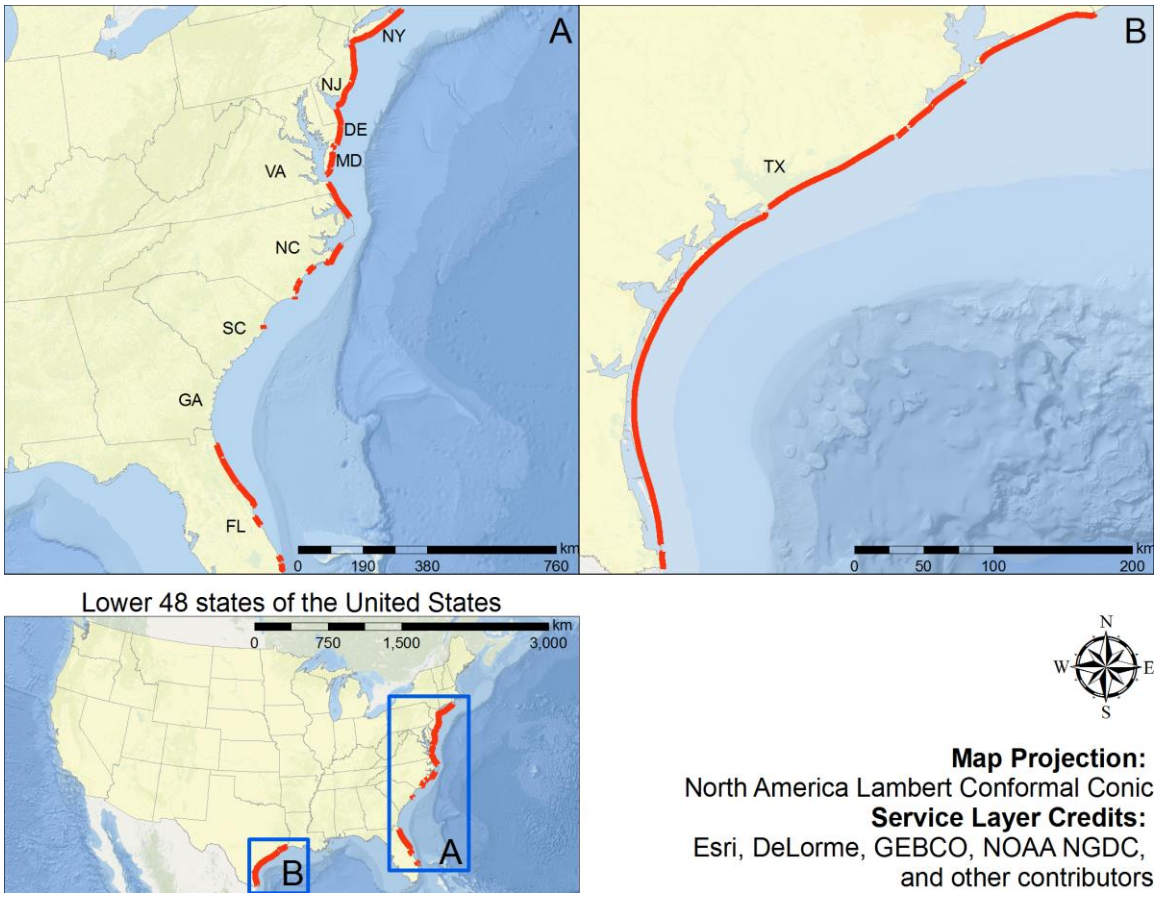

Figure 2.3: The extent of the shorelines considered in our study.

Here we investigate whether the relationship between shoreline curvature and shoreline change is evident on larger timescales and in a wider range of locations than have previously been examined. We build on the work of Lazarus and Murray (2007) by investigating the influence of alongshore plan-view shape of sandy shorelines of the US Gulf and Atlantic Coasts (Figure 2.3) on long-term (decades to centuries) coastline change, to determine on what spatial and temporal scales shoreline curvature is important when interpreting or predicting shoreline change rates. We address the question of whether the diffusive, smoothing signal found by Lazarus and Murray

(2007) will be apparent over longer time and space scales, and in a broad range of locations. In our results, we identify this smoothing signal on the wave-dominated sandy shorelines of the U.S. East and Gulf coasts over decadal to centurial time and several kilometer space scales.

2.2 Methods

We analyzed barrier island shorelines along the US Texas gulf coast and sections of the US Atlantic coast ranging from Florida to New York (Figure 2.3). We obtained shorelines as shapefiles from the Geophysical Data System (GEODAS) Coastline Extractor v 1.1.3 (https://www.ngdc.noaa.gov/mgg/geodas/geodas.html). Shorelines in the Coastline Extractor come from the Global Self-consistent, Hierarchical, High-resolution Geography (GSHHG) database (Wessel and Smith, 1996). After importing the shorelines from the Coastline Extractor into ArcGIS, we broke them into sections defined by geologic (e.g. inlets) and anthropogenic (e.g. groynes) boundaries.

In ArcGIS, we placed points along the shoreline at 1 m increments and created a reference line following the linear trend of the shoreline by connecting the endpoints of the shoreline section. We moved the reference line 2000-3000 m offshore so that the entirety of the shoreline was on the landward side of the reference line. Assuming that the shoreline has relatively low curvature, the distance along the reference line and the distance from the reference line correspond to xy coordinates for each point on the shoreline.

We remove 0.5 km from the ends of each shoreline section to reduce the potential effects of inlets, which can cause convex bulges to form on the shoreline that respond to changes in tidal channels and deltas (Davis and Fitzgerald, 2004). If jetties are present at the ends of the shoreline section, we do not remove this 0.5 km, as the shoreline change and resultant curvature caused by the jetty is a result of the creation of gradients in alongshore transport. Jetties result in the accumulation of sand (and therefore in shoreline accretion) updrift of their location. This results in a concave curvature, and the accretion propagates further updrift of the jetty. This behavior (concave curvature and accretion) results in a smoothing signal in our analysis.

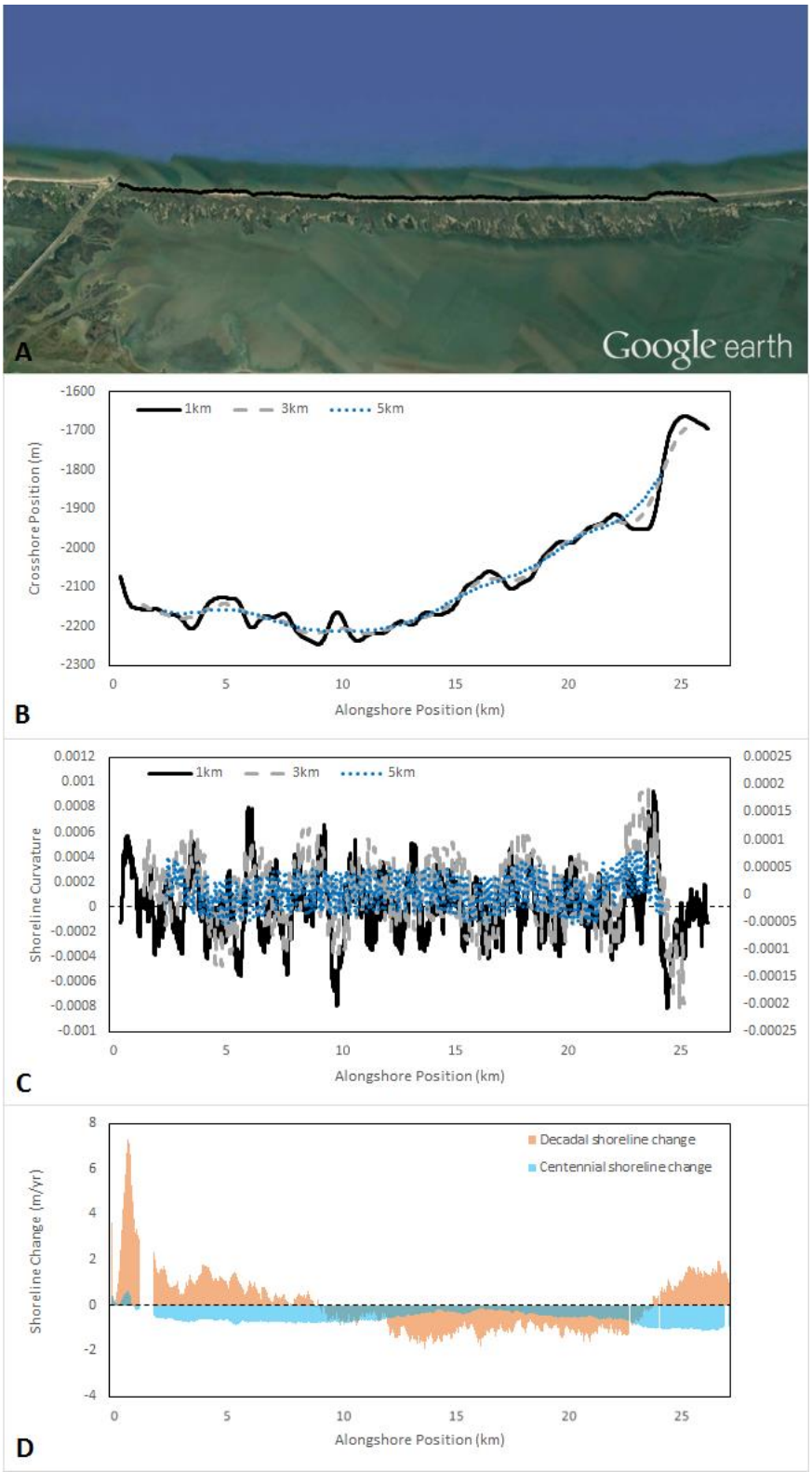
A
Google earth
B
1km
3km
5km
Crosshore Position (m)
-1600
-1700
-1800
-1900
-2000
-2100
-2200
-2300
0
5
10
15
20
25
Alongshore Position (km)
C
1km
3km
5km
Shoreline Curvature
0.0012
0.001
0.0008
0.0006
0.0004
0.0002
0
-0.0002
-0.0004
-0.0006
-0.0008
-0.001
0.00025
0.0002
0.00015
0.0001
0.00005
0
-0.00005
-0.0001
-0.00015
-0.0002
-0.00025
0
5
10
15
20
25
Alongshore Position (km)
D
Decadal shoreline change
Centennial shoreline change
Shoreline Change (m/yr)
8
6
4
2
0
-2
-4
0
5
10
15
20
25
Alongshore Position (km)

Figure 2.4: A) A satellite image of the shoreline overlaid with the shoreline from the Coastline Extractor, B) the shape of the shoreline after it is smoothed at 1, 3, and 5 km scales, C) shoreline curvature and D) shoreline change data for Texas 8. In C), curvature values for the 1 and 3 km smoothing windows are plotted on the primary y-axis and values for the 5 km smoothing window are plotted on the secondary y-axis.

Using the generated xy-coordinates, we then smooth the shoreline sections over 1, 3, and 5 km scales to remove the effects of small scale undulations and reveal the large-scale curvature of the shoreline (Lazarus and Murray, 2007) (Figure 2.4b). We use a running average weighted by a Gaussian distribution with a length scale of $\frac{L}{4}$ as our smoothing window such that:

$$f(x) = \frac{1}{\frac{L}{4}\sqrt{2\pi}} e^{-\frac{1}{2}\left(\frac{x-\mu}{\frac{L}{4}}\right)^2} \quad (1)$$

where *L* is equal to 1, 3, or 5 km. Truncating the tails of the Gaussian results in a total sum of the weights of slightly less than 1 (~0.95). This truncation allows us to retain more shoreline length for analysis, reducing the number of points needed to calculate a single value. This method differs slightly from that used by previous work (i.e. Lazarus and Murray, 2007), but the window is comparable in size (Figure 2.5). As increasing the window size reduces the number of independent data points which can be obtained from a length of shoreline, in the case that a shoreline segment is not long enough to allow for smoothing at all three length scales (1, 3, and 5 km) the analysis is only performed at the appropriate scales .

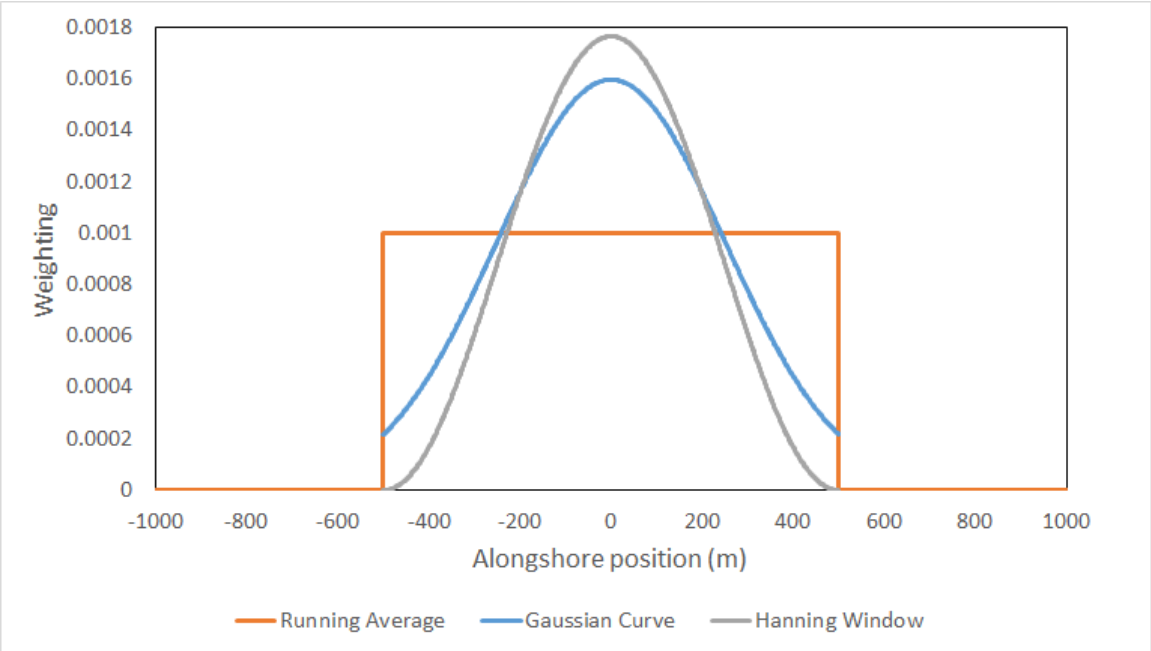

Figure 2.5: Comparison of three possible 1 km smoothing windows on a hypothetical 2 km long shoreline section. We use a Gaussian curve (blue) and define the length scale as L/4. As such, the lowest weighting falls off to 13.5% of the central value and we lose 2.5% on each side of the curve, meaning the sum of all the weights approximates 0.95. When compared to the Hanning window (gray), where the lowest weighting falls off to 1% of the central value and the sum of all the weights approximates 0.99, the weights obtained from the Gaussian are slightly smaller on average. As a result, the results from smoothing with a Gaussian are most comparable to those of a Hanning window when multiplied by 1.5 (e.g., a 1 km Gaussian smoothing window would compare most directly to a Hanning window of 1.5 km).

We calculate the curvature as the second derivative of the shoreline using the smoothed xy-coordinates generated in reference to the linear reference line. In our formulation, concave seaward curvature areas have negative curvature, and convex seaward areas have positive curvature (Figure 2.6; see Figure 2.4C for example data). Shoreline change data is obtained from the USGS's National Assessment of Shoreline Change Project (Morton et al., 2004; Morton and Miller, 2005). In this database, a single

long-term (centurial scale) rate of shoreline change was obtained from a linear regression of shoreline change data from the 1800s, 1920s-1930s, 1970s, and 1998-2002. A short-term (decadal scale) shoreline change rate was obtained using an end-point method and the data from the 1970s and 1998-2002. From here on, the values obtained will be referred to as long or short term. Positive values of shoreline change represent accretion, and negative values correspond to erosion (Figure 2.6; see Figure 2.4D for example data). In the case that large sections of a particular shoreline segment do not have shoreline change data available, we remove the segment from the analysis or break it up into smaller pieces for which data are available. We then calculate a correlation coefficient to determine the strength and direction of the relationship between curvature and shoreline change rate for each shoreline segment. Using the sign conventions described above, a positive correlation signifies that the shoreline is roughening, and a negative one that the shoreline is smoothing (Figure 2.6).

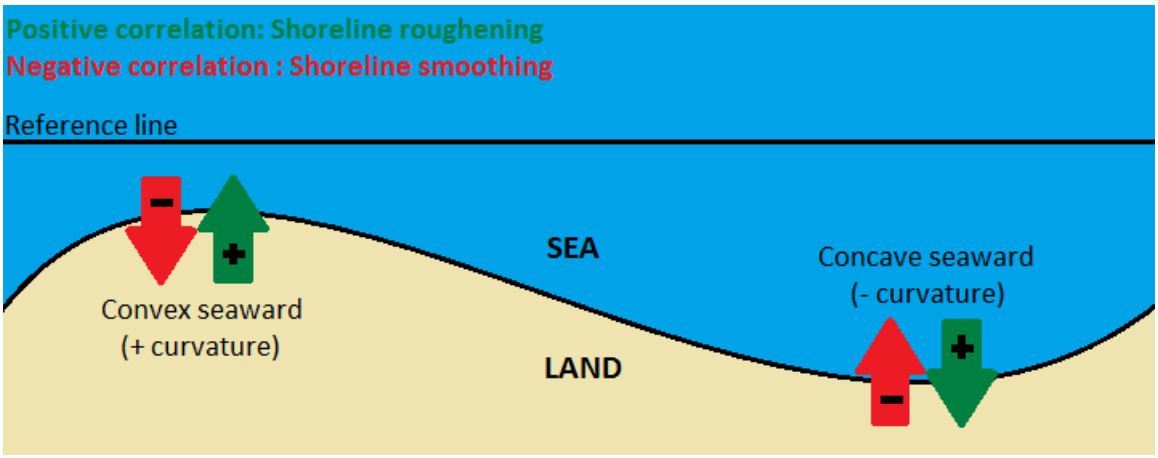

Figure 2.6: Illustration of the sign conventions used in this analysis. Convex (concave) seaward curvature is defined as positive (negative). Accretion (erosion) is positive (negative) shoreline change. A positive (negative) correlation represents roughening (smoothing) of the shoreline.

Finally, we identified shoreline sections that have experienced nourishment using data from the USGS National Assessment of Shoreline Change Project (Miller et al., 2004; Miller et al., 2005). In the case of Texas and the Mid-Atlantic, we included these shoreline sections in the analysis for the sake of discussion. For North Carolina and Florida, we removed nourished shoreline sections from the analysis. Depending on the extent of nourishment, we removed some islands entirely and cut others into more than one piece or removed sections from one or both ends. (See Table 2.1 to identify nourished shoreline sections which were retained in the analysis.) We discuss the implications of nourishment on this type of analysis below.

Table 2.1: Correlation coefficient data for all space and time scales for all shoreline sections. Shoreline sections are numbered moving from south to north (e.g. New York 1 is the southernmost section of New York's shoreline). Bold shoreline section names have not experienced nourishment, unbolded section names have experienced nourishment. Bold values are significant at a 95% confidence interval.

Shoreline section	Correlation Coefficient					
	Short term shoreline change			Long term shoreline change		
	1 km	3 km	5 km	1 km	3 km	5 km
New York8	0.070324	**-0.12827**	**-0.1582**	-0.03502	**-0.20957**	**-0.36577**
New York7	0.111674	**0.372689**	0.129199	-0.01643	**-0.26676**	-0.18264
New York6	**-0.16447**	**-0.2139**	0.094883	0.072898	**-0.35544**	**-0.41847**
New York5	-0.04217	-0.01076	0.02657	-0.01125	-0.02875	-0.08844
New York4	-0.00042	0.026879	**0.164316**	**-0.07888**	**0.202794**	**0.11143**
New York3	0.019078	-0.06927	**-0.54342**	0.027861	-0.06655	0.023931
New York2	**-0.59108**	**-0.69198**	**-0.6239**	**-0.1626**	-0.04233	**0.164476**
New York1	**-0.39928**	0.094831	**0.309797**	**0.305994**	0.079137	**-0.23789**
New Jersey9	**-0.08228**	**0.053764**	**0.205561**	**0.107832**	**0.348556**	**0.332377**
New Jersey8	**0.145729**	**0.205536**	-0.00939	0.045185	**0.10853**	0.052792
New Jersey7	**0.291612**	**0.552746**	**0.412828**	**0.213461**	**0.624899**	**0.515199**
New Jersey6	**0.217063**	0.117759	0.120676	**0.17374**	**0.402628**	**0.220784**
New Jersey5	**-0.2044**	**-0.16818**	**-0.48515**	**0.381102**	**0.570934**	**0.612524**
New Jersey4	0.102028	**0.339569**	**0.282275**	0.10447	0.008002	0.082873
New Jersey3	**-0.61737**	**-0.83374**	**-0.40891**	**0.415036**	**0.569583**	**0.581117**
New Jersey2	-0.06871	0.011789	**0.351761**	0.089031	**0.353269**	**0.226332**
New Jersey1	-0.10345	0.105707	-0.10639	**0.419118**	**0.726764**	**0.608737**
Delaware1	**-0.17877**	**-0.4055**	**-0.26207**	0.003589	**-0.09073**	**-0.30117**
Maryland1	0.005773	0.073997	**0.242193**	-0.02634	0.017682	**0.150606**
Virginia12	**-0.10359**	**-0.16801**	**-0.19339**	0.029798	0.059715	0.055696
Virginia11	**-0.40403**	-0.14275	0.24763	-0.02237	**0.520963**	0.141626
Virginia10	**-0.37967**	**-0.34945**	0.000728	-0.02503	**0.257716**	**0.571434**
Virginia9	-0.06196	-0.00568	-0.08664	0.145887	**0.238378**	0.164923
Virginia8	-0.15521	**-0.36874**	**-0.6393**	**0.45665**	**0.42626**	**0.501026**
Virginia7	**-0.25557**	**-0.74775**	**-0.7111**	0.088547	0.106359	**0.61136**
Virginia6	0.037561	0.120676	**0.746808**	**-0.26258**	**-0.39069**	**-0.68728**
Virginia5	**-0.54848**	N/A	N/A	-0.94385	N/A	N/A
Virginia4	**-0.96205**	**-0.66748**	N/A	**0.925424**	**0.857653**	N/A
Virginia3	0.064669	-0.21759	N/A	0.111884	0.363048	N/A
Virginia2	0.125624	**0.759211**	**0.803326**	0.02661	**0.620772**	**0.891446**
Virginia1	**0.744398**	N/A	N/A	-0.01646	N/A	N/A
North Carolina P96	**0.144269**	**-0.10529**	-0.00876	**-0.10541**	**-0.18824**	**-0.13276**

North Carolina P92	**0.349557**	**-0.27417**	**-0.31334**	0.025203	**-0.28839**	**-0.2133**
North Carolina P91	-0.25219	N/A	N/A	0.145667	N/A	N/A
North Carolina P90	**0.250724**	0.039114	0.142102	0.017522	-0.01094	0.143771
North Carolina P89	0.021587	**0.218485**	0.102581	**-0.24125**	-0.01805	-0.18751
North Carolina P88	**0.079472**	0.050025	0.04052	-0.06983	-0.06712	-0.06532
North Carolina P87	**-0.19644**	**0.324325**	**0.550742**	0.027631	**0.254313**	**0.579232**
North Carolina P85	**-0.37264**	**-0.83128**	N/A	**-0.51683**	**-0.91692**	N/A
North Carolina P84	-0.0911	**0.525982**	N/A	0.124373	**0.591191**	N/A
North Carolina P83	-0.01929	-0.08488	0.122145	-0.00162	**-0.25567**	**-0.24168**
North Carolina P81	**-0.30684**	-0.21183	**-0.34157**	**-0.65238**	**-0.33897**	**0.316539**
North Carolina P80	**-0.21832**	0.071481	-0.06178	0.17744	**0.422571**	-0.12204
North Carolina P78	**-0.56693**	**-0.78673**	**-0.70293**	**-0.51285**	**-0.69875**	-0.10446
North Carolina P76	-0.09098	0.140232	-0.14015	0.067391	**0.501133**	0.1847
South Carolina P68	-0.10677	**-0.44164**	**-0.68018**	**-0.33971**	**-0.81407**	**-0.90549**
Florida P19	0.025201	**0.099415**	**0.279159**	0.054233	**0.095545**	**0.12083**
Florida P18	0.124249	-0.04477	-0.13314	-0.04349	**-0.37348**	**-0.55988**
Florida P17	-0.03337	0.052037	0.01319	-0.00258	0.040937	0.033951
Florida P16_2	**0.093654**	**0.1549**	**0.255917**	0.005374	0.006049	-0.02489
Florida P16_1	**-0.09532**	**-0.11464**	-0.05769	-0.08013	**-0.09641**	-0.0637
Florida P15	0.021525	0.053018	-0.02001	0.020112	0.024078	0.036264
Florida P10	**-0.16552**	**0.161041**	**0.271616**	-0.05879	**-0.13993**	-0.09773
Florida P9	0.087139	**-0.15064**	**-0.21389**	**0.299981**	-0.01654	0.10858
Texas14	-0.00358	**-0.12428**	**-0.27463**	0.035979	0.008918	0.000558
Texas13	0.050743	0.004555	-0.04873	0.045255	0.016686	-0.00247
Texas12	-0.04612	**0.135178**	**0.13365**	**-0.04115**	**-0.1909**	**-0.575**
Texas11	-0.03796	**-0.37634**	**-0.37393**	-0.04811	0.074985	0.071233
Texas10	-0.07537	**-0.13733**	**-0.20475**	**-0.1033**	-0.07987	**-0.19432**
Texas9	-0.03402	**-0.0859**	**-0.14875**	-0.00463	0.021958	-0.03221
Texas8	**-0.11271**	0.061099	0.044159	**-0.12668**	0.029944	**0.104228**
Texas7	-0.06834	**-0.17361**	**-0.28095**	-0.10502	**-0.1840**	**-0.25799**
Texas6	**-0.19458**	**-0.5778**	**-0.71853**	**-0.19394**	**-0.54149**	**-0.66695**
Texas5	-0.05542	**-0.25435**	**-0.43196**	-0.00979	0.037675	-0.00574
Texas4	0.009212	-0.03978	**-0.05869**	-0.01434	**-0.06512**	**-0.08189**
Texas3	0.003582	-0.06113	**-0.08572**	0.003729	0.006362	-0.01497
Texas2	-0.04068	**-0.07482**	**-0.09748**	-0.00601	-0.01158	0.017724
Texas1	-0.06139	**-0.58019**	**-0.7515**	-0.13321	**-0.50223**	**-0.63403**

2.3 Results & Interpretations

2.3.1 Texas

The Texas Gulf Coast is characterized by very long sandy barriers with relatively stable inlets (Kraus, 2007). It is a wave-dominated system with minimal tidal influence (mean tidal range 0.6 m; Kraus, 2007). We broke the shoreline up into 14 segments, ranging in length from 10.2 km to 95.9 km. The shoreline sections for TX 2 (South Padre Island), 11, 12 and 13 (Galveston Island) have experienced nourishment (Figure 2.7).

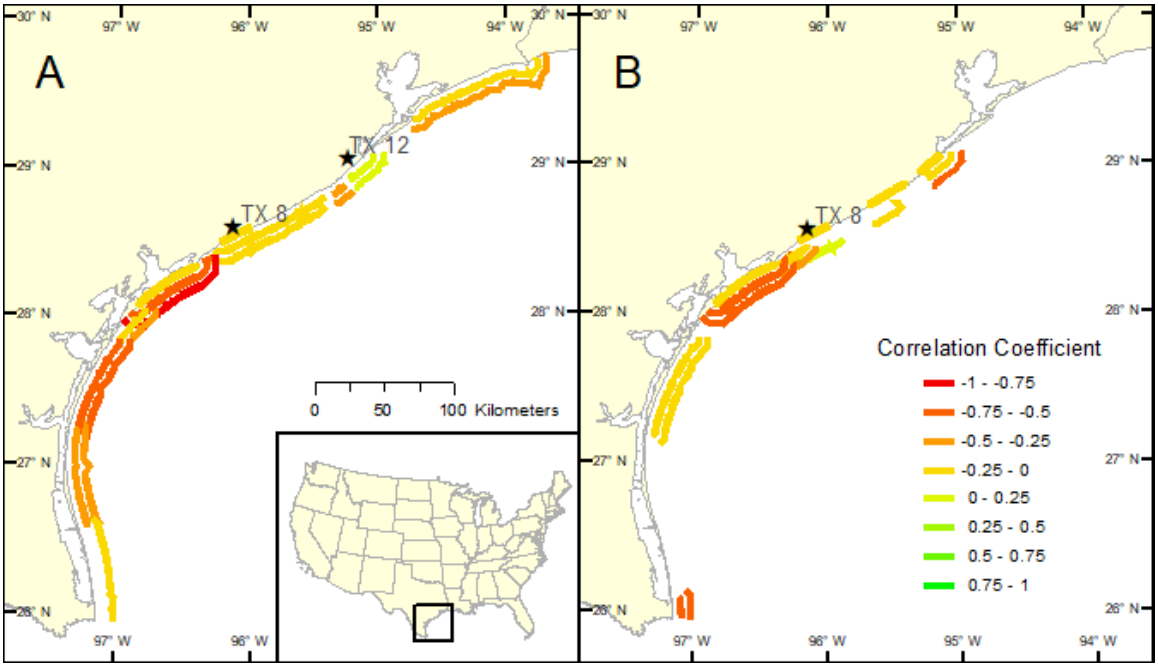

Figure 2.7: Map showing the significant correlation coefficients between shoreline curvature and shoreline change found for the Texas Gulf Coast. A) Correlations between shoreline curvature and short-term (decadal) shoreline change. B) Correlations between shoreline curvature and long-term (centurial) shoreline change. For both timescales, data is plotted in the following order: moving away from the coast, 1 km, 3 km, and 5 km smoothing.

The data typically exhibit a significant ($p < 0.05$) negative correlation over all space and time scales analyzed (Figure 2.7), indicating smoothing of the shoreline. Correlation coefficients range from -0.75 to 0.06 for short term shoreline change, and from -0.63 to 0.1 for long-term shoreline change (see Table 2.1 for all data). The correlation coefficients increase in maximum magnitude and range as the spatial scale increases. While the smoothing signal can be found at all three spatial scales (1, 3, and 5 km), values are more negative and there are more significant values (i.e. the smoothing signal is stronger) at larger spatial scales.

While a few shorelines in Texas appear to have a roughening signal, the correlations in these cases are much smaller in magnitude than those of the smoothing signal and are often not significant. In most cases, for example Texas 8 (the northern part of what is now one island fronting Matagorda Bay; Figure 2.4; Figure 2.7), this signal can be explained by local history. Texas 8 has a positive correlation coefficient indicating a roughening rather than smoothing signal for the 3 and 5 km smoothing windows at both short and long time scales (this signal is significant only at the 5 km, long-term scale). A convex seaward bump along the southern end of the shoreline segment, combined with comparison of that shoreline segment and historical satellite imagery (via Google Earth), reveals that an inlet was formerly present in this location which has now filled in. The inlet, an ephemeral inlet or hurricane pass identified as Greens Bayou (Kraus, 2007) is visible in satellite imagery from December 1942, and is no longer visible in imagery from December 1984. Since the inlet was initially present and then closed during the period covered by our shoreline change data, this roughening signal is likely the result of the shoreline becoming locally convex in shape as waves swept the relict ebb tidal delta onshore. The formation and continued accretion of the resulting convex bulge drives the roughening signal reflected by the analysis.

Nourishment can also introduce a roughening signal as it increases beach width resulting in a bump on the shoreline where the nourishment occurred. This influence can be seen on Texas 12, which exhibits a significant, positive (roughening) signal on 3

and 5 km scales for short-term shoreline change (Figure 2.7a) and is known to have experience nourishment. Nourishment and other processes that introduce shoreline curvature or alter shoreline change rates are discussed in detail in Section 4.3.

2.3.2 North Carolina

2.3.2.1 New Analysis

Similar to the Texas coast, the North Carolina coast is characterized by long sandy barrier islands. Nourishment is more extensive here than on the Texas coast, resulting in the removal of several shoreline pieces (NC 77, 79, 82, 86, 93, 94, and 95) from the analysis. Additionally, a few of the shorelines (NC 84, 85, 91) are too short to be analyzed at all three length scales. As in Texas, smoothing signals dominate in North Carolina, but roughening signals are more common and are higher in magnitude (Figure 2.8; Table 2.1). Correlation coefficients range from -0.83 to 0.55 for short term shoreline change and -0.91 to 0.59 for long-term.

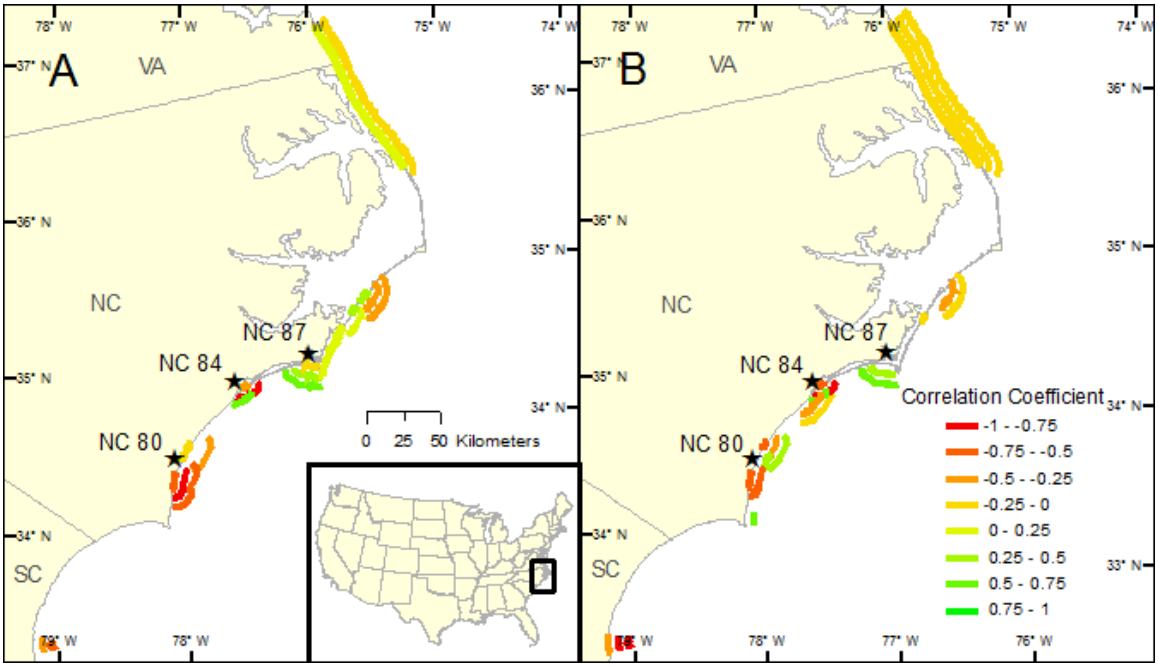

Figure 2.8: Map showing the significant correlation coefficients between shoreline curvature and shoreline change found for the North and South Carolina coasts. A) Correlations between shoreline curvature and short-term (decadal) shoreline change. B) Correlations between shoreline curvature and long-term (centurial) shoreline change. For both timescales, data is plotted in the following order: moving away from the coast, 1 km, 3 km, and 5 km smoothing. Stars mark shoreline sections discussed in detail in the text; NC 87 is Shackleford Banks, NC 84 is Browns Island, and NC 80 is Figure Eight Island.

Some of these roughening signals can be explained by local factors. For example, Shackleford Banks (NC 87) has a significant, positive correlation at the 3 and 5 km scales for both short and long-term shoreline change (Figure 2.8). This apparent roughening signal is likely due to wave shadowing effects leading to a local variation in wave climate. As the waves often come from the east and northeast, and Shackleford Banks is just west of Cape Lookout (NC 88), it does not directly experience the same wave climate as other parts of the coast. Starting from the eastern end of Shackleford banks

and moving from the west, the shoreline is affected more frequently and more strongly by waves from the east and northeast (after diffracting or refracting around Cape Lookout for some wave-approach directions). This gradient in wave shadowing creates a gradient in net alongshore sediment transport; net transport toward the west increases moving west. This gradient in transport tends to cause shoreline erosion, which tends to create a concave shoreline, leading to a roughening signal. (When waves approach from the south, so that wave shadowing is not a factor, the concavity will tend to produce accretion—a smoothing influence that will interact with the roughening effect from the wave shadow.)

Another island which appears to be roughening, Figure Eight Island (NC 80), is a private island and so while it is known to undergo nourishment, it was not included in the database we used to eliminate nourished shorelines. Similarly, NC 84 (Browns Island) is occupied by Camp Lejeune, a U.S. military base, and so shoreline stabilization data is not available.

2.3.2.2 Comparison to Previous Analysis

A section of the Northern North Carolina Outer Banks, stretching roughly from Oregon Inlet to Virginia (NC P96 in our study), was also analyzed by Lazarus and Murray (2007). As our method differs from that used in the previous study, we performed additional analysis on this shoreline section to more directly compare our methods and our results. In addition to the shoreline and shoreline change data used in

the rest of our study, we performed our analysis for this section on the LIDAR shoreline and the multi-annual shoreline change data used by Lazarus and Murray (2007). The previous study smoothed the curvature values and the shoreline change values, whereas we smooth the shoreline itself. We compared the results of smoothing the shoreline to smoothing the curvature values, and found no difference in the final curvature values calculated. Additionally, we found a negligible difference in the correlation coefficients when smoothing or not smoothing the shoreline change data. The length scales and distributions of the smoothing windows used in the analyses also differ slightly (Figure 2.5). When we change the shape of our Gaussian so that it resembles the Hanning window used by Lazarus and Murray (2007) (i.e. so that the sum of the weights is about 0.99 and the lowest weight is about 1% of the central value) the length scale differs by a factor of about 1.5. In other words, we have to reduce our length scale ($\frac{L}{4}$ in Equation 1) by $\frac{2}{3}$ to make our Gaussian have comparable weights to the Hanning window, and so our data smoothed at a 1 km scale is most directly comparable to Lazarus and Murray (2007)'s 1.5 km scale.

When the results of this additional analysis are compared with the data from Lazarus and Murray (2007), the same trends can be seen, and our values are within a factor of 2 of the original values (Table 2.2). For both analyses, over the time scales

involved, the correlation becomes less strong as the length scale increases and is stronger at longer (decadal) than shorter (annual) time scales.

Table 2.2: Comparison of results from Lazarus and Murray (2007) and this study. Bold values are significant at a 95% confidence interval. The most directly comparable smoothing windows (1500 m for Lazarus and Murray (2007) and 1000 m for this study) are in italics.

Time Period	Window Size (m)									
	Lazarus and Murray, 2007							This study		
	100	500	1000	*1500*	2000	2500	3000	*1000*	3000	5000
1996-1997	**-0.15**	**-0.25**	-0.24	*-0.21*	-0.18	-0.14	-0.11	***-0.19***	**-0.15**	**-0.15**
1997-1998	**-0.13**	**-0.22**	-0.17	*-0.14*	-0.12	-0.11	-0.11	***-0.12***	**0.08**	**0.14**
2004-2005	**-0.20**	**-0.30**	**-0.30**	*-0.27*	-0.27	-0.28	-0.28	***-0.19***	**-0.12**	**-0.13**
1997–2004	**-0.11**	**-0.28**	**-0.32**	***-0.34***	-0.34	-0.34	-0.33	***-0.29***	**-0.16**	**-0.05**
1996-2005	**-0.10**	**-0.28**	**-0.42**	***-0.48***	**-0.51**	**-0.53**	-0.53	***-0.32***	**-0.31**	**-0.27**

2.3.3 Additional Analysis

We also analyzed sandy, barrier island shorelines from New York, New Jersey, Maryland, Delaware, Virginia, South Carolina, and Florida (see Table 2.1 for complete results). We did not include the US Atlantic coast between the wave dominated coasts of the Carolinas and Florida. This stretch of coast, similar to the Virginia Barrier Islands (discussed in Section 3.3.2 below), is characterized by a large number of estuaries, large tidal ranges, and thus large tidal prisms. Barriers islands, when present, are short, have strong tidal inlet influences. In addition, the islands between North Carolina and Florida

are often heavily developed and stabilized. Therefore, they are not appropriate for this type of analysis.

2.3.3.1 Mid-Atlantic (New York to Virginia)

Shorelines in this region, stretching from Montauk Point, New York, in the north to Assateague Island, VA, in the south, range from 9.26 - 79.86 km in length. Virtually all of the shorelines along the coast of New York and New Jersey have been nourished or have stabilization structures such as groynes or seawalls in place. This stabilization of the shoreline prevents erosion from occurring, masking natural signals of shoreline change (Hapke et al., 2013). This phenomenon will be discussed in more detail below. Correlation coefficients in this area range from -0.42 to 0.73 for long-term change, and from -0.83 to 0.55 for short-term change (Table 2.1). See Figure 2.9 for a map of the significant data.

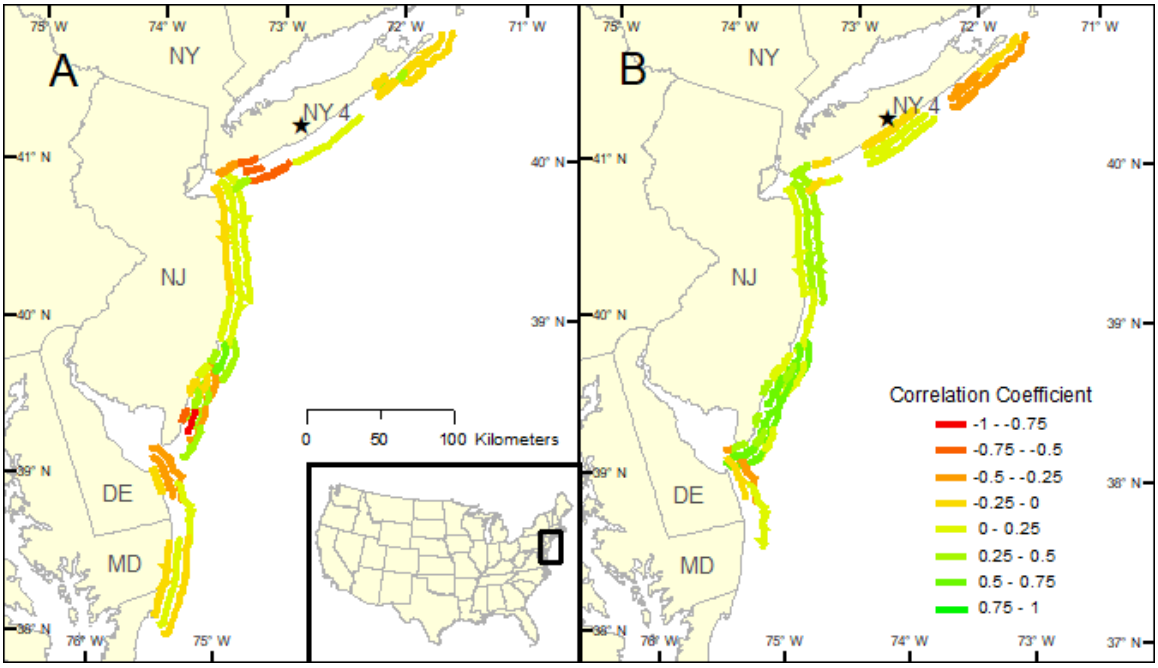

Figure 2.9: Map showing the significant correlation coefficients between shoreline curvature and shoreline change found for the Mid-Atlantic Coast (from New York to Assateague Island, Virginia). A) Correlations between shoreline curvature and short-term (decadal) shoreline change. B) Correlations between shoreline curvature and long-term (centurial) shoreline change. For both timescales, data is plotted in the following order: moving away from the coast, 1 km, 3 km, and 5 km smoothing.

One of the shoreline sections, NY 4 (Fire Island, Figure 2.9), displays a roughening signal on both short-term and long-term timescales despite not undergoing nourishment. This signal can be attributed to the presence of shoreface-attached sand ridges located offshore (e.g. Safak et al., 2017). We discuss this interpretation and its implications for this analysis in Section 4.3.

2.3.3.2 Virginia

The Virginia Barrier Islands are characterized by short, uninhabited islands with a strong tidal influence. Islands range in length from 3.09 to 15.69 km. Tidal and inlet effects are at least as important as wave influence in determining island behavior. Many of the shorelines are too short to evaluate at greater than the 1 km length scale, and others (e.g. Wallops Island, a NASA flight facility) do not have historic shoreline change data available. In addition, the timescales of analysis in this project do not match the timescales of shoreline change in that area. While our shoreline change data is on decadal or centurial time scales, the Virginia Barrier Islands are rotating and shifting on much faster timescales, so that there is little overlap between the current position (and curvature) of the shoreline and the position (and curvature) of the shoreline at the start of the time spanned by the shoreline change data. In one example, Hog Island, shoreline change rates can be higher than 5 m/yr, accreting on the northern end of the island and eroding on the southern (Hayden et al., 1991). A town on the island which was several kilometers from the beach in 1903 was abandoned in the 1930s because the shoreline had eroded through the town, and its former location is now several hundred meters offshore.

As a result of the mismatch between shoreline change rates and the duration over which shoreline change is calculated in this study, no clear signal can be found, and most trends are on the extreme ends of the range of correlations, signifying a strong

smoothing or roughening signal (see Table 2.1 for data). Many of the islands are short enough that few points remained for analysis, allowing outliers to have a strong influence on the overall trend. Few values are significant, and the mismatch in timescales means it is unlikely the trends have any physical meaning, especially on such long timescales as 100 years. Although we did not perform our analysis for the short, tidally-influenced barrier islands of South Carolina and Georgia, we would expect similar results.

2.3.3.3 Florida

Though characterized by long sandy barriers like the coasts of North Carolina and Texas, the Florida coast is also heavily developed and therefore subject to large and frequent nourishment projects. Due to the extent of nourishment, as well as some concerns about the quality of the shorelines obtained from the coastline extractor, we analyzed only a small portion of the Florida coast. Further analysis could be performed using shoreline data from an additional source, such as LIDAR data, but is beyond the scope of this study.

We analyzed 7 shorelines, one of which was broken into two sections. Correlation coefficients range from -0.56 to 0.3 for long-term shoreline change, and -0.21 to 0.28 for short-term change (see Figure 2.10 for significant data, and Table 2.1 for all data).

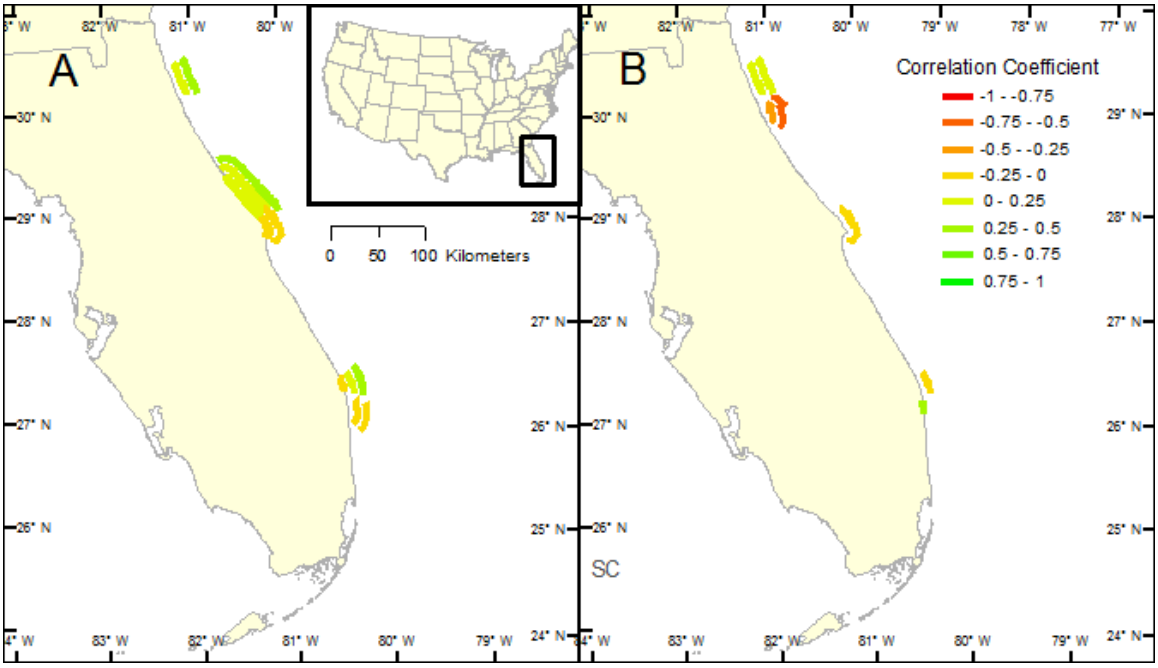

Figure 2.10: Map showing the significant correlation coefficients between shoreline curvature and shoreline change found for the Atlantic Coast of Florida. A) Correlations between shoreline curvature and short-term (decadal) shoreline change. B) Correlations between shoreline curvature and long-term (centurial) shoreline change. For both timescales, data is plotted in the following order: moving away from the coast, 1 km, 3 km, and 5 km smoothing.

2.4. Discussion

2.4.1 Variability in Wave Climate and Effective Diffusivity

The combination of long islands, a tendency for islands to change slowly, and dominance of wave forcing in shaping island morphology makes the Texas Gulf Coast an ideal site for this method of analysis. In fact, the results from our analysis, showing strong, significant, smoothing signals for most of the Texas coast closely matched our expected results (Figure 2.7). Though the coast of North Carolina is similarly wave

dominated, the correlation coefficients resulting from our analysis are more frequently positive (indicating roughening) than might be expected (Figure 2.8).

This result is especially surprising given that we included sections of Texas's shoreline which had been nourished in our analysis, while we removed sections of North Carolina's coast which had been nourished. The positive coefficients for North Carolina are also of higher magnitude than those for Florida (Figure 2.10), for which almost the entire coastline has experience nourishment. This discrepancy is likely due to local variation in wave climate and therefore in effective diffusivity. Unlike Texas or Florida, which both feature predominately low-angle regional wave climates, the coast of North Carolina is subject to a high-angle dominated regional wave climate (Ashton and Murray, 2006a,b). While wave shadowing and shoreline reorientation make the local wave climates almost all low-angle dominated (Ashton and Murray, 2006a,b), the effective diffusivity of local wave climates is likely lower (less strongly smoothing) than the local wave climates of Texas or the East Coast of Florida. This comparison demonstrates the importance of considering local wave climate for this type of analysis.

Though the smaller effective diffusivity of local wave climates decreases the magnitude of the correlation between shoreline curvature and shoreline change in North Carolina, as compared to Texas, the correlations are still significant; the relationship between shoreline curvature and shoreline change still explains part of the shoreline erosion and accretion.

2.4.2 Space and Time Scales of Relevance

In a simple diffusional system, we would expect to be able to see relationships between shoreline curvature and shoreline change down to small (km) spatial scales for short time scales. However, the longer the span of time considered, the more likely you are to lose small scale relationships, as the memory of small-scale shoreline bumps present in the initial coastline diffuses away over time, and the long-term shoreline diffusion becomes dominated by larger scale undulations. This is evident in our results which involve relatively long-timescale shoreline change data; there are stronger correlations for the larger spatial scales (e.g. 5km) than the smaller ones (1, 3 km) and this trend is more evident for the centurial timescales than the decadal ones (see Figures 2.7 and 2.9, Table 2.1).

Unsurprisingly, however, the time and space scales over which our analysis is meaningful varies due to the wide variety of environmental conditions and morphological processes which can affect shoreline change. In some cases, signals which did not fit our expectations were related to events in the shoreline's history. For example, the roughening signal obtained for Texas 8 appears to be due to a change in the processes acting on the island during the time covered by our shoreline change data; during the beginning of the time covered by our analysis, the shoreline was broken up by an inlet, and the formation and subsequent onshore movement of an ebb tidal delta caused the shoreline to accrete. If we had used a shoreline or shoreline change data from

a different period in time (for example, after the inlet closed and the convex shoreline bulge was created), the analysis would likely have resulted in a smoothing signal.

The Virginia Barrier Islands present another example in which the timescale of the shoreline-change data sets does not match the timescale for the reshaping of the shoreline. When the final shoreline shape differs so dramatically from the initial shape (and from the shape at intermediate times), the record of cumulative shoreline change does not bear a strong relationship to the curvature of the final shoreline.

If the fact that shoreline change operates on a faster timescale than our decadal and centurial shoreline change timescales was the only obstacle, we could overcome it by using shorter-term (e.g. annual) shoreline change data. However, the strong tidal influence and rotational nature of the short Virginia Barrier Islands means that waves are not the only strong influence shaping these islands; while gradients in wave-driven alongshore transport are tending to smooth out some portions of the coastline, tidal-inlet processes are generating or exaggerating shoreline bulges in other portions. With the combination of smoothing and roughening signals, we would not necessarily expect the shoreline curvature to have a simple relationship with shoreline change rates. These examples lead to a broader consideration of processes that can create shoreline curvature, in opposition to the tendency for alongshore-transport gradients reduce curvature.

2.4.3 Nourishment and Other Injected Signals

Just as tides and inlets obscured the shoreline change signal from wave-driven shoreline curvature in the Virginia Barrier Islands and in Texas 8, other processes can inject shoreline change signals that complicate or obscure the relationship between shoreline curvature and shoreline change. Prominent examples include injection of shoreline bulges from nourishment (Dean and Yoo, 1992; Browder and Dean, 2000; Dean 2002) or underlying geology (Valvo et al., 2006). If these injected signals are strong enough, they can obscure the diffusional signal from the waves.

On highly developed coasts such as those of the mid-Atlantic (e.g. New York, New Jersey), the influence of humans can be so strong that there is no correlation between the geomorphology of the area and shoreline change rates (Hapke et al., 2013; see also our results in Figure 2.9). Shorelines which in historic times experienced shoreline erosion can now exhibit net accretional shoreline change signals resulting from the cumulative impact of nourishment projects. In these cases, over long timescales the natural erosional signal is completely obscured by human activity.

Nourishment complicates the relationship between shoreline curvature and shoreline change as the artificial widening of the shoreline (and resulting convex shoreline shape) looks like a roughening signal. This effect makes learning about shoreline change from an analysis such as ours difficult on nourished coasts. If shorelines and shoreline change data was available for periods of time in between

nourishment events, the analysis would be straightforward; the convex beach would typically erode and the shoreline would typically smooth as a result (e.g. Dean and Yoo, 1992; Browder and Dean, 2000; Dean 2002).

The presence of hard stabilization structures such as groynes can also artificially create shoreline curvature. Groynes interrupt alongshore currents, influencing where erosion and accretion occur by altering local gradients in alongshore transport. Updrift, locally concave shorelines and accretion result, similar to the jetties discussed above (shoreline smoothing). Downdrift, the effect of a groyne locally involves wave shadowing; the resulting gradient in alongshore transport results in a locally concave shoreline and erosion (roughening).

Heterogeneity in underlying geology or offshore bathymetry can also inject signals of shoreline change. Offshore bathymetric features, such as shoreline-attached sand ridges, can influence both shoreline shape and shoreline change. Fire Island, NY, provides a clear example: the island displays a roughening signal on scales greater than 1 km in our analysis (Figure 2.9, Table 2.1). Shoreline undulations on the order of 1 km have been identified on Fire Island, and their presence is attributed to the presence of shoreface-connected sand ridges offshore (Safak et al., 2017). These features apparently act as a cross-shore source of sediment, resulting in accretion and subtle convex bumps along the shoreline. In a low-angle wave climate such as is found here, we would expect gradients in alongshore sediment transport associated with the convex curvature to

result in erosion. However, in this case it appears that the rate of cross-shore sediment flux building the undulations is greater than the rate sediment is being removed by alongshore transport gradients related to shoreline curvature. It seems that alongshore transport is not the only process playing a significant role in shaping this coastline.

Variations in the composition of underlying geology alongshore can also result in injections of shoreline curvature (Lazarus and Murray, 2011; Valvo et al., 2006). As an eroding coastline encroaches on alongshore heterogeneities in the material that the shoreface is eroding into, on some portions of the coastline, weathering and erosion on the shoreface will produce less material that is coarse enough to stay in the nearshore system. For example, if shoreline weathering and erosion produce sediment composed largely of silt and clay, that fraction of the sediment produced will be lost. As a result those portions of the coastline will begin to erode more rapidly. This locally enhanced erosion will tend to produce concave curvature. Portions of the coastline where the shoreface is eroding into material that is coarser than adjacent portions of the coastline will tend to produce subtle convex bumps in the coastline (Lazarus and Murray, 2011; Valvo et al., 2006). This curvature is then diffused away by the smoothing action of waves, but new shoreline curvature signals are injected as the shoreline transgresses through alongshore-variable substrate (Lazarus and Murray, 2011). The reintroduction of these signals could explain why shorelines on even wave-dominated, pristine

coastlines that are being diffused still retain curvature after millennia of smoothing (Lazarus and Murray, 2011).

2.5 Implications

Our results demonstrate that shoreline curvature can correlate significantly along many coastlines with shoreline change rates over several kilometer and decade to century space and time scales. The presence of a significant correlation between shoreline change and shoreline curvature on many coastlines, however small the correlation coefficient may be, demonstrates the importance of the relationship between coastline curvature and shoreline change in understanding shoreline dynamics. This relationship is strongest on wave-dominated coasts with long, sandy barriers and relatively slow rates of shoreline change, but can help explain shoreline behavior even on shorter islands with competing influences (e.g. tides). Large magnitude, significant correlations between shoreline curvature and shoreline change in some locations (e.g. Texas, North Carolina) suggest that considering shoreline curvature in analyses of historical and predicted shoreline change could help improve agreement between models and data on low-lying, sandy coastlines where models have historically underperformed (e.g. Gutierrez et al., 2011; Yates and Cozannet, 2012).

The demonstrated role of shoreline curvature in determining shoreline change rates has implications for managing as well as for understanding sandy coasts. Shoreline change prediction models have previously had limited success in these environments

(Gutierrez et al., 2011; Yates and Cozannet, 2012). Even in areas with positive correlations (roughening signals), the results of the analyses presented here are often significant. Although practical application is limited to wave-dominated coastlines, this analysis is broadly applicable to many types of shoreline- and shoreline-change data, across a range of time and space scales. Calculating shoreline curvature is simple, and the results of correlation analyses exhibit low sensitivity to variations in methodology (see Section 3.2.2). Thus, the results presented here support the inclusion of correlations between curvature and shoreline change in risk assessment and modelling efforts pertaining to sandy shorelines.

2.6 Acknowledgements

A grant from the National Science Foundation, Dynamics of Coupled Natural-Human Systems Program (ICER-1715638) supported this work. We also thank Kenny Ells, Evan Goldstein, and Andrew Ashton for insightful conversations.

3. Effects of marsh edge erosion in coupled barrier island-marsh systems and geometric constraints on marsh evolution

Rebecca Lauzon, Dr. A. Brad Murray, Dr. Laura J. Moore, David C. Walters, Dr. Matthew L. Kirwan, and Dr. Sergio Fagherazzi

Lauzon, R., Murray, A.B., Moore, L.J., Walters, D.C., Kirwan, M.L., and S. Fagherazzi. In Revision. Effects of marsh edge erosion in coupled barrier island-marsh systems and geometric constraints on marsh evolution. Journal of Geophysical Research – Earth Surface

3.1 Introduction

Salt marshes and barrier islands are ecosystems of great economic and ecological importance; barrier islands are often heavily populated and serve as vacation destinations, and salt marshes provide a number of ecosystem services including water filtration, flood protection, and habitat for commercially and ecologically important species (Barbier et al., 2011). Both barrier islands and salt marshes are dynamic environments that, because of their low relief, are especially vulnerable to future changes in sea level and storm intensity (Fitzgerald et al., 2008; Kirwan and Megonigal, 2013).

Salt marshes tend to maintain their elevation relative to rising sea level through the deposition of mineral sediment and the production of organic matter (e.g. Reed, 1995; Friedrichs and Perry, 2001; Fitzgerald et al., 2008; Kirwan and Megonigal, 2013;

D'Alpaos, 2011). As sea level rises, in the absence of flood protection measures, marshes tend to be flooded for longer periods of time and can therefore trap more inorganic sediment, resulting in vertical accretion of the marsh platform (Marani et al., 2010). However, this feedback is limited by inorganic sediment supply and relative sea level rise (RSLR) rates. If RSLR rates are too high relative to sediment supply, a marsh will drown, decreasing in elevation to the level of an adjacent tidal flat (Reed 1995; Morris et al., 2002; Marani et al., 2007; Kirwan et al., 2010; Day et al., 2011). Even in the absence of RSLR, if the basin is deep enough for waves capable of eroding the marsh edge to form, significant loss of marsh can occur due to lateral erosion of the marsh platform by wind waves (e.g. Schwimmer, 2001; Nyman et al., 2006; Marani et al., 2011; Mariotti and Fagherazzi, 2013; Fagherazzi et al., 2013). As the marsh boundary erodes laterally, the basin's fetch increases, allowing larger waves to form and leading to enhanced erosion. Conversely, if sediment concentrations are high enough for the marsh edge to prograde, fetch decreases, making waves smaller and accelerating progradation. Previous research has shown that because of these paired feedbacks the existence of a partially filled marsh basin is an unstable state (Mariotti and Fagherazzi, 2010), and that there is a critical basin width (determined chiefly by suspended sediment concentrations) below which marshes tend to prograde until they completely fill a basin and above which wave action is sufficiently strong to erode marshes completely, leaving an open bay (Mariotti and Fagherazzi, 2013).

In response to RSLR barrier islands and barrier spits tend to migrate landward and maintain elevation relative to sea level (Bruun, 1988). Barrier migration is facilitated by storms that erode sediment from the beach and nearshore seabed (the 'shoreface') and deposit it via overwash processes on the top and back side of an island, raising island elevation and moving the shoreface, shoreline, and barrier landward. The rate of RSLR, the composition and erodibility of underlying stratigraphy (Moore et al., 2010), and substrate slope (Wolinsky and Murray, 2009; Moore et al., 2010; Brenner et al., 2015) affect island migration, which will tend to occur at the rate necessary to liberate sufficient sediment from the shoreface to maintain island elevation relative to sea level (Wolinsky and Murray, 2009; Moore et al., 2010). If sufficient sand cannot be eroded from the shoreface, or if sand cannot be supplied to the island interior to maintain island elevation (e.g. where shoreline fortifications prevent overwash from occurring), a barrier may disintegrate (e.g. Masetti et al. 2008; Moore et al., 2014; Lorenzo-Trueba and Ashton, 2014).

Although the impacts of climate change and sea-level rise on marshes and barrier islands have been the topic of many previous studies, we are only recently beginning to understand that interactions between these two adjacent environments are important in determining how barrier-marsh systems evolve (Fitzgerald et al., 2008; Walters et al., 2014; Brenner et al., 2015; Walters and Kirwan, 2016). For example, when a barrier migrates over a back-barrier marsh platform less sand is required to raise the elevation

of the back of the island than would be required if the barrier progrades into a back-barrier bay (Wolinsky and Murray, 2009). The tendency of the back-barrier marsh to keep up with RSLR reduces the accommodation space that the barrier needs to fill, thereby allowing for a slower island migration rate (Walters et al., 2014; Brenner et al., 2015) and reducing the likelihood of barrier disintegration. In this scenario, fine-grained marsh sediment can eventually become exposed on the shoreface, reducing the amount of sand available to the barrier and resulting in an increase in island migration rate (Brenner et al., 2015). This scenario can also result in a loss of marsh extent if the back-barrier marsh cannot prograde into the bay as fast as the island is migrating (Deaton et al., 2016). On the other hand, overwash from barriers can be an important source of sediment for back-barrier marshes (e.g. Walters et al., 2014; Walters and Kirwan, 2016), allowing a marsh that would otherwise drown to maintain its elevation, resulting in a long-lasting "narrow marsh" state (e.g. Figure 3.1), identified in model results and in satellite observations of marsh widths for the Virginia Barrier Islands (Walters et al., 2014). For some time, a narrow marsh in this state will maintain its elevation while mainland-attached marshes farther away from the sediment source (here, a barrier) will drown.

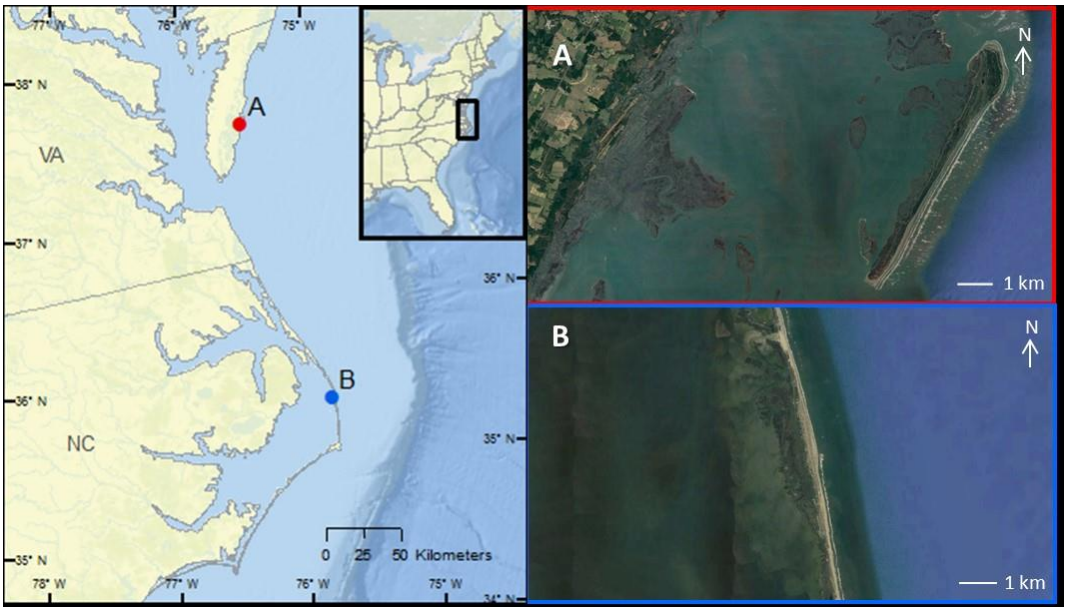

Figure 3.1: Illustrative examples of two narrow back-barrier marshes on the East Coast of the United States. A) is Hog Island, Virginia, and B) is a section of Cape Hatteras National Seashore, North Carolina.

In Walters et al. (2014), in the long-term this narrow marsh state almost always eventually progrades to fill the basin or drowns. However, Walters et al. (2014) did not consider the effects of wave edge erosion, which is a primary cause of marsh loss (e.g. Leonardi and Fagherazzi, 2014; Priestas et al., 2015; Marani et al., 2011). Such model simplification and the intentional omission of the some of the processes and interactions occurring in complex natural morphodynamic systems can facilitate insights about what processes and interactions are most important in those systems (Murray, 2003). To increase the level of realism of the model framework of Walters et al. (2014), and to test the importance of wave-edge erosion in the evolution of marsh-barrier systems, we expand on the morphological behavior model GEOMBEST+ (Geomorphic Model of

Barrier, Estuarine, and Shoreface Translation + Marsh; developed by Walters et al., (2014)) to include the addition of wave effects on back-barrier marshes and create GEOMBEST++ (GEOMBEST+ + Waves). GEOMBEST+ is a 2-D morphological behavior model representing the evolution of a cross-shore transect from the base of the shoreface to the mainland and including a barrier, marsh, and bay. GEOMBEST+ combines the conservation of mass with geometric constraints on sediment availability and placement, given some commonly employed assumptions (chiefly involving equilibrium elevations and shapes of some parts of the cross-shore profile, representing negative morphodynamic feedbacks). GEOMBEST+ facilitates exploration of barrier island evolution on long timescales, as influenced by spatially varying stratigraphy and topography/bathymetry, possibly representing real world settings (e.g. Moore et al., 2010). With the addition of back-barrier processes represented in the model (Walters et al., 2014), and the improvements to those processes in this work, GEOMBEST++ offers an opportunity to further examine the interactions between barriers and back-barrier environments. A more detailed model description, including model assumptions, follows in Section 2.

Our goals are to further investigate the persistence of the overwash-sustained narrow marsh state identified by Walters et al. (2014). We do not seek to represent any particular barrier island-marsh system, but more broadly to improve our understanding of how interactions between barrier islands and marshes can influence the evolution of

the system as a whole. In the process, we explore the consequences of some assumptions and simplifications commonly employed in models of marsh/bay morphodynamics. Our results highlight the constraints that geometry and conservation of mass impose on back-barrier basins as they evolve in response to RSLR, and build on our understanding of how wave edge erosion can increase marsh resilience (e.g. Mariotti and Carr, 2014).

3.2 Model Description: GEOMBEST and GEOMBEST+

GEOMBEST (Geomorphic Model of Barrier, Estuarine, and Shoreface Translation) tracks the evolution of a two-dimensional, cross-shore coastal transect extending from the mainland to the base of the shoreface, as this profile responds to RSLR and sediment supply over timescales of decades to millennia (Stolper et al., 2005; Moore et al., 2010; Brenner et al., 2015). The model tends to maintain an equilibrium profile extending across the barrier island and shoreface (e.g., Rosati et al., 2013; Murray and Moore, 2018), and operates on the principle of sediment conservation, representing the effects of the transport of sand among three domains: shoreface, barrier island and back-barrier (Figure 3.2A). As sea level rises, the profile moves upward to maintain its elevation relative to sea level (representing negative morphodynamics feedbacks; Murray and Moore, 2018) and landward to the cross-shore position required to conserve sand, which is redistributed among the three domains. While stratigraphy in natural back-barrier systems is complex (e.g. Hein et al., 2012; Rodriguez et al., 2018; Odezulu et al., 2018), stratigraphy in the model is by necessity simplified: the user can define

stratigraphic units and establish the erodibility and proportions of sand and mud for each (thus approximating the important influence stratigraphy can have on barrier migration through variations in yield strength). Stratigraphic units have distinct boundaries, but this assumption is relaxed in the back-barrier in recent versions of the model (GEOMBEST+ and GEOMBEST++); the sand content of the marsh can vary temporally and spatially.

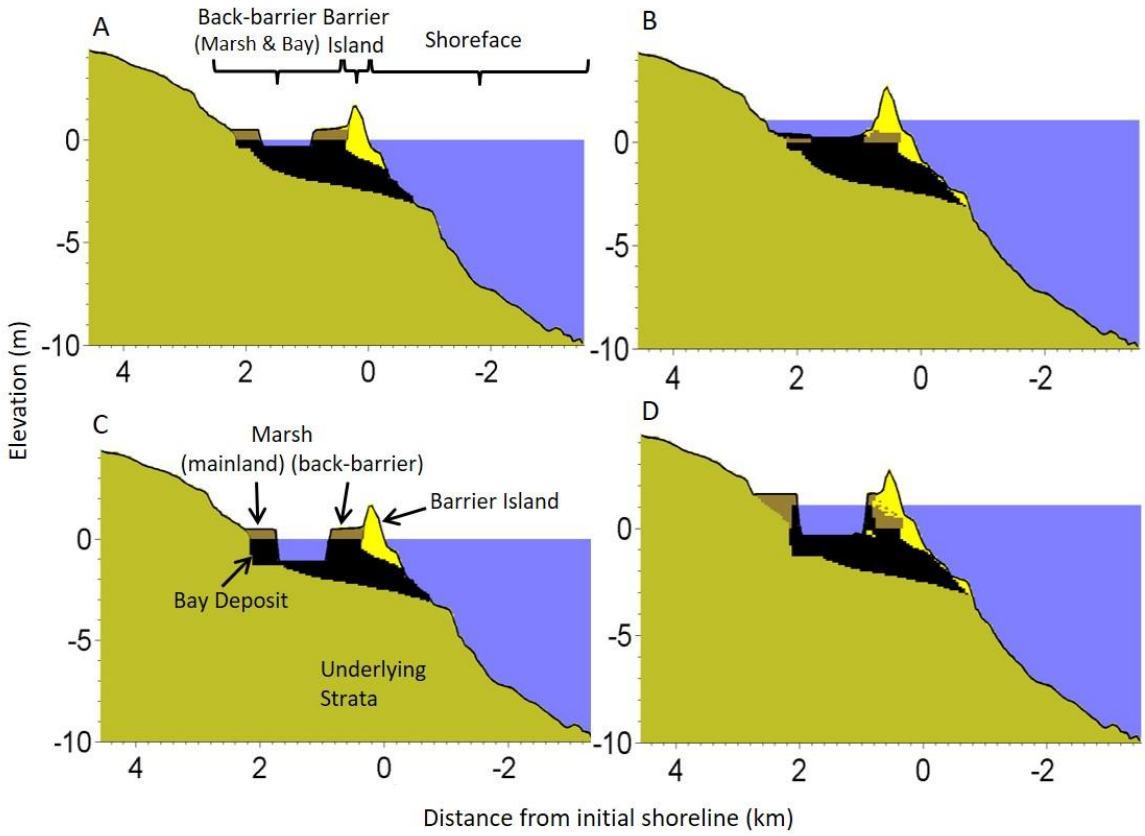

Figure 3.2: Initial condition (A) and model output after 1 m of total RSLR (B) for a GEOMBEST+ simulation of an initially narrow marsh without wave edge erosion (e.g. from Walters et al. (2014)). Initial condition (C) and model output after 1 m of total RSLR (D) from GEOMBEST++ (including wave edge erosion). For both simulations, overwash volume flux = 1.4 m^2/yr and BAR/RSLRR ≈ 0.3; simulations are identified with a black box in Figure 3.3A, C. A) also shows the 3 model domains and C) shows the stratigraphic units and the deeper equilibrium of the bay compared to Walters et al. (2014).

Designed to represent the cumulative effects of storms over decadal to millennial timescales, the barrier component of the model operates on a 10 year time step. As a result, the model does not resolve events of individual storms such as erosion of dunes or individual overwash events, but instead represents a long-term average of the island

profile. The height and/or volume of the sandy part of the barrier can, however, change over time as the profile tends towards equilibrium. The model allows the user to set a sediment import/export rate, representing influx or loss of sediment from gradients in alongshore transport, which can be an important cause of shoreline retreat (e.g. Cowell et al., 1995). However, as we are specifically interested in the interactions between overwash and marsh width, we focus on the cross-shore impacts of SLR and increasing storm frequency (via overwash volume flux) in this study and do not consider alongshore transport. As we focus in this study on the behavior of the back-barrier, we describe the evolution of this model domain in detail below. For more information on the shoreface and barrier components of the model, we refer the reader to Moore et al., (2010).

GEOMBEST+ (Geomorphic Model of Barrier, Estuarine, and Shoreface Translation + Marsh), developed by Walters et al. (2014), adapts components of the marsh-tidal flat model from Mariotti and Fagherazzi (2010) into GEOMBEST so that the back-barrier domain, including marsh and/or shallow bay, evolves dynamically according to rates of SLR and fine-grained sediment supply. In this version of the model, GEOMBEST+, which we use and further expand upon in this study, evolution of the back-barrier geometry depends on the rate of RSLR and the rate of sediment supply (including both overwash sand and fine-grained sediment). Overwash is represented as a characteristic volume flux of sand from the barrier to the back-barrier; the model does

not resolve individual overwash events, but sand deposited in the back-barrier is conserved and layers of sand are preserved in the marsh stratigraphy. GEOMBEST+ does not explicitly include flood tidal deltas, which can be important sources of sand to the back-barrier over long time scales (e.g. Hein et al., 2012). The flux of sand into the back barrier termed 'overwash' could, for the purposes of sediment budgets, be considered to consist of both overwash and sand transported through breaches or ephemeral inlets. However, because sand washed over the island is the main source of sand for the back-barrier (barrier-attached) marshes of interest in our study, we focus here on that mechanism. The model does not include aeolian transport of sediment, as it is negligible at distances away from the dune which are smaller than typical cell sizes (which are on the order of 50-100 m) (Rodriguez et al., 2013). Although sand is conserved in all three domains, fine-grained sediment is only conserved in the back-barrier, because once fine-grained sediment is exposed on natural barrier shorefaces by prolonged shoreface erosion it can be eroded but not redeposited in this high-energy environment.

While the barrier component of GEOMBEST+ still operates on a 10-yr timestep, back-barrier (marsh and bay) processes occur over a shorter sub-timestep, determined by the time it takes for the bay to reach a user-defined maximum depth (d_R) approximating the equilibrium depth (the depth at which vertical accretion and erosion are equal, or for the net deposition rate equals the rate of RSLR). Bay bottom erosion in

GEOMBEST+ (E_B) decreases with depth (d) until reaching zero at the approximated equilibrium depth (d_R) such that:

$$E_B = E_{max}\left(\frac{1-d}{d_R}\right). \quad (1)$$

where E_{max} is a user-defined maximum erosion rate (see Table 3.1 for list of variables). The gross sediment deposition rate (A_B) within the bay (representing riverine and/or net coastal sediment input) is obtained by distributing the net import of sediment to the bay (Q_B) over the width of the bay.

Table 3.1: Definitions of variables and abbreviations.

Variable/abbreviation	Definition
RSLR	Relative sea-level rise
d_R	User-defined maximum bay depth
E_{max}	User-defined maximum erosion rate
E_B	Gross bay bottom erosion rate; previously referred to by *Walters et al.* (2014) as "bay bottom erosion rate"
d	Bay depth
u_b	Orbital velocity
τ	Shear stress
ρ	Water density
f_w	Friction factor
τ_c	Critical shear stress
a	A constant used in gross bay bottom erosion calculation
A_B	Gross bay deposition rate
Q_B	Net import of fine-grained sediment to the bay
E_m	Wave edge erosion
W	Wave power
H	Wave height
c_g	Group velocity
h	Height from bay bottom to surface of marsh platform
k_e	Erodibility coefficient for marsh edge
BAR	Basin accretion rate; Q_B divided by basin width
BAR/RSLRR	Ratio of basin accretion rate to RSLR rate
Q_{OW}	Overwash flux volume
d_b	Depth of the bay relative to MHWL
d_m	Depth of the marsh platform relative to MHWL
R	RSLR rate
L	Cross-shore width of the basin
$Q_{s,in}$	Net volumetric sediment input rate
Q_{OM}	Contribution of organic matter to accretion of marsh platform
Q_d	Organic matter lost to decomposition or dispersal

During each model time step, the back-barrier environment evolves through 5 main stages: (1) sea level rises; (2) barrier island sand is moved into the back-barrier through overwash; (3) Q_B is distributed evenly across the bay; (4) bay bottom erosion occurs according to Equation 1; and (5) fine-grained sediment eroded from the bay bottom is used first to build the marsh platform up to mean high water level and then preferentially deposited on the edges of the bay allowing the marsh to prograde (Mariotti and Fagherazzi, 2010). Stages (3) through (5) comprise the back-barrier component of the model which operates on a faster sub-timestep and so iterate multiple times in one model timestep. The landward and back-barrier sides of the bay each receive half of the total available fine-grained sediment distributed in stage (5). Once the marsh platform has reached mean sea level, 50% of the sediment used to build it up to mean high water comes from the creation of organic material (the remaining 50% comes from fine-grained sediment). This ratio of organic to fine-grained sediment comes from field data collected by Walters et al. (2014). Where a marsh is present, accretion rate in the model does not depend on elevation or flooding frequency. Instead, when sufficient inorganic sediment is available, marsh accretion rate matches the rate of SLR, representing the long-term effects of a dependence on elevation/flooding frequency (e.g. Morris et al., 2002). The model does not resolve the profile shape of marsh boundary because its location is representative of the net effects of erosion and progradation including small and large events (such as mass wasting).

3.3 Methods

We develop a new version of this model - which we will call GEOMBEST++ (Geomorphic Model of Barrier, Estuarine, and Shoreface Translation + Marsh + Waves) - in which we 1) replace the formulation for bay bottom erosion with a more physically based approach and 2) incorporate erosion of the marsh edge by wind waves.

Bay bottom erosion in GEOMBEST+ is depth dependent, decreasing with depth until reaching zero at the equilibrium depth (Equation 1). Because the equilibrium depth of a bay is dynamic in natural systems, varying with the size of the waves and the amount of fine-grained sediment input (Fagherazzi et al., 2007), we replace the previous formulation with a more physically based one driven by shear stress. In GEOMBEST++, we calculate wave height and wave period using the relationships between wave height and energy developed by Young and Verhagen (1996) and then use the orbital velocity (u_b; based on linear wave theory) - a function of bay depth, fetch, and wind speed - to calculate the shear stress (τ) according to

$$\tau = \frac{1}{2} f_w \rho u_b^2 \qquad (2)$$

(Dean and Dalrymple, 1992), where ϱ is water density and f_w is a friction factor equal to 0.03. (We experimented with different values of f_w, but changing this value did not affect the results significantly so for simplicity we chose a reasonable constant value for a smooth bed (Wikramanayake and Madsen, 1991).) Gross bay bottom erosion (E_B;

replacing Equation 1) is then related to the difference between shear stress and the critical shear stress τ_c through

$$E_B = a(\tau - \tau_c) \quad (3)$$

where a is a constant equal to 4.12 x 10^{-4} kg/(m^2 s Pa) (Mariotti and Fagherazzi, 2010) and τ_c is 0.2 Pa (consistent with values used in Mariotti and Fagherazzi (2013) and Fagherazzi and Wiberg (2009)). For simplicity and to enhance the clarity of insight, we assume an equant basin and do not consider anisotropic wind. Instead, we use the cross-shore bay width as the fetch. (If there was a predominant wind direction, the two sides of the marsh/bay could experience different amounts of erosion, which would introduce a translation of the bay (which we do not investigate in this work) as well as a change in size. As in GEOMBEST+, the gross sediment deposition rate (A_B) within the bay (representing riverine and/or net coastal sediment input) is obtained by distributing the net import of sediment to the bay (Q_B) over the width of the bay. The gross bay-bottom erosion rate (E_B, Equation 3) depends on sediment characteristics (through τ_c) as well as on wave characteristics and depth (through τ). Net erosion or deposition is determined by the difference between A_B and E_B. Because E_B decreases with depth, bay depth tends to converge to a steady state value in which deposition balances erosion plus RSLR (Fagherazzi et al., 2007). For greater depths, deposition outpaces erosion ($A_B > E_B$ and net deposition occurs), and the depth shallows toward the equilibrium (and vice versa). We use this dynamic formulation to calculate equilibrium depth (at which E_B + RSLR rate =

A_B) in the model. The time to reach this equilibrium sets the timestep for the back-barrier component of the model, meaning that the bay adjusts to equilibrium instantaneously in the model (i.e. we do not resolve smaller timescales). This treatment represents the results of previous modeling showing that the timescale for approaching equilibrium depth is very small compared to the timescale for changes in bay width (Mariotti and Fagherazzi, 2013).

We calculate wave edge erosion (E_m) using the wave power (W) following the methods of Mariotti and Fagherazzi (2013) and Marani et al. (2011)

$$W = \frac{\rho g}{16} H^2 c_g \quad (4)$$

$$E_m = \frac{W k_e}{h} \quad (5)$$

where wave height (H) is again calculated from Young and Verhagen (1996), c_g is the group velocity (assumed equal to $\sqrt{gd}$ for shallow water waves), h is the height from the bay bottom to the surface of the marsh platform, and k_e is an erodibility coefficient for the marsh edge equal to 0.14 $m^3y^{-1}W^{-1}$. Altering the value of k_e would alter the rate at which sediment is mobilized from marsh erosion for the same wave power, which would tend to alter the rate at which the back-barrier evolves in the model. This value is within the range of values for k_e calculated by Mariotti and Fagherazzi (2013).

We represent four stratigraphic units in the model: an underlying stratigraphy (75% sand), bay facies (100% fine-grained sediment), marsh facies (50% organic material,

50% fine-grained sediment), and barrier island facies (100% sand) (Figure 3.2C). We distinguish sand and fine-grained sediment on the basis of grain size and settling velocity, and represent cohesion not through sediment properties but by treating erosion as dependent on bed shear stress (see Equation 3 above). Across the entire model domain we use a cell size of 50 m (cross-shore width) by 0.1 m (height).

The algorithm for distributing sediment in the back-barrier in GEOMBEST++ is much the same as in GEOMBEST+, but with the addition of wave edge erosion it is modified to: (1) sea level rises; (2) barrier island sand is moved into the back-barrier through overwash; (3) Q_B is distributed evenly across the bay; (4) bay bottom erosion occurs according to Equations 2 and 3; (5) wave power is calculated from Equation 4 and wave edge erosion occurs according to Equation 5; and (6) fine-grained sediment eroded from the bay bottom and the marsh edge is combined and used first to build the marsh platform up to mean high water level and then preferentially deposited on the edges of the bay (resulting in net progradation of the marsh edge if deposition outpaces erosion) (Mariotti and Fagherazzi, 2010). As in GEOMBEST+: the landward and back-barrier sides of the bay each receive half of the total available fine-grained sediment distributed in stage (6); between mean sea level and mean high water half the sediment used to build the marsh comes from the creation of organic material; and the profile shape of the marsh boundary is not resolved. Stages (3) through (6) operate on the faster back-barrier sub-timestep (determined by the length of time required to reach the equilibrium depth),

and so iterate multiple times in one model timestep. Because coarser grain sizes are unlikely to travel far in natural bays (in the absence of high tidal current velocities, not considered here), if sand is eroded from the edge of the marsh in step (5), it is redeposited on the bay bottom in the same location it was eroded from before sediment is redistributed in step (6). Organic material eroded as part of the marsh unit is lost from the system, representing decomposition and/or dispersal.

We consider only one tidal range, though we acknowledge that previous research has shown that marshes with higher tidal ranges experience less bottom erosion from wind waves (D'Alpaos et al, 2012) and are generally more stable and more resilient to RSLR (e.g. D'Alpaos et al, 2012; Kirwan and Guntenspergen, 2010; D'Alpaos et al., 2011). The tidal range could affect the rates of marsh erosion (by affecting the proportion of the marsh platform sediment column that contains organic matter), but this is beyond the scope of this study. All fine-grained sediment, from both marsh and bay stratigraphic units, is conserved in the back-barrier - i.e. we do not consider sediment export to the ocean. We discuss this important simplification in Section 5.1.

Our model runs span a range of fine-grained sediment input rates, RSLR rates, and overwash volume fluxes across the parameter space defined by Walters et al. (2014) (Figure 3.3). Walters et al. (2014) demonstrated that marsh width increases with Q_B and decreases with RSLR rate, and that both dependencies can be expressed through the ratio of basin accretion rate (BAR; i.e. the accretion rate that results when Q_B is spread

across the initial width of the basin) to RSLR rate (BAR/RSLRR). Thus, we examine the effects of varying BAR rather than varying the Q_B and RSLR rate individually. When the BAR/RSLRR ratio is 1 the fine-grained sediment input is sufficient for the basin to accrete at a rate equal to the rate at which space is created by RSLR. Thus, a high BAR/RSLRR value (>1) means that sediment input is high compared to the rate of space creation, and a low value (<1) means that space is being created faster than fine-grained sediment input can fill it. We considered five BAR/RSLRR values evenly spaced on a log scale between 0.1 and 10. Overwash flux volume (Q_{OW}) ranges from 0.2-2 m^2/yr in increments of 0.6. For each BAR/RSLRR and overwash volume flux combination we ran model simulations with an initially full basin (an 1800 m wide basin filled with marsh) and an initially narrow marsh (about 500 m wide on both sides of the 1800 m wide basin), resulting in a total of 40 simulations. These initial marsh widths are the same as in Walters et al. (2014), however, in our experiments bay depths are greater because the new dynamic bay bottom erosion calculation results in a deeper equilibrium depth for the bay than the previous formulation (Figure 3.2; see the Discussion for potential impacts of this change on our findings relative to those of Walters et al. (2014)). Following Mariotti and Fagherazzi (2013) we use a wind speed of 8 m/s for all simulations, because average wind events make the greatest contribution to marsh edge erosion (Leonardi et al., 2016). We run the model for 100 years with no RSLR and the necessary Q_B and Q_{OW} inputs to establish the initial condition of a full basin or narrow

marsh. This also ensures the bay has reached the appropriate equilibrium depth for the marsh width. To ensure that the barrier moves over the same section of underlying substrate in each simulation (and thereby to control for the effect of substrate slope on simulation outcome) model simulations then run for 1 m of total RSLR, regardless of the RSLR rate. Thus, simulations run for 120-1000 model years (not including spin-up), with longer runs corresponding to slower RSLR rates.

Although marshes form on both the back-barrier and landward sides of the basin, we measure only the width of the back-barrier attached marsh (from the dune limit to the landward marsh edge, see Figure 3.2C), because the width of this marsh is directly influenced by Q_{ow} and the migration rate of the barrier. Therefore, when discussing a marsh width in reference to the model, unless otherwise noted we are always referring to the back-barrier (barrier-attached) marsh. We use the same categories of marsh widths defined by Walters et al. (2014) to classify our results; full basins (> ~800 m), narrow marshes (150-400 m), and empty basins (<150 m).

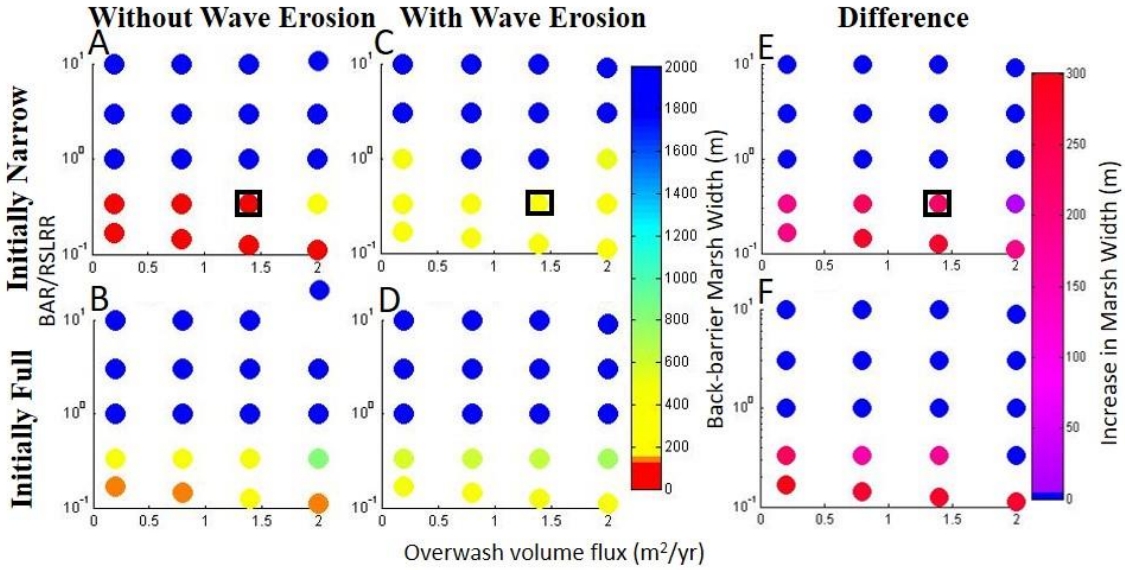

Figure 3.3: Phase diagram showing the distribution of back-barrier marsh widths after 1 m of total RSLR for a selection of initially A) narrow marshes and B) full basins from the experiments of Walters et al. (2014)) (without wave edge erosion using GEOMBEST+) and the same initially C) narrow marshes and D) full basins using GEOMBEST++ (including wave edge erosion). E) and F) show the increase in marsh widths between A and C (initially narrow marshes) and B and D (initially full basins), respectively. Black boxes in A and C correspond to the images in Figure 3.2B and 2D, respectively.

3.4 Results

Overall, the addition of wave edge erosion to GEOMBEST+ results in back-barrier marshes that are on average wider after 1 m of total RSLR than when wave edge erosion is not included (Figure 3.3E,F).Without wave edge erosion, for both initial conditions (initially narrow marshes and initially full basins), final marsh widths fall into all three categories (full basins (> ~800 m), narrow marshes (150-400 m), and empty basins (<150 m), (Walters et al., 2014)) (Figure 3.3A, B) after 1 m of RSLR (Walters et al., 2014). With the inclusion of wave edge erosion, for the initial condition of a full basin,

narrow marshes remain as wide as 700 m after 1 m of RSLR (Figure 3.3D). Initially narrow marshes fall into the range of 150-450 m wide after 1 m of RLSR (Figure 3.3C). For both initial cases, final marsh widths are approximately 200m wider on average than they are when wave edge erosion is not accounted for (Figure 3.3D,E), and narrow marshes survive under a wider range of conditions in the presence of wave edge erosion. In addition, none of the runs reach the empty basin state, and narrow marshes exist at lower Q_{ow} values and lower BAR/RLSR rates when the effects of wave edge erosion are included. After an additional m of RSLR, the results are qualitatively the same as those of Walters et al. (2014): whereas 18 of our 40 model runs yield narrow marshes after 1 m of RSLR, all but 5 simulations have converged from the narrow marsh state to the full or empty basin state after 2 m of total RSLR (Figure 3.4A).

The new formulation for equilibrium depth of the bay is sensitive to wind speed. However, the choice of wind speed (and therefore the equilibrium depth of the bay) does not affect the final outcome of our model experiments; rather it changes the timescale (Figure 3.4B). For higher wind speeds (and deeper bays) marshes erode more slowly, but the choice of wind speed does not determine whether the marsh is filling the basin or eroding away. We discuss this counter-intuitive model behavior below.

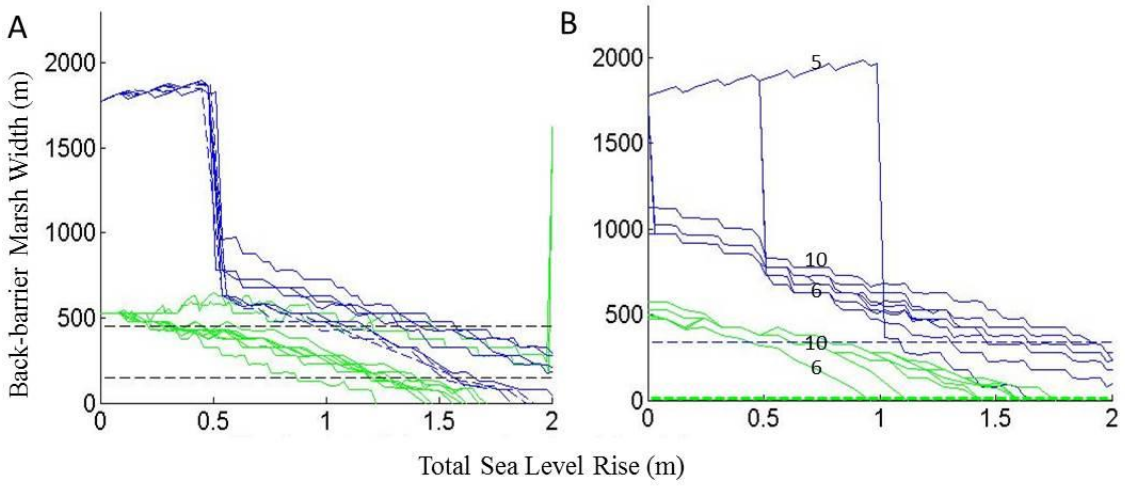

Figure 3.4: A) Evolution of marsh widths over 2m of total RSLR (we run the model for a total amount of sea level rise rather than a set length of time). Initially full basins are in blue and initially narrow marshes are in green. The dashed lines represent the range of marsh widths defined in Walters et al. (2014) as narrow (150-450 m). The apparent sudden increase in marsh width for the initially narrow marshes that fill the basin occurs when the narrower back-barrier marsh merges with the wider mainland-attached marsh, and the width of contiguous marsh behind the barrier suddenly increases to the combined width. B) Sensitivity to wind speed. Evolution of marsh width for an initially full basin (blue; overwash volume flux = 0.2 m2/yr, BAR/RSLRR ≈ 0.3) and an initially narrow marsh (green; overwash volume flux = 1.4 m2/yr, BAR/RSLRR = 0.125) for wind speeds ranging from 5 – 10 m/s. The lines for 6 and 10 m/s are labeled. The dashed lines of corresponding color represent the marsh width for the same input conditions after 1 m of total RSLR from the results from Walters et al. (2014) (i.e. without wave edge erosion and therefore without any dependence on wind speed). After 1 m of RSLR slight changes in the landscape slope change the basin area, resulting in the shift from a full to narrow basin for the 5 m/s wind speed at 1 m of total sea level rise.

3.5 Discussion

3.5.1 Geometry and conservation of mass constraints

Understanding these results requires consideration of the roles that geometry and conservation of mass play in determining the rate at which a marsh erodes laterally. RSLR rate and basin width determine the rate at which accommodation space is created

in a basin, whereas sediment inputs (e.g. fine-grained contributions (here Q_B), production of organic material, and overwash delivery (Q_{OW})) determine the rate at which space is filled. The balance between these factors then determines whether a basin is emptying or filling with sediment. In the model, as in nature, this can occur through 1) changes in bay depth, 2) changes in the elevation of the surface of the marsh relative to sea level and/or 3) changes in the location of the marsh edge (i.e. through progradation or lateral erosion).

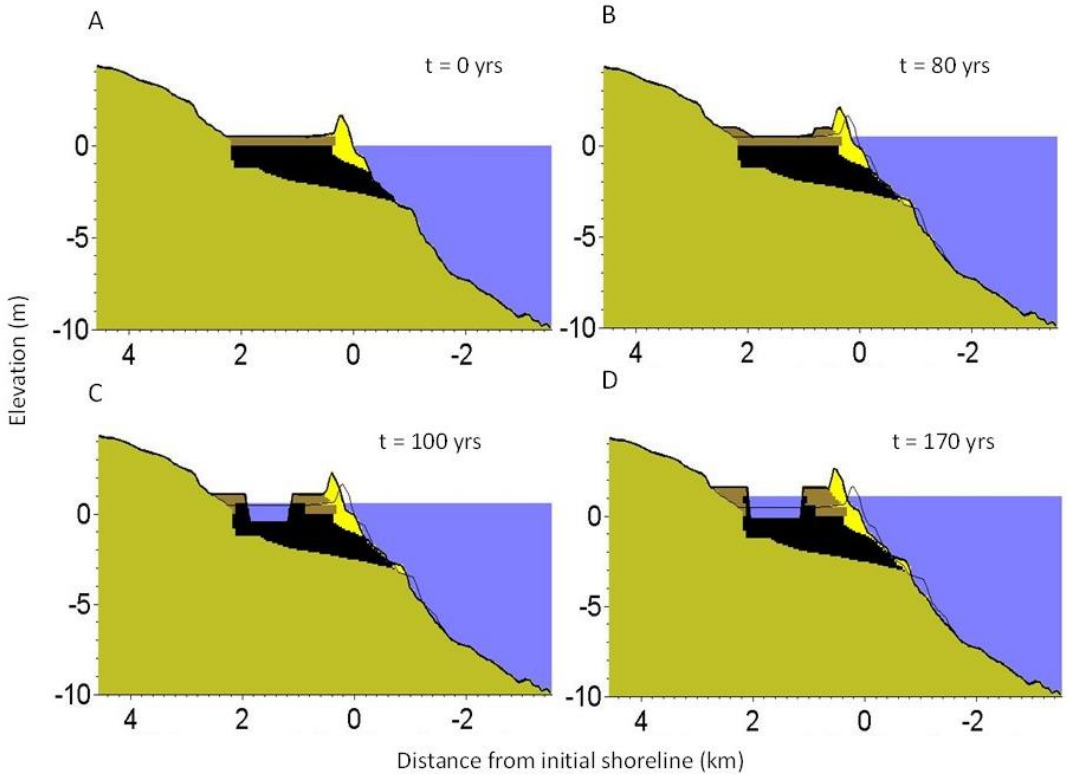

Figure 3.5: Evolution of an initially full marsh over 1 m of total RSLR. A) Initial condition of a full marsh. B) The center of the marsh, farthest from the sediment sources, cannot maintain its elevation. C) The center of the marsh drowns, and as waves begin to form in the resulting bay it quickly deepens and widens, eroding the marsh edge. D) Final condition of a narrow marsh (~475 m wide) after 1 m of RSLR. The black outline on B, C, and D shows the initial landscape.

In our experiments, bay depth can change over time as it adjusts to the equilibrium depth determined by the width of the bay (which changes more slowly than depth) and the size of the resulting waves, sediment supply rate, and RSLR rate. This process is most apparent in the initially full basin case (see Figure 3.5 for an example). If Q_B is too low to allow the entire marsh to keep up with RSLR, the middle of the marsh

drowns. Recall that sediment eroded from the marsh and bay is deposited preferentially on the edges of the basin (after Mariotti and Fagherazzi (2010)); this, combined with the spatial dependence on Q_{OW}, makes the middle of the marsh the farthest from sediment sources. The drowning of the middle of the marsh creates a small, shallow bay and allows waves to form in the back-barrier. (The tendency of the Young and Verhagen (1996) wave model to overestimate bed shear stress values for shallow depths may affect the timescale for the bay to become deep enough for bay bottom erosion to commence, and then for the depth to approach equilibrium. However, erosion would inevitably begin as the marsh continued to drown, and because we assume that the timescale for depth adjustments is very fast compared to the timescale for adjustments in marsh width, we do not expect the results to depend on which wave model we use.) These waves result in further marsh loss through marsh edge erosion which increases the bay fetch, resulting in increased wave heights and a deeper bay (Figure 3.5B, C). Thus, in this initially full basin case, the basin is emptying of sediment through all three types of adjustment: changes in bay depth, erosion of the marsh edge, and erosion of the marsh surface (i.e. drowning).

These considerations of geometry and conservation of mass provide an insight into why marshes in the initially full-basin cases are wider after 1 m of RSLR than those of Walters et al. (2014) (Figure 3.2). As the marsh drowns in the center of the basin and a bay forms, sediment is eroded from the bay bottom and deposited on the edges of the

marsh. The equilibrium depth in our formulation depends dynamically on the strength of the waves (which depends on the width of the basin and the wind speed), and is deeper than the equilibrium depth chosen by Walters et al. (2014). Because the bay erodes to a deeper depth and sediment is conserved, more sediment is moved to the marsh edge resulting in a wider marsh.

While this behavior may seem counterintuitive, we can understand it by considering the relationship between marsh width and wind speed in the model (Figure 3.4B). Recall that although changing the wind speed (and therefore the equilibrium depth) does not change the final outcome of a model experiment, it does change the timescale. Higher wind speeds lead to deeper equilibrium depths and taller marsh edges, which produce more sediment per increment of lateral erosion. Therefore, if the balance between sediment supply and rate of RSLR remains the same, to create space at the same rate, the marsh edge must erode more slowly for a higher wind speed (i.e. a taller marsh). This is consistent with suggestions that the volumetric marsh erosion rate, rather than the lateral erosion rate, is proportional to wave power (e.g. Marani et al., 2011; McLoughlin et al., 2015). (We discuss the relevance of this result to natural marshes in section 4.3.) The model runs of Walters et al. (2014), with their shallower equilibrium depth, could be equated to having a lower wind speed. In fact, the lowest wind speeds we tested produce results most similar to those of Walters et al. (2014) at 1 m of RSLR (see the dotted lines in Figure 3.4B).

Turning to the case of the initially narrow marsh, the change in bay depth over the course of a model run is small (Figure 3.2C,D), and the amount of fine-grained sediment made available from erosion of the bay bottom is negligible compared to the amount made available by edge erosion. This is because the increase in bay fetch, and therefore in wave height, is not as large as that of the initially full basin, and so the equilibrium depth does not change significantly from the initial equilibrium condition. Erosion of the marsh edge leads to an increase in sediment available for deposition on the marsh surface, preventing drowning as sediment is redistributed from the bay bottom and marsh edges to the marsh surface (e.g. Mariotti and Carr, 2014). Because edge erosion prevents marsh drowning, we can infer that both the marsh platform and the bay bottom are keeping up with RSLR (e.g. Marani et al., 2007; Marani et al., 2010).

Given the considerations of geometry and mass conservation discussed above, if both the marsh platform and bay bottom keep up with RSLR, then the third type of adjustment, marsh edge progradation or erosion, is the only way the basin can fill with or empty of sediment. In this case, because the balance between the rate of space creation and the rate of sediment input (potentially including riverine input, exchange through inlets, and overwash) controls whether the marsh edge erodes or progrades, we can actually make predictions about what is happening to the marsh edge without representing the mechanisms of marsh progradation and erosion. For example, if the rate of sediment input is not sufficient to balance the rate of space creation then the

amount of open water in the basin must be increasing (i.e. the basin must be emptying of sediment), and thus, if both the marsh surface and bay bottom are keeping up with RSLR, the marsh edge must be eroding laterally. In addition, the rate of lateral erosion can be predicted by the difference between the rate of sediment input and the rate of space creation. In other words, if w is the width of one side of the marsh (Figure 3.6), then

$$2\frac{dw}{dt}(d_b - d_m) = Q_{s,in} - RL \quad (6)$$

where d_b and d_m are the depths of the bay and marsh relative to mean high water level, R is the RSLR rate, and L is the cross-shore width of the basin. RL is the rate of space creation, and $Q_{s,in}$ is the net volumetric sediment input rate. In our model formulation, $Q_{s,in}$ consists of

$$Q_{s,in} = Q_B + Q_{OW} + Q_{OM} - Q_d \quad (7)$$

where Q_{OM} is the contribution of organic matter to the accretion of the marsh platform, and Q_d is the organic matter lost to decomposition or dispersal as the waves remobilize sediment on the marsh edge. When $Q_{s,in}$ is greater than RL (rate of sediment input is greater than rate of space creation) the marsh will prograde, and vice-versa.

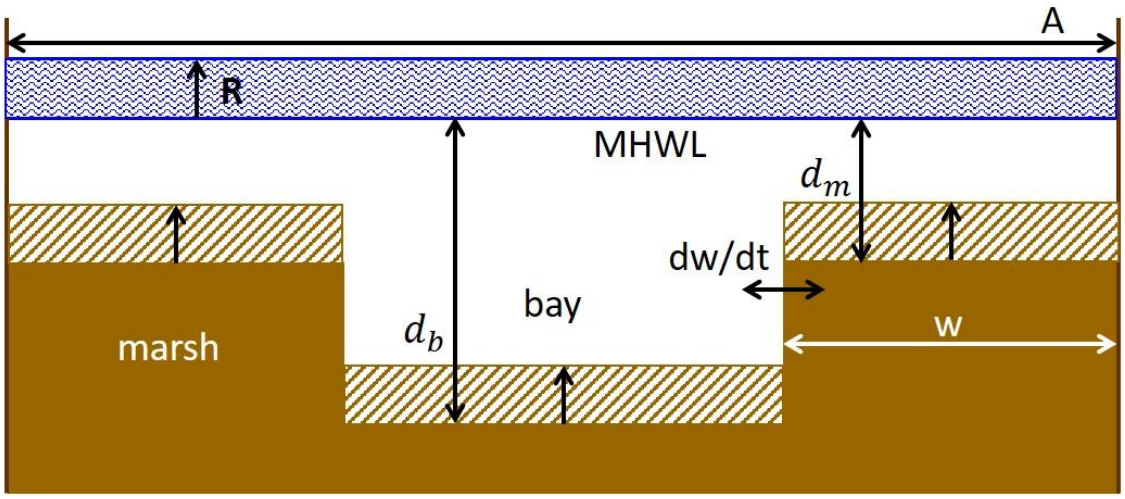

Figure 3.6: Schematic of a case where the marsh and bay are keeping up with sea level and so the only way the basin can empty and fill with sediment is by moving the location of the marsh boundary. A is the area of the basin, R is the amount of RSLR, d_b is the depth of the bay, d_m is the depth of the marsh, w is the marsh width, and dw/dt is the rate of change of the marsh width. The blue stippled area represents the space created by RSLR during a unit of time, and the brown hatched area represents the space filled by vertical accretion of the marsh and bay-bottom surfaces. If the volumetric rate of net sediment input equals the rate space is being created by RSLR, w cannot change. However, if the rate of sediment input is greater than (less than) the rate space is being created, the marsh boundary must prograde (erode).

3.5.2 Stratigraphy and composition constraints

Although the difference in equilibrium depth between our formulation and that of Walters et al. (2014) provides extra sediment to the marsh in the initially full basin case, in the case of the initially narrow marsh, the bay is already at its equilibrium depth and the initial marsh is the same width as in Walters et al. (2014) (see Figure 3.2A, C for a comparison of the initial conditions in our formulation and that of Walters et al. (2014)). Given that sediment provided from net bay bottom erosion is negligible in this case, the change in the formulation of the equilibrium depth cannot fully explain the

increase in marsh width. So why are initially narrow marshes still wider after 1 m of total RSLR than they were without wave edge erosion? One part of the answer is that taller marsh edges need to erode more slowly (they yield more sediment per unit of lateral erosion) to satisfy the constraints of geometry and conservation of mass, as discussed above. A second part of the answer involves stratigraphy and sediment compositions; the marsh edge is a more efficient sediment source than the marsh surface.

Without wave edge erosion, sediment redistributed to the marsh platform comes only from vertical erosion of the bay bottom or other, drowned parts of the marsh surface. However, with wave edge erosion, it also comes from lateral erosion of the marsh edge. A portion of the sediment volume eroded from the marsh (50% in our experiments) is not conserved, representing organic matter which would be lost to decomposition or dispersal. Therefore, vertical erosion of the drowned marsh surface yields proportionally less fine-grained sediment than lateral erosion of the marsh edge, which includes both marsh and underlying bay sediment (e.g. Figure 3.7). Because edge erosion liberates more inorganic, fine-grained sediment per total volume of sediment eroded relative to vertical erosion of the marsh surface, less of the marsh platform needs to be eroded to provide an adequate fine-grained sediment supply to maintain elevation in the remaining marsh. This mechanism for moving sediment to the top of a marsh platform temporarily prevents narrow marshes from drowning, allowing marshes to

keep up with RSLR under lower BAR/RSLRR conditions (higher rates of RSLR and/or lower sediment inputs) than they otherwise would. This behavior, and the fact that the narrow marshes remaining after 1 m of RSLR have largely disappeared after 2 m of RSLR (Figure 3.4A), agrees with previous findings (i.e. Mariotti and Carr, 2014) that edge erosion temporarily increases marsh resilience, but that under sufficiently high RSLR rates or sufficiently low sediment supply rates marshes will eventually drown.

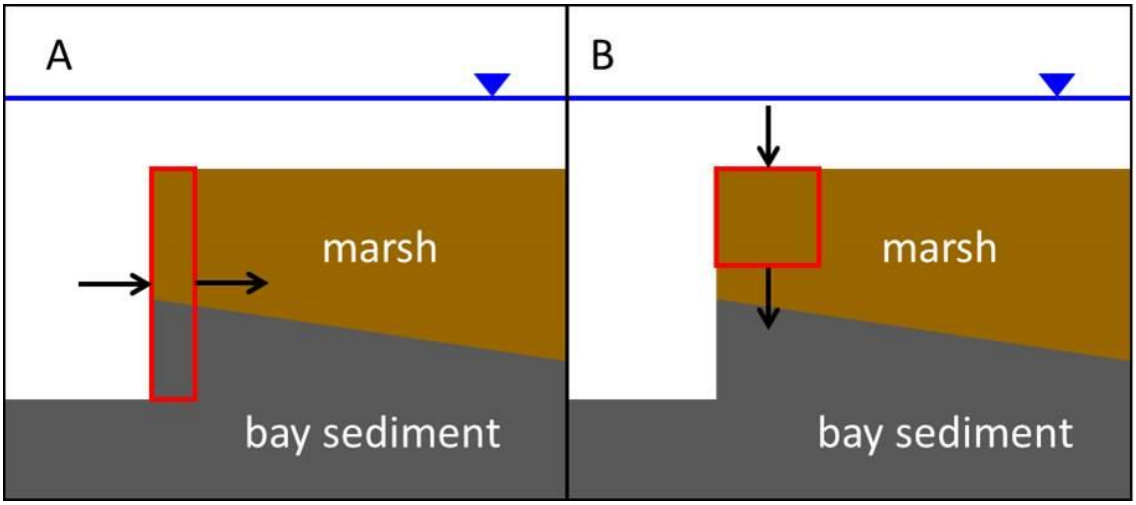

Figure 3.7: Difference in efficiency as a sediment source between lateral erosion and vertical erosion of the marsh platform. A) Lateral erosion of a certain volume of the marsh platform erodes both marsh (50% organic material and 50% fine-grained sediment) and bay sediment (100% fine-grained sediment). B) Vertical erosion of the same volume of sediment erodes only marsh sediment, resulting in only half the amount of fine-grained sediment being remobilized as through lateral erosion.

3.5.3 Limitations

Some of our results seem counterintuitive, especially those arising from the constraints of geometry and conservation of mass. The results depend on assumptions represented in the model parameterizations. How relevant to natural marshes the results

are depends on the realism of those model assumptions. One key assumption is that an equilibrium depth is established rapidly compared to the timescales for horizontal marsh change. This assumption, consistent with and widely employed in previous modeling investigations (e.g. Mariotti and Fagherazzi 2013; Walters et al., 2014), is supported by observations of bimodal elevation distributions in well-studied marsh systems (e.g. the Mississippi delta (Wilson and Allison, 2008), Venice lagoon (Fagherazzi et al., 2006; Carniello et al., 2009), and Virginia Coast Reserve) where bed erosion primarily depends on wave characteristics.

In the model, when bay bottom and marsh are both keeping up with RSLR, elevations are typically restricted to the levels of those two features. In natural marshes, elevations are less cleanly divided into the two modes. For example, in some basins where a marsh edge is eroding, a portion of the previous marsh platform remains at an intermediate elevation between that of the marsh and the tidal flat, without being eroded immediately to the level of a tidal flat (e.g. Wilson and Allison, 2008). However, this intermediate elevation zone can be a transient feature, so that the shape of the boundary of the marsh translates marshward in an approximately steady state without affecting the sediment budget. (In the model, we do not resolve the shape of the marsh boundary, implicitly assuming that the zones of intermediate depth are smaller than our cell size, 50 m consistent with Wilson and Allison (2008). In this case, the height of the retreating profile – the elevation difference between tidal flat and marsh – is the only

quantity relevant to the mass balance.) In the case of a transient zone of intermediate depth along a moving marsh boundary, model results can be related to natural environments despite the strong model tendency towards bimodality of elevations. In some basins, however, the assumption of bimodal depths is not a good approximation. For example, bays with a large influence from tidal currents (e.g., the Scheldt estuary (Wang and Temmerman, 2013)) exhibit a range of bay depths rather than one equilibrium tidal-flat depth. For a given basin, the less applicable our model assumption of wave-driven equilibrium bay depths is, the less relevant our model results will be.

In some natural circumstances, bay depth could vary not only spatially, but temporally – again limiting the relevance of the assumption of a well-defined equilibrium depth. For example, consider a basin subjected to a highly variable wind regime, and in which fine sediment is conserved in the back-barrier environment. During high-wind events, the bed may be eroded to a relatively deep depth. However, if the marshes are already at an equilibrium elevation influenced by the sediment concentrations during the high wind events, the sediment will ultimately be redeposited on the bay bottom. The result of intermittently strong winds and sediment conservation could be a bay in which the depth is typically small, but with a significant thickness of poorly consolidated mud. In such a circumstance, present for example in some areas of the NC Outer Banks, the relationship between wind speed and marsh edge erosion would likely be very different than in the model results (Figure 3.4B).

In this model, as in other models (e.g. Mariotti and Fagherazzi, 2013; Mariotti and Carr, 2014), we neglect temporal variations in wind speed for simplicity. A constant wind speed implies a single, constant equilibrium depth. In this case, stronger wind corresponds to a deeper equilibrium depth (and therefore taller marshes). For a given difference between space creation rate (RSLR times the basin area) and net sediment input rate, taller marsh edges tend to create more space per increment of erosion, and therefore to erode more slowly (given the constraints of geometry and conservation of mass). Therefore, in the model results, higher wind speeds lead to more slowly eroding marsh edges. However, these results are not likely to be relevant for natural basins in which bay depth fluctuates with wind speed. In such a natural circumstance, the intermittent high wind events would be eroding marsh edges that are short (relative to a basin where wind speeds are consistently high), at least early in the event, and marsh progradation during the calm periods would be accentuated by the more-typical shallow bay depths. For this reason we do not take the counterintuitive relationship between higher wind speed and wider marshes (Figure 3.4B) as a literal prediction about what to expect in natural basins.

A last key model assumption involves sediment import and export. In GEOMBEST++ and previous iterations, sediment import is specified as a forcing variable. This treatment differs from some other studies such as Mariotti and Fagherazzi (2013), in which net sediment import/export was related to the difference between the

concentration of sediment in the bay and in the ocean. This latter approach best represents a system with limited riverine input and significant inlet exchange (such as the Virginia Barrier Islands; Figure 3.1A), whereas the approach in GEOMBEST++ is more representative of a system with riverine input and little sediment exchange with the ocean (such as the North Carolina Outer Banks, where inlets are spaced far apart (e.g. Jalowska et al., 2015; Figure 3.1B); recall, however, that we do not seek to represent any specific location with our model experiments). We explored a variable sediment export rate in GEOMBEST++ by conducting model experiments in which a fixed percentage of sediment remobilized by waves is lost from the system, representing sediment loss via exchange with the coastal ocean. Such a loss can be expected to result in an exponential loss of marsh width, as bay widening leads to increases in wave power and thus increases in the amount of sediment eroded and the amount of sediment lost. In our experiments the treatment of the underlying stratigraphy of the basin dominates and prevents this from occurring, and we do not present these model experiments.

3.5.4 Implications

Neither of the approaches discussed above for representing net sediment import/export rates is appropriate for all situations, and the limitations of both approaches demonstrate the need for a new kind of marsh model, which allows suspended sediment concentrations and sediment exchange to evolve dynamically, accounting for sediment input from rivers as well as variable sediment exchange with

the ocean, which depends on the concentration of sediment in the basin. At the limit in which tidal prism (tidal range) is small and river water discharge is relatively large, the sediment concentrations in the basin at the end of the flood tide would be dominated by the concentration in the river, and (assuming the concentration during ebb tide is in equilibrium with the waves and is lower than the river sediment concentration) river sediment would be deposited mostly in the basin with little lost offshore. This scenario is closer to that represented in GEOMBEST++. On the other hand, if river water discharge is small relative to tidal prism, the effective concentration imported to the basin would be dominated by the concentration in coastal waters (as net sediment import/export would depend on the difference between the concentration produced by waves and that in the coastal ocean) as in Mariotti and Fagherazzi (2013), and Mariotti and Carr (2014).

However, we believe that the insights arising from considering geometry and conservation of mass remain important when sediment exchange with the coastal ocean is considered. In that case, knowing the net rate of sediment input depends on the sediment concentration in both the bay and in the ocean, and sediment concentration in the bay depends on the rate of marsh edge erosion. Still, in both cases, if the net rate of sediment input, the rate of space creation at a snapshot in time, and the height of the marsh edge are known, the rate of erosion or progradation of the marsh edge can be predicted (assuming that the bay bottom and marsh surface are keeping up with sea

level). With collection of the appropriate data, this model prediction is testable. The rate of space creation could be determined by the basin area and SLR rate. The rate of net sediment import or export could be determined with river discharge, tidal prism, and sediment concentration (in the river, surrounding ocean, and in the bay during ebb tide). Then, given data verifying that the bay bottom and marsh surfaces were keeping up with sea level, you could predict the rate of marsh edge erosion or progradation (using the elevation difference between the marsh and the bay bottom) and compare it with historical data.

One of the main implications of the GEOMBEST++ model experiments, consistent with Mariotti and Carr (2014), is that marsh edge erosion tends to slow marsh loss. This result should be relevant to all natural basins prone to drowning. However, in basins for which sediment exchange with the open ocean is important, an opposing tendency comes into play: marsh edge erosion tends to increase sediment concentrations during ebb tide, decreasing the net sediment input rate, making bays expand laterally faster than they would if sediment exchange with the ocean were negligible. In such basins, if marshes are not threatened with drowning, marsh edge erosion could increase marsh loss (as intuitively expected). In basins for which sediment exchange with the open ocean is negligible, this opposing tendency does not come into play, and edge erosion will consistently tend to increase marsh resilience.

These competing tendencies could also have implications for the management of natural marshes. For example, stabilizing marsh shorelines by installing rip-rap or 'living shorelines', which prevent marsh edge erosion (without affecting marsh inundation), may have unintended consequences, depending on the conditions of the basin. For basins in which marshes are not threatened in the near future with drowning, and sediment exchange with the open ocean dominates the sediment budget, marsh edge stabilization will likely have the desired effect of increasing marsh resilience. However, if marshes are imminently threatened with drowning, marsh edge stabilization may lead to marsh loss (relative to what would happen in the absence of stabilization). These implications suggest that factors affecting marsh drowning (local RSLR rate, sediment concentration, and vegetation type) should be accounted for when marsh protection is considered. This exploratory research points to the need to better understand back-barrier processes to provide reliable bases for management decisions and suggests a strategy that is customized for basin type and characteristics may be more effective than a one-size-fits-all management approach.

The newly recognized distinction between erosion of marsh edges and marsh surfaces, in terms of their efficiency in producing sediment useful for maintaining remaining marshes, (and which is the case regardless of the boundary conditions for sediment input/output), demonstrates the importance of considering the effects of stratigraphy and compositional differences in the evolution of back-barrier marsh

systems. The differences in inorganic sediment liberation rate resulting from the erosion of marsh edges versus marsh surfaces can shift the balance between the rate of space creation and space filling, potentially influencing marsh resilience by affecting how much marsh can be maintained or how rapidly it is lost.

Deaton et al. (2016) show that under some circumstances the sediment input and basin geometry do not allow a back-barrier marsh to prograde as quickly as the associated barrier island is migrating, ultimately resulting in loss of the back-barrier marsh due to burial of the marsh by the island. However, given the interdependencies between barrier islands and back-barrier marshes, increased resilience for back-barrier marshes, even if only temporary, has important implications for barrier islands. As long as a back-barrier marsh continues to exist, it will reduce the accommodation space that the associated barrier needs to fill – decreasing the likelihood that the barrier-marsh system will disintegrate. In turn, survival of barrier islands affects how long back-barrier marshes, supported by localized overwash deposition from the sandy part of barriers, will ultimately persist (Walters et al., 2014). Our modeling result that these overwash-sustained narrow marshes persist in the presence of wave edge erosion, combined with existing observational evidence (a statistically significant peak in distribution of satellite observations of marsh widths in the Virginia Barrier Islands for narrow marshes of ~400 m (Walters et al., 2014; Walters and Moore, 2016)), strengthens the conclusion of Walters et al. (2014) that overwash can temporarily support marshes under conditions with

lower sediment availability and higher RSLR rates than would otherwise be possible. Thus, lateral erosion of marsh edges, through its effect on the sediment input/output balance and sediment redistribution, can influence the overall evolution of the coupled marsh-barrier island system.

3.6 Conclusions

Overwash from barrier islands provides an important sediment source for back-barrier marshes, sustaining them under SLR rate or sediment supply conditions under which they would otherwise drown. This important relationship between marshes and barrier islands and the existence of a resulting long-lasting narrow back-barrier marsh state, proposed by Walters et al. (2014), persists even in the presence of marsh edge erosion by wind waves. However, it is a temporary state; even in a closed system such as our model, without sediment loss to the ocean, the narrow marsh is transient and the basin tends towards the stable states of completely full or completely empty of marsh, similar to the results of Mariotti and Fagherazzi (2013). Our results also suggest that wave edge erosion may enhance marsh resilience not only by providing a mechanism to move sediment from the marsh edge to the marsh surface and prevent drowning (e.g. Mariotti and Carr, 2014), but also, dependent on the stratigraphic composition of the marsh, by providing a more efficient sediment source than vertical erosion of drowned marsh platform. Older marsh sediments eroded from the lower part of the marsh scarp may have a higher concentration of inorganic sediment which can be redeposited on the

marsh, while newer surface layers may have a higher proportion of organic material which may be lost to decomposition or dispersal when eroded. Combined, these results emphasize the first-order control that geometry and stratigraphy can have on the evolution of marsh-barrier systems. Where a marsh and bay both maintain equilibrium elevations relative to sea level, and the net sediment budget is known, the behavior of the marsh edge (the rate of erosion or accretion) can be predicted based on basin geometry and the rates of sea-level rise (space creation) and sediment supply. If the rate of sediment import or export is known, for instance at a snapshot in time, this control on marsh evolution applies regardless of basin conditions or model assumptions about sediment exchange with the ocean (i.e. to both open and closed systems).

3.7 Acknowledgements

We thank Andrea D'Alpaos, anonymous reviewers, and the editors for insightful and helpful comments that lead to improvements in the manuscript. This work was supported by the Virginia Coast Reserve Long-Term Ecological Research Program (National Science Foundation DEB-123773) via a sub-award to the University of North Carolina at Chapel Hill. GEOMBEST++ can be downloaded from the online Community Surface Dynamics Modeling System model repository. Many of the model output animations are available on YouTube as part of an educational activity available through the Scientific Research and Education Network (Theuerkauf and Ridge, 2014).

4. Comparing the Cohesive Effects of Mud and Vegetation on Delta Evolution

Rebecca Lauzon, Dr. A. Brad Murray

4.1 Introduction

Deltas are home to half a billion people worldwide (Syvitski et al., 2009), and countless others depend on them for their food or livelihood, making it important to understand the processes which govern their evolution. Muddy, cohesive sediment can have a significant influence on delta morphology and the dynamics of delta channel networks. Compared to deltas built of non-cohesive sediment, mud leads to increased stability of bars and channel banks, deepened and elongated channels, increased shoreline rugosity and decreased channel mobility (Edmonds and Slingerland, 2009; Hoyal and Sheets, 2009; Liang et al., 2015a; Caldwell and Edmonds, 2014; Straub et al., 2015). Vegetation also introduces cohesive effects, and has been hypothesized to play a similar role in delta evolution (Edmonds and Slingerland, 2009; Straub et al., 2015; Hoyal and Sheets, 2009).

In rivers, vegetation can stabilize channels and prevent braiding (Gran and Paola, 2001; Murray and Paola, 2003; Tal et al., 2004; Tal and Paola, 2010). Braiding is sustained by lateral transport of sediment (i.e. from channel banks into channel beds), and the introduction of cohesion from sediment (Murray and Paola, 1997) or vegetation (Gran and Paola, 2001; Murray and Paola, 2003; Tal et al., 2004; Tal and Paola, 2010)

stabilizes channel banks and favors a single channel over braiding. In wetland as well as river environments, vegetation concentrates flow into channels by decreasing velocities within vegetation patches (Temmerman et al., 2005; 2007), decreases bank erosion (including lateral transport) by introducing cohesion from stabilization by roots (Gran and Paola 2001; Tal et al., 2004; Millar, 2000; Schwarz et al., 2013; Ameen et al., 2017), and introduces friction and roughness and therefore flow resistance (e.g. Solari et al., 2015; Vargas-Luna et al., 2015; Nepf, 2012a,b). These effects could have a significant influence on the morphology and evolution of deltas and their channel networks.

However, investigations of the direct effects of vegetation on river deltas are limited (Nardin and Edmonds, 2014; Nardin et al., 2016, Lorenzo-Trueba et al., 2012; Rosen and Xu, 2013). It has been inferred that the effects of vegetation are similar to the effects of delivering cohesive sediment to a delta (Edmonds and Slingerland, 2009; Straub et al., 2015; Hoyal and Sheets, 2009), without specifically exploring the cohesive effects introduced by vegetation. While vegetation likely does, as hypothesized, introduce many of the same cohesive effects as mud, it is also possible that the cohesion introduced to deltaic systems by mud and by vegetation differs in important ways.

Vegetation can only shape the delta if conditions are favorable for it to establish. These conditions include elevations at or near sea level. Sediment delivery rates and sediment composition influence the rates at which potential habitat is created, with the sand fraction playing a significant role in initial land building (Kim, 2012). Even once

land has been established, high flow velocities or high sediment discharges can result in sediment transport processes, and associated erosion or accretion, acting on very fast timescales (Orton and Reading, 1993; Hoyal and Sheets, 2009). If the timescales for erosion or deposition are shorter than the timescale for vegetation growth, vegetation will not strongly influence delta morphology or dynamics (e.g. Murray and Paola, 2003; Pasquale et al., 2013; Perona et al., 2012).

To directly assess similarities or differences in cohesion introduced by vegetation or by cohesive sediment, over the time and space scales of the evolution of deltas and channel networks, we use the model of delta formation DeltaRCM (Liang et al., 2015a). This cellular, rule-based model provides a platform for representations of vegetation dynamics and vegetation effects on physical processes that are simplified to enhance the clarity of potential insights (Murray, 2003; Paola and Leeder, 2011) about which processes and interactions might be most important in this context. We adapt DeltaRCM to include two key effects of vegetation: 1) stabilizing channel banks and 2) increasing flow resistance. We then directly investigate the morphology and behavior of deltas and deltaic channel networks with and without the influence of vegetation and cohesive sediment, in order to compare and contrast the cohesive effects they introduce.

4.2 Model Description and Vegetation Rules

DeltaRCM's model algorithm consists of a rule-based flow routing scheme and a set of sediment transport rules. In each time step, water and sediment "parcels" enter

the domain through a fixed inlet channel and are routed by a weighted random walk. Weights are determined by the average downstream direction (inertia), the water surface gradient (gravity), and a depth dependent resistance to flow. The proportion of sediment parcels which are sand (f_{sand}) can be specified; remaining parcels are mud and each has a different set of erosion and deposition rules. After the water parcels are routed, the depth-averaged flow field and then the water surface profile are updated, the sediment parcels are routed, and finally the bed elevations are updated. A more detailed description of the model can be found in Liang et al. (2015a), and an assessment of the hydrodynamics of the model can be found in Liang et al. (2015b). Model deltas have also been extensively compared to a number of observational, experimental, and numerical-model (Delft3D) datasets (Liang et al., 2016).

We incorporate a simplified representation of emergent vegetation such as marsh grasses into the model. The vegetation is characterized by a rooting depth (d_{root}), stem diameter (d_{stem}), growth rate (r), and carrying capacity (K). We do not consider the growth of individual plants, but rather a fractional cover of vegetation (representing biomass density) in each cell (f_{veg}). Vegetation is established at the end of each timestep in any cell where the water depth is less than 0.5 m and the magnitude of bed elevation change in that timestep was less than 1% of d_{root} (i.e. the bed is essentially not moving) at a fractional cover of 5%, and grows logistically up to the maximum density ($f_{veg} = 1$). We do not consider lateral propagation of vegetation, or growth of vegetation patches

within a model cell; vegetation establishes in a cell whenever model conditions become favorable—representing the assumption that the dispersion of seeds through the channel network would not limit growth over the timescales involved in delta evolution, and that new land would be colonized effectively as soon as it becomes suitable. Both erosion and deposition cause mortality within a cell (Pasquale et al., 2013; Perona et al., 2012): f_{veg} is reduced during a timestep by an amount equal to amount of bed elevation change divided by d_{root} (with a minimum f_{veg} value of 0). Thus, we assume that there will always be a small number of small or weak plants which can easily be uprooted or buried. We do not consider organic sediment production as we are interested specifically in the cohesive effects of vegetation.

As the model assumes bankfull flow conditions (Liang et al., 2015a), we incorporate a flood length and flood frequency. Mortality occurs at the end of each timestep, and growth occurs after every n^{th} timestep where n = the number of timesteps equal to the flood length. We use a flood length of 3 days and a flood frequency of 100 days, giving about 10 days of bankfull flow per year (Caldwell and Edmonds, 2014; Liang et al., 2016). Our formulation for mortality results in approximately the same net effect for many short floods as a few long floods, so the vegetation dynamics are not sensitive to the flood timescales if the flood duration/year is held constant. For simplicity, we do not consider seasonality of floods or of plant growth.

We explicitly represent two main effects of vegetation in the model: it 1) stabilizes channel banks, decreasing lateral transport of sediment and 2) increases resistance to flow by introducing friction. Lateral transport of sediment (q_{s_lat}) is a function of local lateral slope (S) and sand flux (q_{s_loc}) so that $q_{s\_lat} = \alpha S q_{s\_loc}$. As f_{veg} increases from 0 to 1, we decrease the lateral transport coefficient α linearly by 2 orders of magnitude (Murray and Paola, 2003).

Flow resistance (R_f), previously depth (h) dependent ($\frac{1}{R_f} = h^{\theta}$; where $\theta = 1$ for water and mud (assumed to follow the water parcels) and 2 for sand parcels (assumed to be transported lower in the water column and preferentially follow deeper flow paths); Liang et al., 2015a), now increases with f_{veg} to incorporate drag from vegetation. As traditional representations of flow resistance such as Manning's coefficient vary with depth in vegetated channels, we adapt a simplified version of a formulation for flow resistance in channels with emergent vegetation developed by James et al. (2004). Now, $\frac{1}{R_f} = \left(h\left(1 - \frac{a\pi d_{stem}^2 K(f_{veg} - b)}{4}\right)\right)^{\theta}$ if f_{veg} is greater than b, and remains the same for $f_{veg} < b$.

The values of a and b are set so that flow obstruction begins at a low stem density and is maximized at a high stem density ($0 << f_{veg} < 1$) but still allows some flow to enter vegetated cells (informed by the experiments of Zong and Nepf, 2010). Though we do not explicitly represent the effect of vegetation trapping to enhance the deposition of

cohesive sediment (Stumpf, 1983), increasing flow resistance will result in a decrease in velocities (e.g. Lightbody and Nepf, 2006) and a reduction in the number of sand parcels entering vegetated cells which combined will indirectly capture this effect by increasing deposition (settling) of mud parcels in vegetated cells (Mudd et al., 2010).

We run a set of model experiments using f_{sand} = 10, 25, 50, and 75%, with and without vegetation. We establish 'base' vegetation parameters of d_{root} = 20 cm, d_{stem} = 6 mm, r = 1 yr^{-1}, and K = 800 stems/m^2 (in the range of those observed for or used to represent emergent marsh grasses; e.g. Widdows et al., 2008; Cranford et al., 1989; Nepf et al., 1997; Zong and Nepf, 2010). We examine the relative influence of each parameter, individually increasing and decreasing each parameter by an order of magnitude (r) or a factor of two (d_{stem}, d_{root}, K) for f_{sand} = 50%. Here we present averages of these 'strong' and 'weak' experiments, as results for each individual variable were of similar magnitude. We use the same model set-up as Liang et al. (2015a, 2016), with a grid size of 240 by 120 50 m^2 cells, constant water input of 1250 m^3/s, sediment input of 1.25 m^3/s, and a timestep of about 7 hours of bankfull flow. We run each experiment in triplicate for 5000 timesteps and present averaged (for calculations) or representative (for images and time series) results.

4.3 Delta Morphology

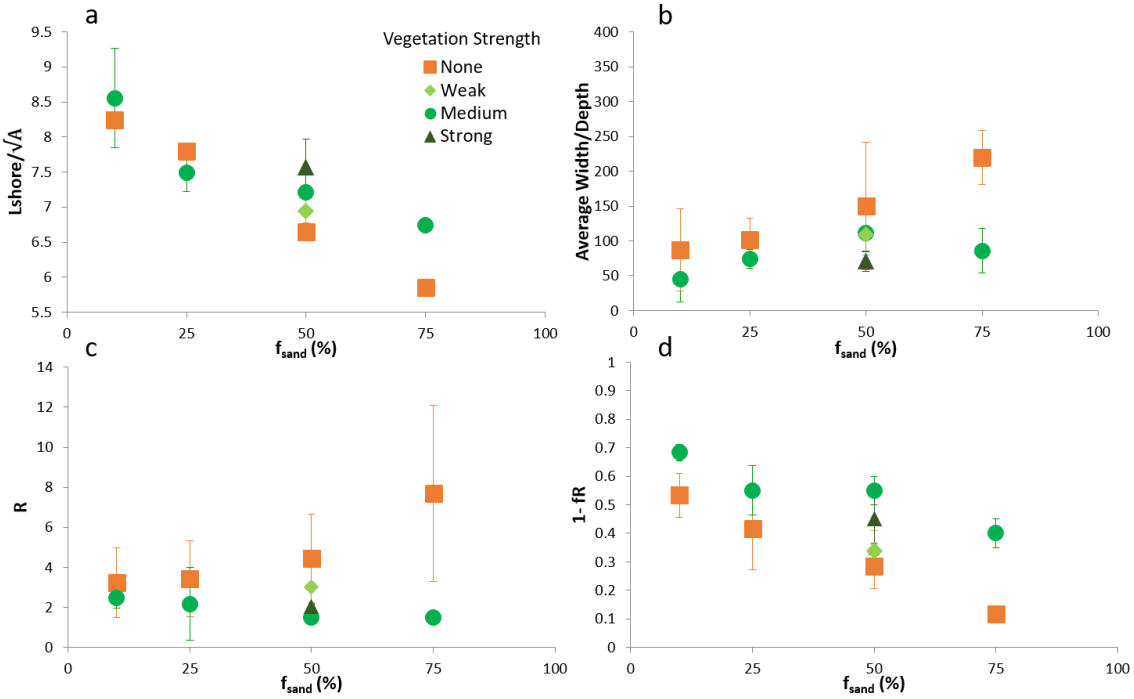

Figure 4.1: a) Shoreline roughness, measured as shoreline length divided by the square root of delta area, and averaged over the second half of each run. b) Average width to depth ratio for channels along the arc of a semi-circle with an area 2/3 that of the delta, measured at the last timestep. c) Decay constant obtained from fitting an exponential decay function to the remaining unreworked fluvial surface, using a varying time lag encompassing the second half of the model run. d) The fraction of the fluvial surface remaining at the final timestep which has not been reworked by the channel network during the second half of the model run. All data presented is averaged across triplicate runs; data for weak and strong vegetation is averaged across all runs.

Shoreline roughness, measured as the shoreline length divided by the square root of the delta area ($L_{shore}/\sqrt{A}$), increases with the percentage of the sediment delivered to the delta that is cohesive ($1 - f_{sand}$), and increases with the presence of vegetation (Figure 4.1a). We identify the shoreline using the opening-angle method (Shaw et al., 2008), with an opening angle of 75° and an elevation threshold of -0.5 m.

With sand-rich compositions, the addition of vegetation increases shoreline roughness by approximately the same amount as decreasing f_{sand} by 25%. The tendency for cohesive sediment to increase shoreline roughness has been previously described (e.g. Liang et al., 2015; Caldwell and Edmonds, 2014); cohesive sediment elongates and deepens channels, limiting deposition to particular sections of the shoreline and producing lobes that extend seaward (Edmonds and Slingerland, 2009). Vegetation roughens the shoreline through a similar mechanism; increasing bank stability and increasing roughness on channel banks confines flow into relatively deep channels, while the vegetation roughness on channel banks also enhances deposition (by decreasing velocities through added friction) of sediment from overbank flow, enhancing levee growth, deepening channels, and confining flow.

The increased stability of channel banks also decreases the average channel aspect ratios (width/depth, Figure 4.1b; calculated along the arc of a semi-circle with an area 2/3 that of the delta). There is a decreasing trend in width-to-depth ratio with cohesive sediment ($1 - f_{sand}$) and with the presence of vegetation. This is consistent with the role cohesive sediment and vegetation play in the transition between braided flow and single channel or anastomosing patterns (Gran and Paola, 2001; Tal et al., 2010), and has also been observed in experimental deltas with cohesive sediments (Hoyal and Sheets, 2009).

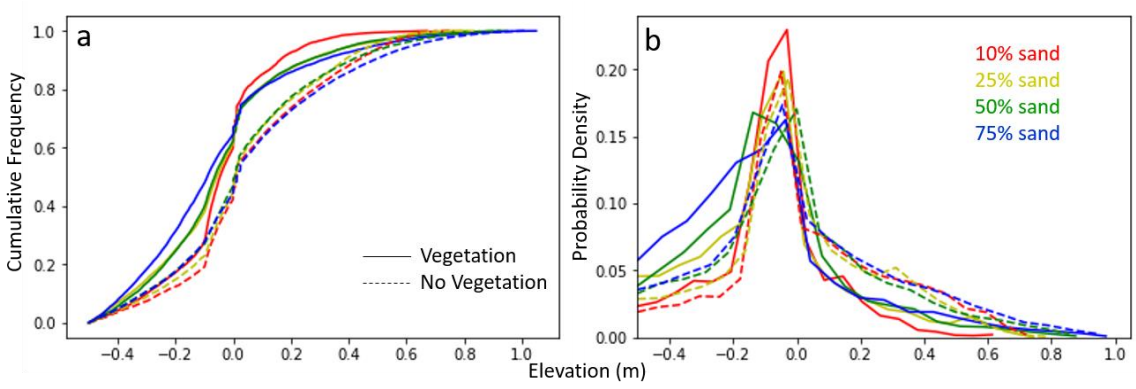

Figure 4.2: a) Cumulative frequency and b) probability density of subaerial (> -0.5 m) delta elevations for the last timestep of representative model runs for 25, 50, and 75% sand with and without vegetation. Data for the 10% sand runs are plotted for t = 3960 (with vegetation) and t = 4670 (without), as all model runs with such high cohesive sediment inputs reach the model domain boundary before the end of the run.

Confining flow into channels (as opposed to more evenly distributed across the delta through sheet flow) results in lower average elevations on the 'subaerial' delta surface (defined as elevations above which vegetation can grow; > -0.5 m) than when vegetation is not present (Figure 4.2). The shift in elevation distributions occurs for all sediment inputs, though it is largest for sandier deltas. We do not observe this effect for cohesive sediment on its own; increased resistance to flow from vegetation on channel banks reduces the likelihood of overbank flow and limits deposition on delta islands. Nardin and Edmonds (2014) observed a similar effect; roughness from vegetation on channel banks caused flow to preferentially remain in channels, resulting in vegetation reducing deposition of fine sediments. This effect could have implications for sediment retention on the delta (Nardin et al., 2016; Straub et al., 2015), or could be balanced out

by alternate mechanisms for sediment redistribution not represented in our study, such as tides, which can have a significant effect on deltaic water and sediment fluxes (e.g. Sendrowski and Passalacqua, 2017; Hiatt and Passalacqua 2014; Leonardi et al., 2015; Hanegan and Georgiou, 2014).

We also observe better sorted delta stratigraphy when vegetation is present. Vertically averaging the fraction of sand deposited in each cell reveals that on sandy deltas with vegetation, channel beds are composed almost entirely of sand (Figure 4.3d). This level of heterogeneity is not found in the channels of sandy deltas with no vegetation (Figure 4.3b), or with the addition of vegetation to a muddy delta (Figure 4.3a, c). Given the tendency of strong levees and roughness on channel banks to confine flow in channels, overbank flow is inhibited. However, in the limited overbank flow that does occur, mud parcels would be far more likely to leave the channel as sand parcels are more heavily weighted toward deeper flow paths, representing their tendency to be transported lower in the water column.

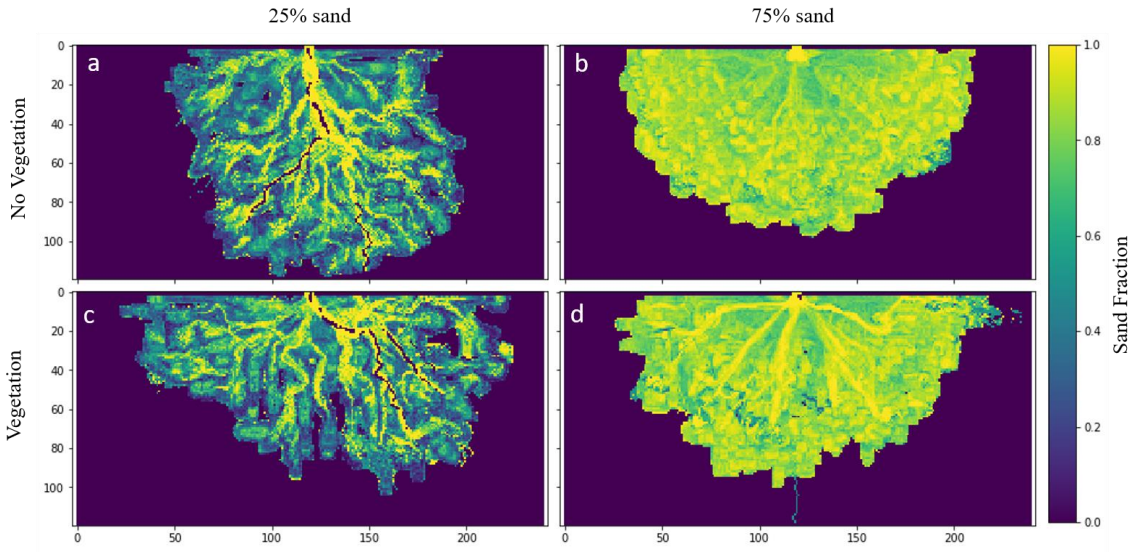

Figure 4.3: Vertically-averaged sand fractions at the end of a model run for representative deltas with a) 25% sand, no vegetation; b) 75% sand, no vegetation; c) 25% sand, vegetation; d) 75% sand, vegetation.

4.4 Channel dynamics

The effects of cohesion from sediment and vegetation on delta morphology also alter the timescales of change in the delta channel networks. Over the second half of a model run, we measure how the fraction of delta area that remains unchannelized decreases over time (after Wickert et al., 2013). Fitting an exponential decay function, we obtain a decay constant R which has been described as the rate dry pixels convert to wet pixels (Liang et al., 2016). R is significantly decreased by the presence of vegetation, while it otherwise increases with f_{sand} (Figure 4.1c). The stabilization of channel banks by vegetation significantly reduces channel migration, holding the channel network in place. While the effect of vegetation on delta morphology appears to be limited by f_{sand} - as seen by the variation in shoreline rugosity and width/depth values with f_{sand} (Figure

4.1a, b) - the value of R is consistent across f_{sand} values. This suggests that vegetation may have a larger effect on the timescales of channel dynamics than on morphology; the channel mobility of vegetated deltas is relatively constant regardless of the amount of cohesive sediment (Figure 4.1c).

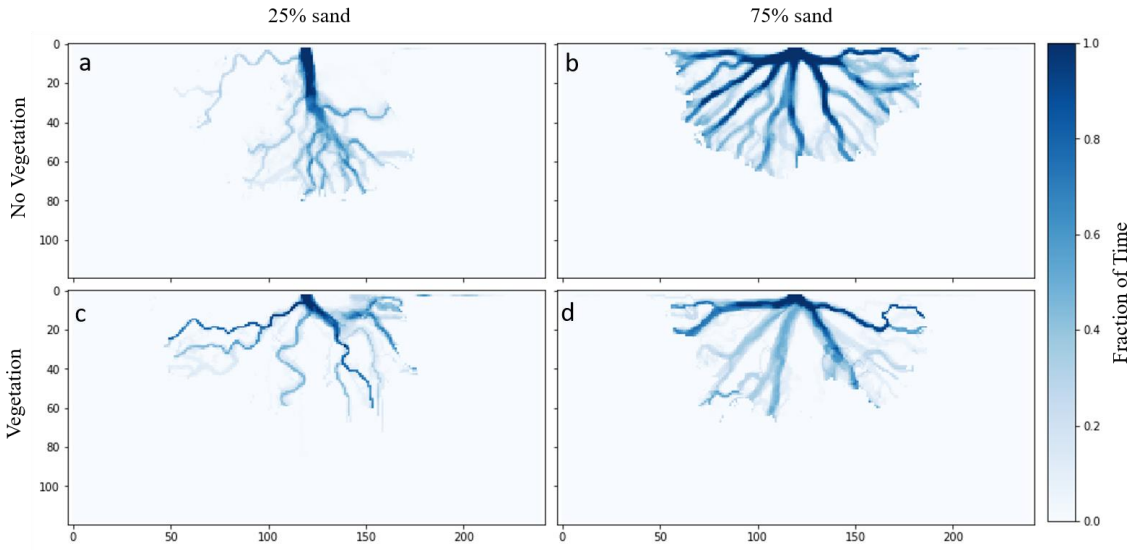

Figure 4.4: Plots of the fraction of time each channel cell spends as a channel during the second half of a run for representative runs with a) 25% sand, no vegetation; b) 75% sand, no vegetation; c) 25% sand, vegetation; d) 75% sand, vegetation.

We also calculated the fraction of time each cell spent as a channel for the second half of each run (Figure 4.4). To account for delta growth, we only considered cells which were within the delta area at the initial (halfway) point. This analysis reveals trends in the spatial and temporal distribution of flow on the delta which suggest differences in avulsion dynamics with the addition of vegetation. Sandy deltas with no vegetation (Figure 4.4b) have many wide channels which contain flow for much of a

model run, reflecting frequent channel switching between many active channels, and flow distributed relatively consistently through time across the delta. The addition of vegetation (Figure 4.4d) reduces the number of channels, and channels are less likely to consistently contain flow. This suggests that vegetation, like cohesive sediment, confines deposition to certain areas of the delta (therefore increasing shoreline roughness; Edmonds and Slingerland, 2009), causing the flow to avulse episodically to lower areas. This is supported by higher values for $1 - fR$, the fraction of the delta surface unreworked by the channel network at the end of a model run, with vegetation and with decreasing f_{sand} (Figure 4.1d). The addition of vegetation has a smaller effect on muddy deltas (Figure 4.4a,c), but does appear to further confine flow to the channel network, and to move avulsion nodes closer to the delta apex, resulting in a less even distribution of flow (and therefore deposition) across the delta.

4.5. Comparison of cohesive effects of vegetation and cohesive sediment

The effect of vegetation on many aspects of delta morphology and evolution in these experiments is similar to that of cohesive sediment; vegetation increases shoreline roughness, decreases channel width to depth ratios, decreases channel migration rates, and limits the spatial distribution of flow and deposition on the delta, which enhances avulsion dynamics. However, our results also highlight some differences; by introducing friction on levees in addition to stabilizing channel banks, further decreasing overbank flow, vegetation shifts the elevation distribution of the delta

surface to lower elevations. As the mechanisms for vegetation to influence delta morphology are similar to those of cohesive sediment, it is not surprising that the effect of adding vegetation is typically larger for sandy deltas than for muddy ones, which already have cohesive sediment. Vegetation, when present (for sandy deltas), tends to alter delta morphology in way that resembles the effects of adding about 25% more cohesive sediment (e.g. Figure 4.1).

We suggest that f_{sand} plays an important role in shaping delta morphology because of the role that sediment composition plays in building the delta subaqueously. As long as the delta remains below an elevation at which emergent vegetation can establish (about -0.5 m in our model), the evolution of the delta will be controlled by the sediment composition. Once the delta becomes subaerial, vegetation can begin to alter the dynamics of the delta, and while it is true that this influence can alter patterns of flow and sediment transport, therefore altering the delta morphology to some degree, the initial formation of new land and of channel networks is strongly controlled by f_{sand}. Take for example the distribution of the channel network (Figure 4.4); even with vegetation, the channel network is more evenly distributed across the delta and the delta is more fan-shaped in the case with 75% sand than with 25%.

This land-building dependence on composition explains why vegetation has a larger effect on the channel dynamics than the delta morphology. While f_{sand} plays a large role in shaping the delta, once vegetation establishes it can play an important role on the

evolution of the channel network through time. This dominant effect can be seen in the essentially constant R values for vegetated deltas across all f_{sand} values, and in the tendency for vegetation to increase avulsions on sandy deltas and to change the avulsion patterns on already cohesive deltas (i.e. to move the avulsion node and to result in more complete rather than partial and reversible avulsions; Tal et al., 2010).

4.6. Implications

The role that cohesive sediment plays in shaping deltas has been often studied recently (Edmonds and Slingerland, 2009; Hoyal and Sheets, 2009; Liang et al., 2015a; Caldwell and Edmonds, 2014; Straub et al., 2015). The results of the model experiments presented here suggest that vegetation can have effects on delta morphology that are comparable to or larger in magnitude than those of increasing the fraction of cohesive sediment. Both cohesive sediment and vegetation can alter delta morphology and channel dynamics in model results, but while sediment cohesion (or lack thereof) appears to be a first-order control on delta morphology, vegetation can have a stronger influence on channel dynamics and stratigraphy. This distinction in model results suggests that caution should be used when interpreting cohesive sediment as a proxy for vegetation in model experiments. The effect of vegetation on channel migration and avulsion styles and timescales, as well as the effect on enhancing sandy channel deposits, may not be captured by the addition of cohesive sediment alone.

Our results also highlight some areas for future work. The tendency of vegetation in our experiments to decrease delta elevations suggests that vegetation confines flow to channels, reducing sediment retention on the delta. However, as we did not explicitly represent sediment trapping, which would tend to increase sediment retention, the role of vegetation in deltaic sediment retention remains unclear (Straub et al., 2015) and should be the focus of future research. The tendency suggested by Nardin and Edmonds (2014) and in our study for vegetation to confine flow to channels has important implications for deltaic channel-island exchange, and for the distribution of sediments and nutrients across the delta (e.g. Hiatt and Passalacqua, 2014). Additionally, the ability of vegetation to exert a dominant influence over channel timescales depends on its ability to establish and grow on timescales faster than those bed elevation changes, which could be enhanced by external factors such as base level rise or high sediment inputs. The interactions between these timescales and those of vegetation growth should be explored. These timescales will also depend on the strength of the vegetation; while no single characteristic appears to have a significant effect on vegetation influence in the range of values tested, increasing vegetation strength by co-varying vegetation parameters may alter vegetation's influence on delta evolution.

The importance of vegetation in influencing cohesive delta behavior means that, in addition to the geology and hydrology of a delta basin, the climate affecting a delta plays an important role in delta evolution. When a basin produces predominantly non-

cohesive sediment, transitions in climate that inhibit or slow vegetation establishment and growth (e.g. toward more arid or cold climates) could cause a shift toward higher channel mobility, more uniform sediment delivery, and smoother shorelines (and vice versa). In addition, the way vegetation can affect stratigraphy in these experiments suggests that when interpreting stratigraphy laid down in delta environments, changes in climate directly affecting the delta, in addition to climate-related changes in base level and sediment delivery to the delta, should be considered.

4.7 Acknowledgements

Grants from the National Science Foundation, Geomorphology and Land-Use Dynamics Program (1324114 and 1530233) supported this work. We would like to thank Wonsuck Kim, Anastasia Piliouras, Katherine Ratliff, and Jim Heffernan for insightful conversations in the early stages of this work.

5. Vegetation influence on delta evolution and dynamics under varying environmental conditions

Rebecca Lauzon and Dr. A. Brad Murray

5.1 Introduction

The evolution of deltas and their distributary channel networks can be controlled by a number of factors, including the balance between river, wave, and tidal influences (e.g. Galloway, 1975; Nienhuis et al., 2015; Geleynse et al., 2011; Leonardi et al., 2015) water and sediment discharge (Powell et al., 2009; Hoyal and Sheets, 2009; Orton and Reading, 1993; Edmonds et al., 2010), fraction of cohesive sediment (Caldwell and Edmonds, 2014; Hoyal and Sheets, 2009; Straub et al., 2013; Edmonds and Slingerland, 2009, Liang et al., 2015a; Tejedor et al., 2016) or cohesion from vegetation (Chapter 4), base level rise (Jerolmack, 2009; Liang et al., 2016a; Martin et al., 2009), and many others. Recent research has focused on the role these factors play in shaping delta morphology and influencing autogenic timescales: the timescales at which deltas undergo cycles of channelization, channel extension and aggradation, avulsion and incision of a new channel (e.g. Hoyal and Sheets, 2009; van Dijk et al., 2009; Kim et al., 2006). Cohesion is thought to alter these timescales, decreasing channel mobility and avulsion frequency (Straub et al., 2015; Edmonds and Slingerland, 2009; Hoyal and Sheets, 2009; Caldwell and Edmonds, 2014; Liang et al., 2015a), favoring progradation even with high cross-levee slopes (Edmonds and Slingerland, 2009) and resulting in rugose shorelines.

Vegetation has many of the same cohesive-like effects as fine-grained sediment – elongating, deepening, and stabilizing channels and increasing shoreline rugosity – and may be even more effective at stabilizing channel networks, resulting in well-sorted sandy channel beds and potentially decreasing deltaic fine-grained sediment retention (Chapter 4; Nardin and Edmonds, 2014). However, while recent research has begun to assess the cohesive effects of fine sediment under varied environmental conditions (e.g. Martin et al., 2009, Liang et al., 2016a,b), vegetation may be sensitive to environmental conditions in ways that cohesive sediment may not be. The influences of SLR rate and water and sediment discharge are particularly important to understand, as SLR rate is predicted to continue to increase over the next century (e.g. Chen et al., 2017) and humans are increasingly modifying the distribution of water and sediment to the coast (e.g. Syvitski and Saito, 2007) which could have important implications for the evolution of natural deltas (e.g. Ericson et al., 2006; Anthony et al., 2014) and the success of engineered and restored deltas (e.g. Kim, 2012; Kim et al., 2009; Paola et al., 2011; Allison and Meselhe, 2010).

Sea level rise increases aggradation on the delta surface, often at the expense of progradation. This increased deposition increases channel mobility and can reduce autogenic timescales (Martin et al., 2009; Jerolmack, 2009; Liang et al., 2016a). Sediment distribution can be optimized by changes in avulsion patterns, from avulsions between local, intra-lobe tributaries to global avulsions and large scale branching as SLR rate

increases (Jerolmack, 2009), or by increased branching (Jerolmack, 2009; Liang et al., 2016a)

Increasing water discharge can increase the number of bifurcations in delta channel networks (Syvitski and Saito, 2007; Edmonds et al., 2010). Delta slope is also (inversely) correlated with discharge, and plays an important role in autogenic cycles (Powell et al., 2012). Increasing water discharge leads to a more organized channel system; channel mobility decreases and sediment transport capacity increases (Powell et al., 2012).

Similar to SLR, increased sediment discharge increases deposition rates, and can increase avulsion frequency and channel mobility as a result (e.g. Orton and Reading, 1993; Hoyal and Sheets, 2009; Bryant et al., 1995). Autogenic timescales generally decrease as sediment discharge increases relative to water discharge (Powell et al., 2012).

The tendencies for SLR and increased sediment discharge to increase deposition rates may have a significant effect on vegetation influence. Enhanced deposition may increase vegetation mortality, as plants are buried or uprooted (Pasquale et al., 2013; Perona et al., 2012), or make areas of the delta less suitable for vegetation colonization. If sediment transport processes act on timescales faster than those for vegetation growth, vegetation will likely not be able to influence delta morphology or dynamics (e.g. Murray and Paola, 2003; Pasquale et al., 2013; Perona et al., 2012).

We use the delta building model DeltaRCM (adapted to include key vegetation effects; Chapter 4) to investigate the effects of different environmental conditions (and therefore different climates) on vegetation's role in shaping delta evolution. We explore the effects of varying SLR rates and water and sediment discharges, and test the hypothesis that high SLR rates or sediment discharges will result in sediment transport processes that outpace the timescales of vegetation growth and establishment, therefore reducing the effects of vegetation.

5.2 Methods

5.2.1 Model Description

DeltaRCM consists of a rule-based flow routing scheme and a set of sediment transport rules governing the behavior of water and sediment 'parcels' which build a small, river-dominated delta. We have modified DeltaRCM to include the effects of vegetation to 1) reduce lateral transport of sediment and 2) increase flow resistance. A brief description of the model and our modifications are below, and a more detailed description of the vegetation rules can be found in Chapter 4. A more detailed description and an assessment of the hydrodynamic component of DeltaRCM can be found in Liang et al. (2015a,b). Model deltas have also been extensively compared to a number of observational, experimental, and numerical-model (Delft3D) datasets (Liang et al., 2016a).

Each model run begins with a 5 m deep basin with an inlet channel of fixed width and depth on one side. In each time step, water and sediment "parcels" enter the domain through the inlet channel and are routed by a weighted random walk. Weights are determined by the average downstream direction (inertia), the water surface gradient (gravity), and a depth dependent resistance to flow. The proportion of sediment parcels which are sand (f_{sand}) can be specified; remaining parcels are mud and each has a different set of erosion and deposition rules. After the water parcels are routed, the depth-averaged flow field and then the water surface profile are updated, the sediment parcels are routed, and finally the bed elevations are updated. The model timestep, *dt*, is set so that a characteristic sediment volume, related to the volume of the inlet channel, enters the domain in each time step. Optimizing computational efficiency and model stability, this volume was determined by Liang et al. (2015a) to be:

$$dt = \frac{0.1 N_0^2 V_o}{Q_s} \quad (1)$$

where V_0 is the volume of one cell of the inlet channel, N_0 is the number of cells in the inlet, and Q_s is the input sediment discharge.

We incorporate two main effects of vegetation (represented as a fractional cover of each cell and representing emergent vegetation such as marsh grasses) into the model: 1) stabilizing channel banks, reducing lateral transport and 2) introducing friction which increases resistance to flow. Lateral transport, otherwise dependent on local slope and sand flux, now also decreases as vegetation cover increases. Flow resistance, previously

depth dependent, now increases with vegetation density representing friction and drag introduced by the plants.

Vegetation can establish in any cell near sea level (elevation > -0.5 m) with bed elevation change over the previous timestep less than 1% of the rooting depth of the vegetation. Fractional cover increases logistically during interflood periods, occurring every n^{th} timestep where n is the number of timesteps in each flood. We set the flood length equal to 3 days and the interflood equal to 100 days, assuming about 10 days of bankfull flood per year. Mortality occurs during floods, and is proportional to the magnitude of erosion and deposition events relative to the rooting depth of the vegetation.

5.2.2 Experimental Set-up

We use a model grid of 120 by 240 50 m^2 cells, and a sediment composition of 50% sand, as Chapter 4 demonstrated that vegetation has a less significant effect on the delta morphology and channel dynamics of already cohesive deltas. We run two sets of experiments: one to explore the effects of SLR rate and one to explore the effects of varying sediment (Q_s) and water (Q_w) discharge. For both sets of experiments, parameters were selected to be in line with those previously used for DeltaRCM (Liang et al., 2015a; 2016a,b); to be varied enough to be expected to influence delta evolution (e.g. an increase in discharge of at least 60%; Edmonds et al., 2010); and to be reasonable

enough for inferences to be made to experimental and natural deltas (Syvitski and Saito, 2007). Details of experimental set-ups can be found in Table 5.1.

The SLR experiments are run with 5, 10, 25, and 50 mm/yr of SLR, and Q_w and Q_s equal to 1250 and 1.25 m^3/s, respectively. These experiments are run for 5000 timesteps (dt ≈ 7 hrs of bankfull flow; total run equivalent to about 150 years, assuming 10 days of bankfull flow per year) with the same strength vegetation as the 'base' case in Chapter 4.

The discharge experiments are run with Q_w values of 1000 and 2000 m^3/s and Q_s values of 0.5, 1, and 2 m^3/s, both with and without vegetation, resulting in 12 unique runs. As the timestep depends on Q_s and the inlet size (N_0; Equation 1), which varies with Q_w, the discharge experiments are run until the same total amount of sediment has entered the model domain, which occurs after fewer timesteps for higher Q_w (see Table 5.1). This amount is about 2/3 of the sediment added in the SLR experiments.

Table 5.1: Experimental setup. Experiments Q1-Q6 are run with and without vegetation.

	f_{sand} (%)	SLR rate (mm/yr)	Qw (m3/s)	Qs (m3/s)	N_0	# of timesteps	dt (hrs)	Time (years)
S5	50	5	1250	1.25	5	5000	≈ 7	≈ 150
S10	50	10	1250	1.25	5	5000	≈ 7	≈ 150
S25	50	25	1250	1.25	5	5000	≈ 7	≈ 150
S50	50	50	1250	1.25	5	5000	≈ 7	≈ 150
Q1	50	0	1000	0.5	4	5000	≈ 11	≈ 230
Q2	50	0	1000	1	4	5000	≈ 5.5	≈ 115
Q3	50	0	1000	2	4	5000	≈ 3	≈ 60
Q4	50	0	2000	0.5	8	1250	≈ 44	≈ 230
Q5	50	0	2000	1	8	1250	≈ 22	≈ 115
Q6	50	0	2000	2	8	1250	≈ 11	≈ 60

5.2.3 Data Analysis

We use a number of established metrics to interpret our model results. To capture the dynamics of the channel network over time we measure the decay in channel planform overlap (Wickert et al., 2013). Using channel maps (determined with a velocity threshold equal to the minimum velocity for sediment transport) for the second half of each run, we measure the overlap in the channel network using a varying time lag. To eliminate differences in the channel network due to delta growth, we consider only the channels within the delta area at the initial time (halfway through the run). We fit an exponential decay function to the channel planform overlap data to obtain a decay constant M. M is a measure of how quickly the spatial configuration of the channel network changes. A high value suggests little similarity in the configuration of the channel network through time, and would be a signature of frequent avulsions to new channels or frequent switching between existing channels. Using the same channel maps, we measure the decay in the fraction of the delta surface unreworked by the channel network to obtain a decay constant R, which approximates the rate dry cells are converted to wet cells. A high value suggests highly mobile channels, reflecting channel migration and/or avulsions to new (rather than previously occupied) channels.

By summing the channel maps analyzed above, we measure the fraction of time that each cell which is ever part of the channel network remains part of the channel network (Liang et al., 2016a). As a measure of channel persistence, we take the ratio of

cells which are channels for greater than 50% of the time over the number of cells which are channels for less than 50% of the time, P_c. A high value suggests a more stable channel network, i.e. the same channels are consistently occupied. These channel maps also allow us to qualitatively assess the spatial distribution of the channel network across the delta and the typical number of channels.

We quantitatively assess the spatial distribution of the channel network in two ways. First, by finding the minimum value of the exponential decay function used to obtain R; $1 - fR$ represents the fraction of the delta surface which remains untouched by the channel network at the end of a model run. Second, we determine channel centerlines (after Isikdogan et al., 2015) from binary channel maps (based on the same velocity threshold as those used to calculate M and R, but including the entire delta area) and use those to calculate total channel length, from which we obtain drainage density. We can obtain a temporal measure of the spatial distribution of flow through the channel network by considering variations in the maximum discharge. We calculate the maximum discharge value for the entire delta at each timestep and consider variations in maximum discharge over time. Large-scale avulsions result in a sharp increase in maximum discharge as flow is concentrated in the newly incising channel. Smaller avulsions do not cause these peaks in maximum discharge as flow remains distributed between multiple channels.

We complement these measures of channel dynamics with an analysis of sediment distribution across the delta. Shoreline roughness (equal to the shoreline length divided by the square root of the delta area; $L_{shore}/\sqrt{A}$; Wolinsky et al., 2010) provides a measure of the evenness of the distribution of sediment across the delta by the channel network, with more stable channel networks tending to build more irregular deltas. We consider time series of delta area throughout a model run to approximate progradation rate. To measure aggradation, we consider probability density functions of subaerial (> -0.5 m) delta elevations at the final timestep of each run. Finally, we measure the distribution of mud and sand across the delta by vertically averaging the stratigraphy to obtain a sand fraction for each cell of the model domain (Liang et al., 2016a).

5.3 Results and Discussion

5.4.1 Sea Level Rise

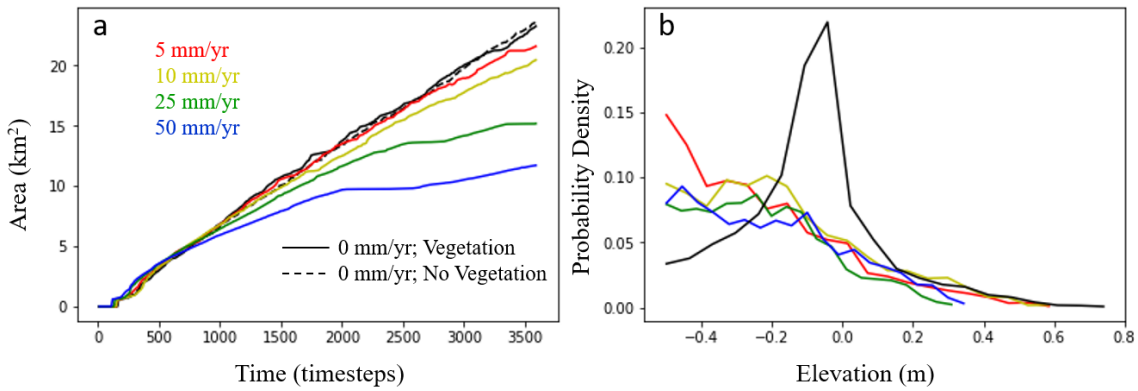

Figure 5.1: a) Delta area through time for no SLR with and without vegetation and for 5, 10, 25, and 50 mm/yr with vegetation. b) probability density function for

subaerial (> -0.5 m) elevations for 0, 5, 10, 25, and 50 mm/yr of SLR with vegetation. Elevations are relative to sea level at the end of the run.

As expected, we find that delta growth rates decrease with increasing SLR rate and that the delta keeps up with sea level (Figure 5.1) as sediment is used for aggradation instead of progradation (Martin et al., 2009; Jerolmack, 2009; Liang et al., 2016a). Increased aggradation requires a denser channel network and more persistent channels, to ensure that sediment is distributed evenly across the delta (Liang et al., 2016a). This is reflected by the maps of the channel network showing the fraction of time that channel cells remain part of the active channel network; at higher rates of SLR, the channel network is more densely distributed across the delta surface and more channel cells remain part of the channel network for all of the run (Figure 5.2). We quantify the distribution of the channel network with drainage density, which increases with increasing SLR rate (Figure 5.3a) and with $1 - fR$; the fraction of the delta surface unreworked by the channel network at the end of a model run decreases from more than 50% with no SLR to about 10% with high rates of SLR (Figure 5.3b). The increase in channel persistence is also quantitatively supported, as P_c increases with SLR rate (Figure 5.3c) from about 20% of channel cells remaining channels for more than half the run with no SLR to over 50% at 50 mm/yr.

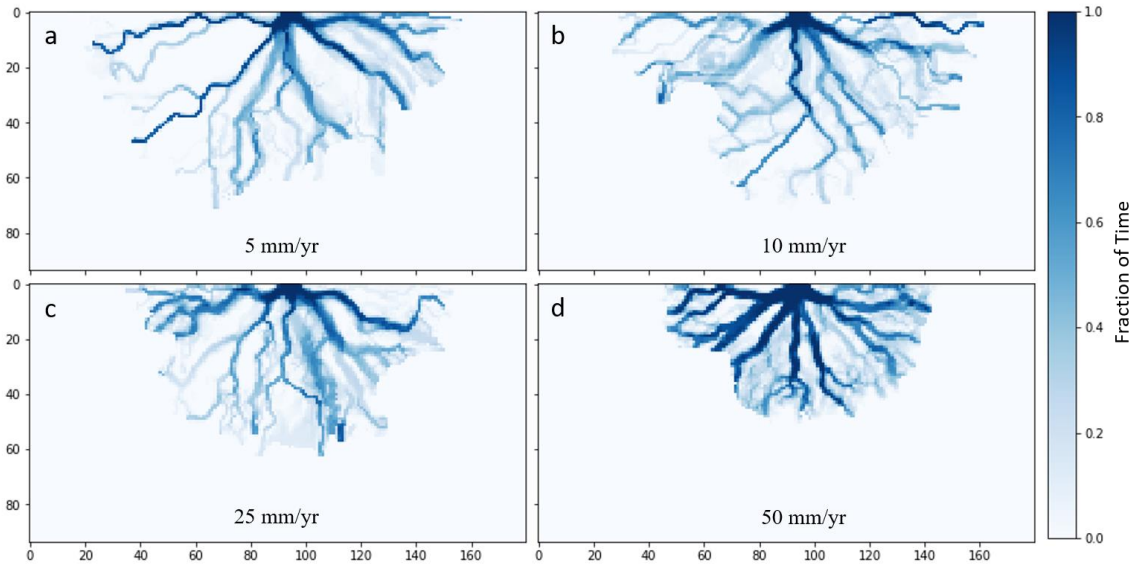

Figure 5.2: Maps of the fraction of time any cell which is part of the channel network during the second half of the run remains part of the channel network for a) 5 mm/yr, b) 10 mm/yr, c) 25 mm/yr, and d) 50 mm/yr of SLR. Cells with a value of zero are never channels, and cells with a value of 1 are always channels.

The even distribution of sediment across the delta surface by more persistent, evenly distributed channels is enhanced by an increase in the rate that channels rework the delta surface. As SLR rate increases, *R*, approximating the rate that previously untouched cells become part of the channel network, increases as well (Figure 5.3d). This reworking of the delta surface likely represents small-scale, partial avulsions (e.g. shifts in flow between bifurcations of a single channel), enhanced channel migration, and potential increases in overbank flow, all supplementing the distribution of sediment by the stable channel network (Figure 5.2d). Liang et al. (2016a) found a similar increase in local avulsions with increasing SLR rate for cohesive deltas without vegetation.

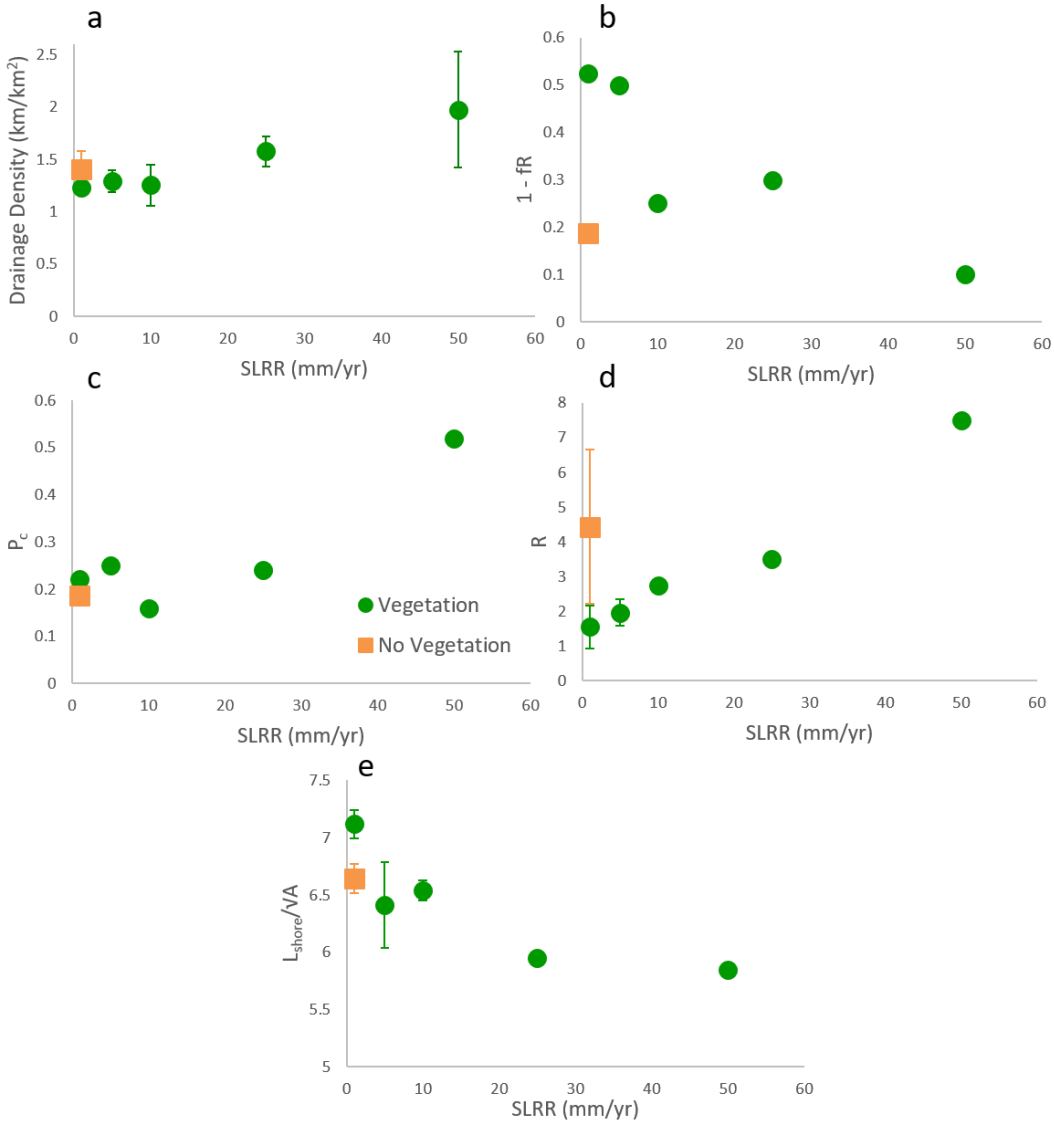

Figure 5.3: a) Drainage density, b) the fraction of the delta surface which has not been reworked by the channel network by the end of the model run (1- fR), c) P_c (the ratio of the number of channel cells which are channels for more than 50% of the time over less than 50% of the time), d) R (the rate of decay in remaining delta surface unreworked by the channel network), and e) shoreline roughness (measured as shoreline length divided by the square root of delta area) for unvegetated deltas with no SLR and vegetated deltas with 0-50 mm/yr of SLR.

These changes in channel dynamics, toward a more spread out, dynamic flow network, suggest a decrease in the effect of vegetation to reduce channel mobility with increasing SLR rate; *R* approaches that for a delta without vegetation or SLR at a SLR rate of 25 mm/yr (Figure 5.3d). The aggradation resulting from SLR would be expected to enhance vegetation mortality (which is directly related to erosional and depositional events) and therefore inhibit vegetation growth, decreasing its ability to strengthen channel banks and levees. Given that the model run encompasses about 150 years, and that the basin is 5 m deep, we could estimate a characteristic deposition rate for a delta with no SLR of about 30 mm/yr, and results from Chapter 4 show that at those timescales vegetation is able to grow fast enough to stabilize channel banks and reduce channel mobility. Assuming that the delta is maintaining elevation with respect to sea level, a SLR rate of 25 mm/yr would nearly double aggradation rates on the delta. The convergence of channel mobility for vegetated and unvegetated deltas at a SLR rate of 25 mm/yr suggests that this may be approximately the limit at which vegetation can stabilize channels; for faster timescales, sediment transport outpaces vegetation growth. This limit is also supported by the trends in $1 - fR$ and P_c; the channel network reworks more of the surface and becomes more persistent than an unvegetated delta with no SLR at SLR rates of about 25 mm/yr (Figure 5.3b, c).

As a result of the increasingly dense and evenly distributed channel network and the shift from global (i.e. entire channel(s)) to local avulsions, shoreline roughness tends

to decrease with increasing SLR rate (Figure 5.3d). Unlike the channel dynamics, which appear to still be strongly influenced by vegetation up to relatively high SLR rates, the tendency of vegetation to increase shoreline roughness is decreased by even small amounts of SLR. This supports the finding in Chapter 4 that delta morphology is more strongly controlled by sediment composition than by vegetation dynamics.

5.3.2 Sediment and Water Discharge

We also find that Q_w and Q_s influence channel dynamics on vegetated deltas (recall that there is no SLR in these experiments). For low values of Q_w, channel mobility (as measured by R, the decay in remaining unreworked fluvial surface) on vegetated deltas increases with Q_s (Figure 5.4a). This suggests that vegetation's ability to decrease channel mobility is, as expected, reduced by increased Q_s (e.g. Murray and Paola, 2003); for the highest Q_s value we tested, channel mobility is comparable on vegetated and unvegetated deltas. However, for high values of Q_w, channel mobility is not strongly influenced by Q_s; values of R converge for all values of Q_s. R values for vegetated runs converge for high Q_w at a lower value than unvegetated runs, reflecting the tendency for vegetation to keep flow in channels by stabilizing and introducing roughness on channel banks. This tendency to increase resistance to flow in vegetated areas likely makes avulsions to previously abandoned channels more likely than the incision of new channels through vegetated areas. For unvegetated runs, R values increase with

increasing Q_w; suggesting that increased Q_w enhances channel migration and increases avulsion frequency (converting dry cells on the delta surface to channels more quickly).

An increase in Q_w increases the number of channels (Figure 5.5) for both vegetated and unvegetated runs, as flow is distributed more evenly across the delta and increasingly through channels instead of overbank flow, reflecting the tendency for increased Q_w to increase channelization (Powell et al., 2012). This tendency is also reflected by an increase in drainage density with increasing Q_w (Figure 5.4b) For unvegetated runs, this results in a lower value of M, slower decay in channel planform overlap (Figure 5.4c), suggesting more similarity in the configuration of the channel network through time with higher Q_w.

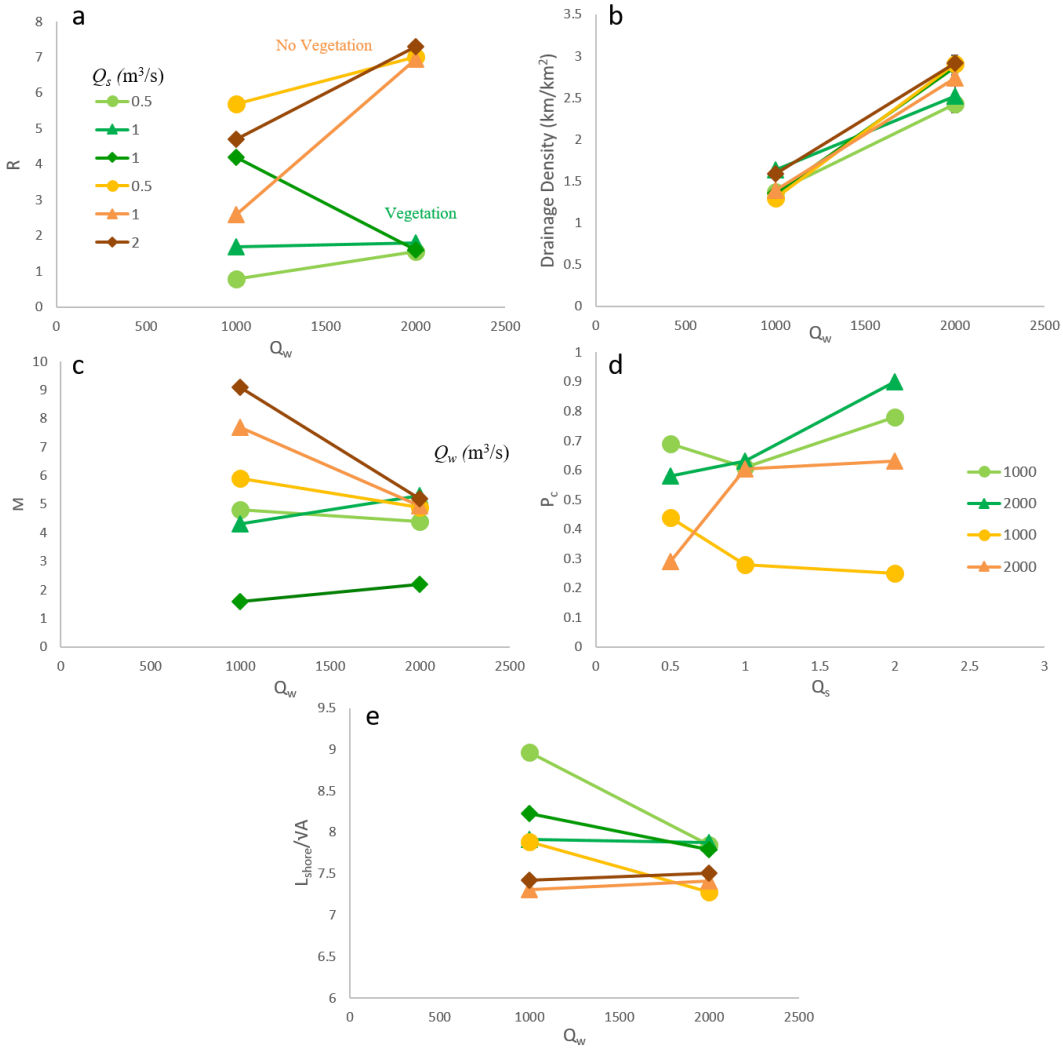

Figure 5.4: a) R (the rate of decay in remaining delta surface unreworked by the channel network), b) drainage density, c) M (the rate of decay in channel planform overlap), d) P_c (the ratio of the number of channel cells which are channels for more than 50% of the time over less than 50% of the time) and e) shoreline roughness (measured as shoreline length divided by the square root of delta area). a, b, c and e are plotted against Q_w,, with Q_s represented by increasing dark shades of orange (for unvegetated deltas) and green (for vegetated deltas). c is plotted against Q_s, with increasing Q_w represented by darker colors.

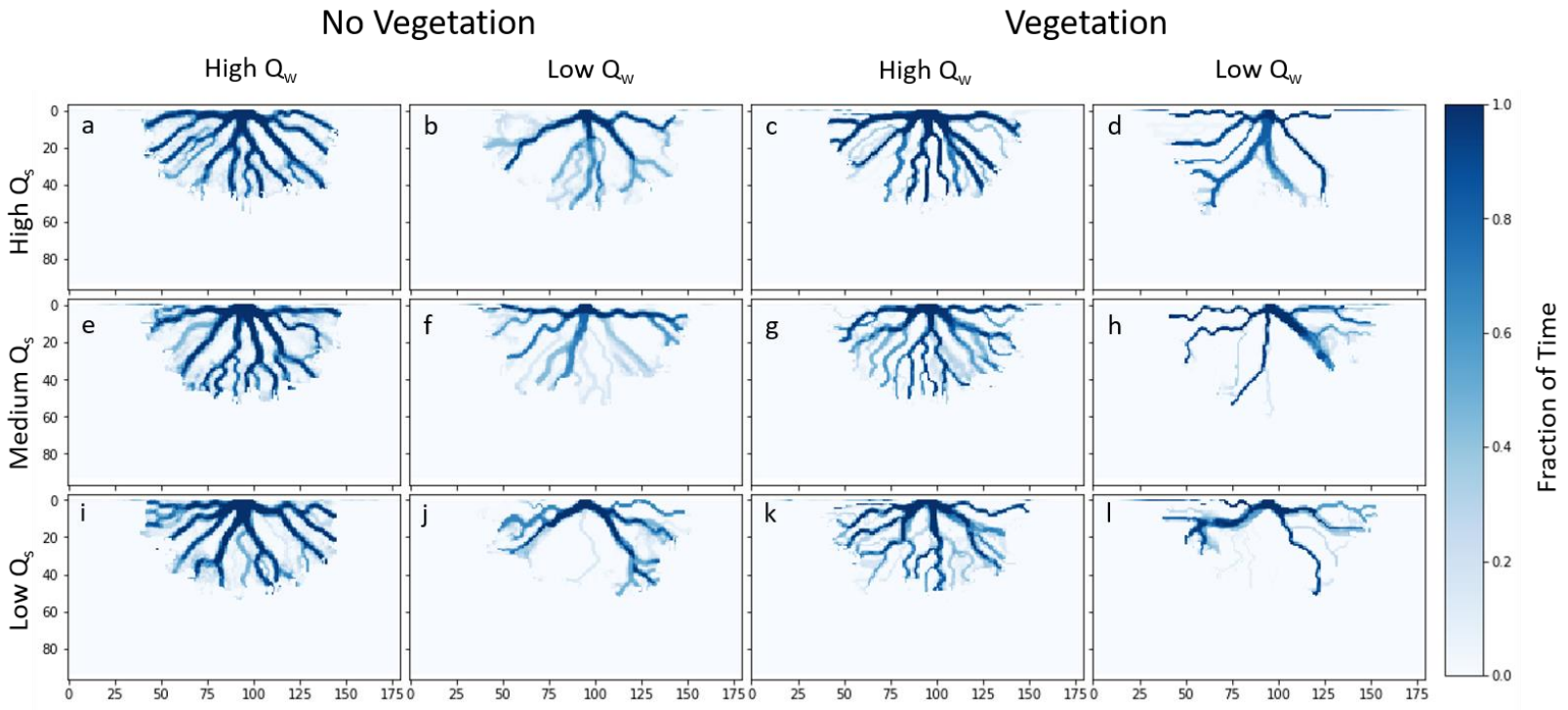

Figure 5.5: Maps of the fraction of time any cell which is part of the channel network during the second half of the run remains part of the channel network. Cells with a value of zero are never channels, and cells with a value of 1 are always channels. For the top row (a – d) Q_s = 2 m³/s, for the middle row (e-h) Q_s = 1 m³/s and for the bottom row (i-l) Q_s = 0.5 m³/s. The first two columns are unvegetated runs and the third and fourth are vegetated. The first and third columns have Q_w = 2000 m³/s and the second and fourth have Q_s = 1000 m³/s.

An increase in similarity in the channel network through time may seem to be at odds with an increase in channel mobility, but we suggest both can be explained by separating spatial and temporal variability in the channel network. We propose a shift from a few active channels that distribute sediment regionally via overbank flow and periodically undergo large-scale (global) avulsions at low Q_w to many channels distributed across the delta with limited overbank flow and frequent local, small-scale avulsions at high Q_w. Such as shift would, as we see, increase R (as channel migration and/or more frequent (but local) avulsions would be required to distribute flow across the delta in the place of overbank flow) and decrease M (as smaller-scale avulsions would result in smaller changes in the configuration of the channel network).

The proposed shift from global to local avulsions is supported by a decrease in the variation in maximum discharge values through time with increasing Q_w (Figure 5.6). Large-scale avulsions tend to introduce sudden increases in maximum discharge as most of the flow is concentrated in the new channel(s) rather than distributed more evenly between channels. Smaller peaks suggest that the number of active channels is higher and more constant, and that avulsions are more likely to be local rather than global.

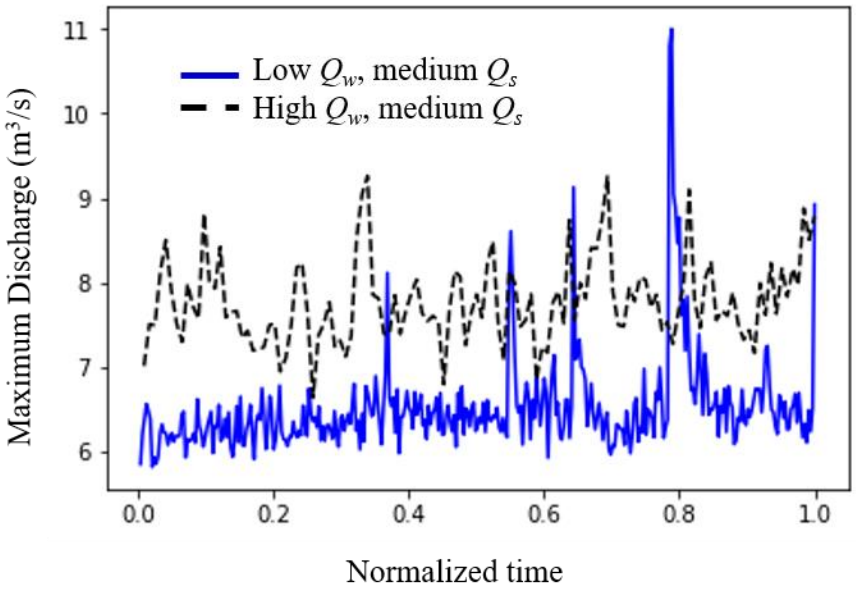

Figure 5.6: Time series of maximum discharge values for the entire delta for low Q_w, medium Q_s (blue solid line) and high Q_w, medium Q_s (black dashed line).

When vegetation is present, M is only determined by Q_s, decreasing with increasing Q_s but remaining relatively constant regardless of Q_w (Figure 5.4c). This suggests that with vegetation, there is more similarity in the configuration of the channel network through time with increasing Q_s, instead of less as would be expected (and is found without vegetation, where M increases with Q_s at low Q_w as rapid avulsions spread sediment across the aggrading delta). This may be due to consistent channel reoccupation during avulsions. Aggradation and increased channel switching frequency prevents vegetation from establishing in less active channels, and as vegetation offers resistance to incising new flow paths, results in frequent channel reoccupation. If the channel network is distributed evenly across the delta surface, consistent channel

reoccupation would still facilitate the even distribution of sediment across the delta necessary for the high aggradation rates typical of high Q_s, likely though overbank flow.

This hypothesis is qualitatively supported by the delta stratigraphy. The effect of high Q_s to increase channel aggradation and avulsion (by increasing cross-levee slopes through aggradation), encouraging even distribution of sediment across the delta, appears to result in less strong channelization of flow, especially when vegetation is present. This is supported by the decrease in the prevalence of sandy channel deposits with increasing Q_s (Figure 5.7c, g, k). It is also quantitatively supported by considering the fraction of time spent as a channel by each cell in the channel network (Figure 5.4d; Figure 5.5). For low Q_w, P_c decreases with increasing Q_s without vegetation, suggesting larger avulsions (supported by an increase in M, Figure 5.4c), but with vegetation the ratio increases (suggesting more persistent channel locations). This increase corresponds with a more even distribution of channels across the delta surface (Figure 5.5d, h, l) supporting the consistent reoccupation hypothesis described above.

A more even distribution and a denser network of channels across the delta surface results in a decreased ability of vegetation to increase shoreline roughness with increasing Q_w. Shoreline roughness is typically higher for vegetated than unvegetated runs (Figure 5.4e); however, the magnitude of the difference decreases with increased Q_w and Q_s. This supports our finding that vegetation's ability to decrease channel mobility is decreased with high Q_s as deposition impedes vegetation growth.

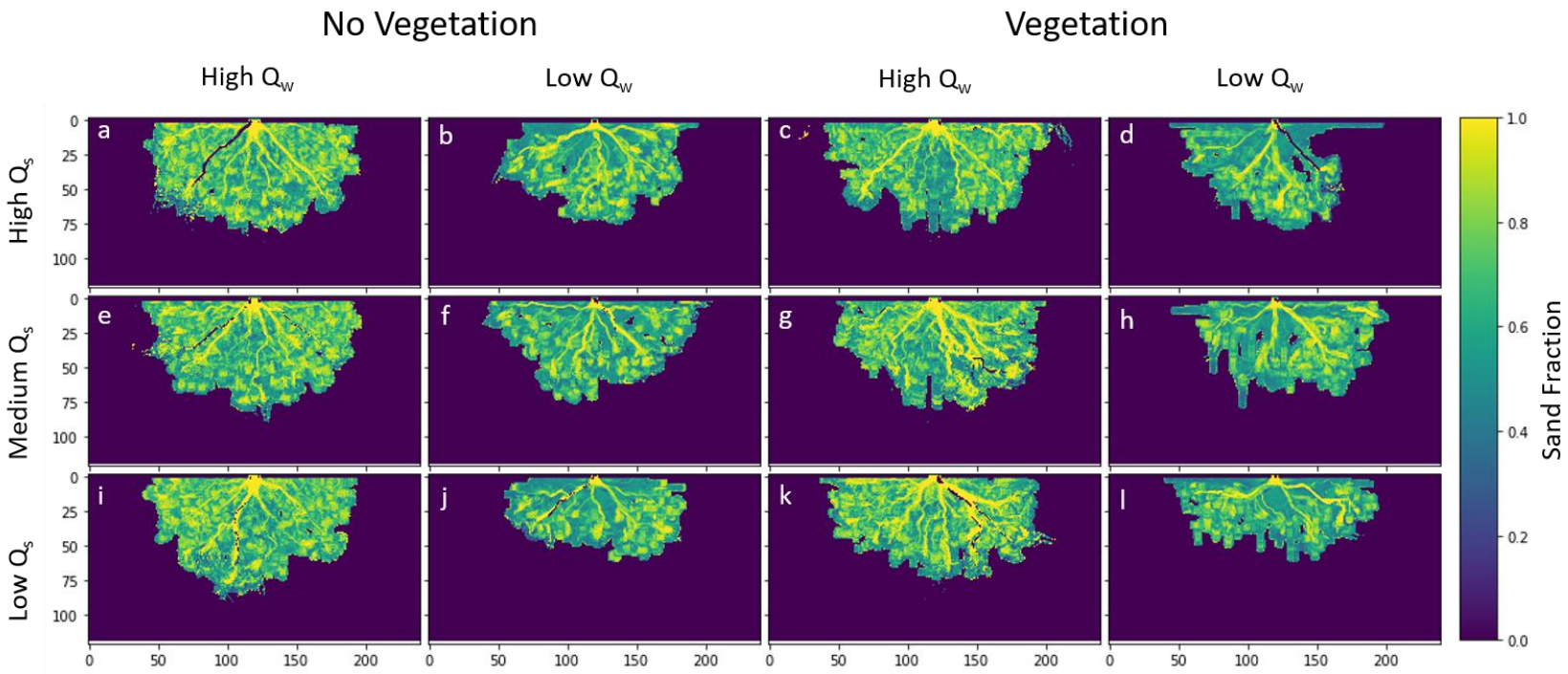

Figure 5.7: Vertically-averaged sand fractions at the end of a model run. For the top row (a – d) $Q_s = 2$ m³/s, for the middle row (e-h) $Q_s = 1$ m³/s and for the bottom row (i-l) $Q_s = 0.5$ m³/s. The first two columns are unvegetated runs and the third and fourth are vegetated. The first and third columns have $Q_w = 2000$ m³/s and the second and fourth have $Q_s = 1000$ m³/s. The composition of the input sediment is 50% sand.

5.4 Potential for Future Work

Our results raise some interesting questions which could be answered by future work. While our results suggest that the effect of vegetation on decreasing channel stability and delta morphology decreases with increasing SLR rate, a comparison of vegetated and unvegetated deltas both experiencing SLR would be necessary to quantify how much the stabilizing effect of vegetation is decreased. Such a comparison would also allow us to evaluate our interpretation of the limiting rate of SLR above which sediment transport processes occur on timescales faster than vegetation growth as about equal to the deposition rate on an unvegetated delta with no SLR (25 mm/yr in our particular model setup). This analysis would also allow us to further investigate the finding from Chapter 4 that vegetation tends to lower elevations on the delta by confining flow in channels. Does vegetation still reduce delta elevations with SLR, or does the faster reworking of the delta surface by the channel network, proposed to involve denser channel networks and unconfined flow, result in similar elevation profiles for vegetated and unvegetated deltas? Additionally, our proposed insights depend on the ability of increased Q_w and Q_s to increase the density of the channel network, which we have assessed quantitatively with only one metric (drainage density). This tendency could be further quantified by a measure such as nearest-edge distance and/or island size (e.g. Edmonds et al., 2011), which would also allow for a better understanding of the spatial distribution of channels on the delta surface.

In natural delta systems, multiple species and types of vegetation (e.g. aquatic plants or trees in addition to marsh grasses) exist in close proximity. In addition to each type of vegetation having different properties and levels of cohesive influence, both competition and facilitation effects could occur which would introduce more spatial and temporal variability in vegetation influence and may enhance or inhibit vegetation's overall level of influence. We have purposefully chosen to include only a simple representation of vegetation dynamics, with one type of vegetation, as a first examination of the basic question of whether cohesion from vegetation has similar effects on delta evolution as cohesion from muddy sediment and how it responds to varying SLR and discharge conditions. With this question in mind, we incorporated only the cohesive effects of vegetation, though other dynamics such as organic sediment production may be important to consider in other contexts (i.e. the sediment retention example in Chapter 4). Similarly, we provide a useful starting point for future research by considering ranges in water and sediment discharge, but our model deltas develop under constant discharge conditions (i.e. they could be considered at equilibrium). Natural deltas are subject to changes in discharge over time due to changing environmental conditions or human alteration of water or sediment fluxes to the coast (Syvitski and Saito, 2007), and so may be expected to experience transient effects as they respond to changing conditions with would not be captured by our equilibrium deltas. In addition to long-term trends in discharge, natural deltas experience stochastic

variations in flow, which would likely have a different effect on vegetation than the constant flood height represented in our model. However, we have provided a valuable foundation by identifying different behaviors in the delta channel networks across different experimental set-ups, which are consistent with experimental studies with changing discharge trends (but no vegetation; e.g. an increase in water discharge increasing the number of channels; Edmonds et al., 2010).

5.5 Summary and Implications

We find that the effects of SLR on vegetated deltas agree with those found by other studies of model and experimental unvegetated deltas: decreased progradation and increased aggradation rates, a denser channel network and increased channel mobility (Martin et al., 2009; Jerolmack, 2009; Liang et al., 2016a). As expected, we find that SLR decreases vegetation's effectiveness at stabilizing and elongating channel networks, resulting in smoother shorelines. Our results suggest that vegetation still has a strong influence on delta morphology and channel dynamics with some amount of SLR, but that there is a limit beyond which sediment transport processes begin to act on shorter timescales than vegetation growth, and the influence of vegetation decreases. This limit appears to be higher for channel dynamics than for delta morphology, supporting the stronger control on channel mobility by vegetation and on morphology by sediment composition found in Chapter 4.

In agreement with previous research, we find that increasing Q_w increases the number of channels (Edmonds et al., 2010), and (at low Q_w) channel mobility increases with Q_s (Powell et al., 2012; Orton and Reading, 1993; Hoyal and Sheets, 2009) and vegetation's ability to decrease channel mobility is decreased (e.g. Murray and Paola, 2003). We also propose two new insights into the evolution of delta channel networks under different discharge conditions: 1) a change in avulsion dynamics without vegetation from a few active channels supplemented by overbank flow and undergoing periodic global avulsions at low Q_w to many active channels experiencing limited overbank flow and frequent local avulsions at high Q_w, and 2) that while vegetation's ability to establish in less active channels is decreased by more frequent channel switching and aggradation under high Q_s conditions, this can increase the persistence of the channel network by favoring reoccupation of abandoned channels over incising new channels through vegetated areas.

The proposed insights into channel dynamics under high Q_w and Q_s conditions have important implications for deltaic channel-island exchange. As vegetation may reduce fluxes between channels and islands (e.g. Chapter 4, Nardin and Edmonds, 2014), a decrease in vegetation's effectiveness to channelize flow with increasing SLR may result in increased channel-island exchange (Liang et al., 2016a), with important implications for sediment and nutrient fluxes to islands (Hiatt and Passalacqua, 2014). On a larger scale, a shift from more lobate delta growth with low Q_w to more fan-like

growth with high Q_w has implications for the delivery of sediment and nutrients across the entire delta through potential changes in network connectivity (e.g. Tejedor et al., 2016; Passalacqua, 2016). These implications will be particularly important for restored or engineered deltas, which are subject to natural delta processes after initial construction (Paola et al., 2011), or for diversions with controlled water and sediment discharges. If restoration efforts aim to build new deltaic land, they will need to consider the implications of discharge and sediment load on channel network configuration and dynamics, including the influence of vegetation.

5.6 Acknowledgements

Grants from the National Science Foundation, Geomorphology and Land-Use Dynamics Program (1324114 and 1530233) supported this work.

6. Conclusions

6.1 Barrier islands and salt marshes

The results presented in Chapter 2 demonstrate that there is a significant correlation between shoreline curvature and shoreline change rates over several kilometer and decade to century space and time scales along many coastlines. This signal is typically a smoothing signal (i.e. in North Carolina, Texas, and Florida), however in some regions (i.e. the Mid-Atlantic) the extent of anthropogenic shoreline stabilization results in a roughening signal. The presence of a significant correlation, even a small one, demonstrates the importance of the relationship between coastline curvature and shoreline change in understanding shoreline dynamics. This relationship is strongest on long, sandy barriers which are wave-dominated and have relatively slow rates of shoreline change, but can help explain shoreline behavior even on shorter islands with competing influences (e.g. tides). Shoreline change prediction models have historically underperformed on low-lying, sandy shorelines such as those considered in this study (e.g. Gutierrez et al., 2011; Yates and Cozannet, 2012); this finding of large magnitude, significant correlations between shoreline curvature and shoreline change in some locations (e.g. Texas, North Carolina) suggests that considering shoreline curvature in analyses of historical and predicted shoreline change could help improve agreement between models and data on these coasts.

As barriers migrate landward, overwash provides an important sediment source for back-barrier marshes, sustaining them under SLR rate or sediment supply conditions under which they would otherwise drown. In Chapter 3 I find that this important relationship between marshes and barrier islands and the existence of an overwash-supported, long-lasting narrow back-barrier marsh state, proposed by Walters et al. (2014), persists even in the presence of marsh edge erosion by wind waves. However, even in a closed system such as this model, without sediment loss to the ocean, the narrow marsh is a temporary state and the basin tends towards the stable states of completely full or completely empty of marsh (Mariotti and Fagherazzi, 2013). I also find that, in addition to providing a mechanism to move sediment from the marsh edge to the marsh surface and prevent drowning (e.g. Mariotti and Carr, 2014), wave edge erosion may enhance marsh resilience by providing a sediment source that is more efficient than vertical erosion of drowned marsh platform. Marsh sediments eroded from the lower portion of the marsh scarp may have a higher concentration of inorganic sediment which can be redeposited on the marsh, while surface layers may have a higher proportion of organic material which may be lost to decomposition or dispersal when eroded. Combined, these results emphasize the first-order control of geometry and stratigraphy on the evolution of marsh-barrier systems. Where a marsh and bay both maintain equilibrium elevations relative to sea level, if the net sediment budget is known the behavior of the marsh edge (the rate of erosion or accretion) can be predicted

based on basin geometry and the rates of sea-level rise (space creation) and sediment supply. So long as the rate of sediment import or export is known, for instance at a snapshot in time, this control on marsh evolution applies to natural and model basins regardless of basin conditions or model assumptions about sediment exchange with the ocean.

6.2 River deltas

In Chapter 4 I find that vegetation and cohesive sediment have similar effects on many aspects of delta morphology and evolution. Vegetation, like cohesive sediment, increases shoreline roughness, decreases channel width to depth ratios, decreases channel migration rates, and limits the spatial distribution of flow and deposition on the delta, which enhances avulsion dynamics. However, my results also highlight some differences; as vegetation introduces friction on levees in addition to stabilizing channel banks, further decreasing overbank flow, it shifts the elevation distribution of the delta surface to lower elevations. Both cohesive sediment and vegetation can alter delta morphology and channel dynamics in model results, but while sediment cohesion (or lack thereof) appears to be a first-order control on delta morphology, vegetation can have a stronger influence on channel dynamics and stratigraphy. These model results suggest that vegetation can have effects on delta morphology that are comparable to or larger in magnitude than those of increasing the fraction of cohesive sediment and that caution should be used when interpreting cohesive sediment as a proxy for vegetation in

model experiments as the effect of vegetation on channel migration and avulsion styles and timescales, as well as the effect on enhancing sandy channel deposits, may not be captured by the addition of cohesive sediment alone.

I also considered, in Chapter 5, the cohesive effects of vegetation under varied environmental conditions. In agreement with previous studies of unvegetated deltas, I find that SLR on vegetated deltas leads to decreased progradation and increased aggradation rates, a denser channel network and increased channel mobility (e.g. Martin et al., 2009; Jerolmack, 2009; Liang et al., 2016a). As expected, in these experiments SLR decreases vegetation's effectiveness at stabilizing and elongating channel networks, resulting in smoother shorelines. My results suggest that while vegetation still has a strong influence on delta morphology and channel dynamics with some amount of SLR, as SLR rates increase sediment transport processes begin to act on shorter timescales than vegetation growth and the influence of vegetation decreases. This appears to occur at higher rates of SLR for channel dynamics than for delta morphology, supporting the conclusion of Chapter 4 that vegetation has a stronger influence on channel dynamics than delta morphology. Also in agreement with previous research, I find that increasing Q_w increases the number of channels (Edmonds et al., 2010), and (at low Q_w) vegetation's stabilizing influence decreases (e.g. Murray and Paola, 2003) and channel mobility increases with increasing Q_s (Powell et al., 2012; Orton and Reading, 1993; Hoyal and Sheets, 2009). I propose two new insights into the evolution of delta channel networks

under different discharge conditions. First, without vegetation, I observe a change in avulsion dynamics with increasing Q_w from a few active channels supplemented by overbank flow and undergoing episodic global avulsions (at low Q_w) to many active channels experiencing limited overbank flow and frequent local avulsions (at high Q_w). Second, I find that vegetation's ability to establish in non-dominant channels is inhibited by increased channel switching and aggradation under high Q_s conditions, and that this can ultimately increase the persistence of the channel network by favoring reoccupation of abandoned channels over incising new channels through vegetated areas.

These insights have important implications for deltaic channel-island exchange. A decrease in vegetation's effectiveness to channelize flow may result in increased channel-island exchange (Liang et al., 2016a), with implications for sediment and nutrient fluxes to islands (Hiatt and Passalacqua, 2014). On a larger scale, a shift from more lobate to more fan-like delta growth with increasing Q_w has implications for the delivery of sediment and nutrients across the entire delta. These implications will be particularly important for restored or engineered deltas or diversions which may have controlled water or sediment discharges but whose evolution is subject to natural delta processes after initial construction (Paola et al., 2011). If restoration efforts aim to build new deltaic land, they will need to consider the implications of discharge and sediment load on channel network configuration and dynamics, including the influence of vegetation.

References

Allison, M. A. and E. A. Meselhe (2010). "The use of large water and sediment diversions in the lower Mississippi River (Louisiana) for coastal restoration." Journal of Hydrology **387**(3-4): 346-360.

Anthony, E. J., N. Marriner and C. Morhange (2014). "Human influence and the changing geomorphology of Mediterranean deltas and coasts over the last 6000years: From progradation to destruction phase?" Earth-Science Reviews **139**: 336-361.

Ashton, A., A. B. Murray and O. Arnoult (2001). "Formation of coastline features by large-scale instabilities induced by high-angle waves." Nature **414**: 296-300.

Ashton, A. D. and A. B. Murray (2006). "High-angle wave instability and emergent shoreline shapes: 1. Modeling of sand waves, flying spits, and capes." Journal of Geophysical Research **111**(F4).

Ashton, A. D. and A. B. Murray (2006). "High-angle wave instability and emergent shoreline shapes: 2. Wave climate analysis and comparisons to nature." Journal of Geophysical Research **111**(F4).

Barbier, E. B., S. D. Hacker, C. Kennedy, E. W. Koch, A. C. Stier and B. R. Silliman (2011). "The value of estuarine and coastal ecosystem services." Ecological Monographs **81**(2): 169-193.

Basco, D. R. (2006). "Seawall impacts on adjacent beaches: Separating fact from fiction." Journal of Coastal Research **39**: 741-744.

Brenner, O. T., L. J. Moore and A. B. Murray (2015). "The complex influences of back-barrier deposition, substrate slope and underlying stratigraphy in barrier island response to sea-level rise: Insights from the Virginia Barrier Islands, Mid-Atlantic Bight, U.S.A." Geomorphology **246**: 334-350.

Browder, A. E. and R. Dean (2000). "Monitoring and comparison to predictive models of the Perdido Key beach nourishment project, Florida, USA." Coastal Engineering **39**(2-4): 173-191.

Bruun, P. (1988). "The Bruun Rule of Erosion by Sea-Level Rise: A Discussion on Large-Scale Two- and Three-Dimensional Usages." Journal of Coastal Research **4**(4): 627-648.

Bryant, M., P. Falk and C. Paola (1995). "Experimental study of avulsion frequency and rate of deposition." Geology **23**(4): 365-368.

Caldwell, R. L. and D. A. Edmonds (2014). "The effects of sediment properties on deltaic processes and morphologies: A numerical modeling study." Journal of Geophysical Research: Earth Surface **119**(5): 961-982.

Carniello, L., A. Defina and L. D'Alpaos (2009). "Morphological evolution of the Venice lagoon: Evidence from the past and trend for the future." Journal of Geophysical Research **114**(F4).

Center, T. H. (2000). Evaluation of Erosion Hazards. Washington, D.C.**:** 203.

Chen, X., X. Zhang, J. A. Church, C. S. Watson, M. A. King, D. Monselesan, B. Legresy and C. Harig (2017). "The increasing rate of global mean sea-level rise during 1993–2014." Nature Climate Change **7**(7): 492-495.

Coelho, C., R. Silva, F. Veloso-Gomes and F. Taveira Pinto (2006). A vulnerability analysis approach for the Portuguese West Coast. Risk Analysis V: Simulation and Hazard Mitigation**:** 251-262.

Cowell, P. J., P. S. Roy and R. Jones (1995). "Simulation of large-scale coastal change using a morphological behavior model." Marine Geology **126**: 45-61.

Cranford, P. J., D. C. Gordon and C. M. Jarvis (1989). "Measurement of Cordgrass, Spartina altemiflora, Production in a Macrotidal Estuary., Bay of Fundy." Estuaries **12**(1): 27-34.

D'Alpaos, A. (2011). "The mutual influence of biotic and abiotic components on the long-term ecomorphodynamic evolution of salt-marsh ecosystems." Geomorphology **126**(3-4): 269-278.

D'Alpaos, A., C. Da Lio and M. Marani (2012). "Biogeomorphology of tidal landforms: physical and biological processes shaping the tidal landscape." Ecohydrology **5**(5): 550-562.

D'Alpaos, A., S. M. Mudd and L. Carniello (2011). "Dynamic response of marshes to perturbations in suspended sediment concentrations and rates of relative sea level rise." Journal of Geophysical Research **116**(F4).

Davis, R. and D. Fitzgerald (2003). Beaches and Coasts, Wiley.

Day, J. W., G. P. Kemp, D. J. Reed, D. R. Cahoon, R. M. Boumans, J. M. Suhayda and R. Gambrell (2011). "Vegetation death and rapid loss of surface elevation in two contrasting Mississippi delta salt marshes: The role of sedimentation, autocompaction and sea-level rise." Ecological Engineering **37**(2): 229-240.

Dean, R. (2002). Beach Nourishment: Theory and Practice. Hackensack, N.J., World Scientific.

Dean, R. and C. H. Yoo (1992). "Beach-nourishment performance predictions." Journal of Waterway, Port, Coastal, and Ocean Engineering **118**(6).

Dean, R. G. and R. A. Dalrymple (1991). Water wave mechanics for engineers and scientists, World Scientific.

Edmonds, D., R. Slingerland, J. Best, D. Parsons and N. Smith (2010). "Response of river-dominated delta channel networks to permanent changes in river discharge." Geophysical Research Letters **37**(12).

Edmonds, D. A., C. Paola, D. C. J. D. Hoyal and B. A. Sheets (2011). "Quantitative metrics that describe river deltas and their channel networks." Journal of Geophysical Research **116**(F4).

Edmonds, D. A. and R. L. Slingerland (2009). "Significant effect of sediment cohesion on delta morphology." Nature Geoscience **3**(2): 105-109.

Ericson, J., C. Vorosmarty, S. Dingman, L. Ward and M. Meybeck (2006). "Effective sea-level rise and deltas: Causes of change and human dimension implications." Global and Planetary Change **50**(1-2): 63-82.

Fagherazzi, S., L. Carniello, L. D'Alpaos and A. Defina (2006). "Critical bifurcation of shallow microtidal landforms in tidal flats and salt marshes." Proceedings of the National Academy of Sciences **103**(22): 8337-8341.

Fagherazzi, S., G. Mariotti, P. Wiberg and K. McGlathery (2013). "Marsh Collapse Does Not Require Sea Level Rise." Oceanography **26**(3): 70-77.

Fagherazzi, S., C. Palermo, M. C. Rulli, L. Carniello and A. Defina (2007). "Wind waves in shallow microtidal basins and the dynamic equilibrium of tidal flats." Journal of Geophysical Research **112**(F2).

Fagherazzi, S. and P. L. Wiberg (2009). "Importance of wind conditions, fetch, and water levels on wave-generated shear stresses in shallow intertidal basins." Journal of Geophysical Research **114**(F3).

Falqués, A. (2003). "On the diffusivity in coastline dynamics." Geophysical Research Letters **30**(21).

FitzGerald, D. M., M. S. Fenster, B. A. Argow and I. V. Buynevich (2008). "Coastal Impacts Due to Sea-Level Rise." Annual Review of Earth and Planetary Sciences **36**(1): 601-647.

Fletcher, C. H., B. M. Romine, A. S. Genz, M. M. Barbee, M. Dyer, T. R. Anderson, S. C. Lim, S. Vitousek, C. Bochicchio and B. M. Richmond (2012). "National Assessment of Shoreline Change: Historical Shoreline Change in the Hawaiian Islands." U.S. Geological Survey Open-file Report **2011-1051**.

Friedrichs, C. T. and P. J.E. (2001). "Tidal Salt Marsh Morphodynamics: A Synthesis." Journal of Coastal Research **27**: 7-37.

Galloway, W. E. (1975). "Process framework for describing the morphologic and stratigraphic evolution of deltaic depositional systems." Deltas; models for exploration: 87-98.

Geleynse, N., J. E. A. Storms, D.-J. R. Walstra, H. R. A. Jagers, Z. B. Wang and M. J. F. Stive (2011). "Controls on river delta formation; insights from numerical modelling." Earth and Planetary Science Letters **302**(1-2): 217-226.

Gibbs, A. E. and B. M. Richmond (2015). "National Assessment of Shoreline Change: Historical Shoreline Change along the North Coast of Alaska, U.S.-Canadian Border to Icy Cape." U.S. Geological Survey Open-file Report **2015-1048**.

Gornitz, V. M., R. C. Daniels, T. W. White and K. R. Birdwell (1994). "The development of a coastal risk assessment database: Vulnerability to sea-level rise in the U.S. southeast." Journal of Coastal Research **12**: 327-338.

Gran, K. and C. Paola (2001). "Riparian vegetation controls on braided stream dynamics." Water Resources Research **37**(12): 3275-3283.

Gutierrez, B. T., N. G. Plant and E. R. Thieler (2011). "A Bayesian network to predict coastal vulnerability to sea level rise." Journal of Geophysical Research **116**(F2).

Hanegan, K. and I. Georgiou (2015). "Tidal modulated flow and sediment flux through Wax Lake Delta distributary channels: Implications for delta development." Proceedings of the International Association of Hydrological Sciences **367**: 391-398.

Hapke, C. J., E. A. Himmelstoss, M. G. Kratzmann, J. H. List and E. R. Thieler (2011). "National assessment of shoreline change. Historical shoreline change along the New England and Mid-Atlantic Coasts." U.S. Geological Survey Open-file Report **2010-1118**.

Hapke, C. J., M. G. Kratzmann and E. A. Himmelstoss (2013). "Geomorphic and human influence on large-scale coastal change." Geomorphology **199**: 160-170.

Hapke, C. J. and D. Reid (2007). "National Assessment of Shoreline Change Part 4: Historical Coastal Cliff Retreat along the California Coast." U.S. Geological Survey Open-file Report **2007-1133**.

Hapke, C. J., D. Reid, B. M. Richmond, P. Ruggiero and J. H. List (2006). "National Assessment of Shoreline Change Part 3: Historical Shoreline Change and Associated Coastal Land Loss Along Sandy Shorelines of the California Coast." U.S. Geological Survey Open-file Report **2006-1219**.

Hayden, B. P., R. D. Dueser, J. T. Callahan and H. H. Shugart (1991). "Long-Term Research at the Virginia Coast Reserve." BioScience **41**(5): 310-318.

Hein, C. J., D. M. FitzGerald, E. A. Carruthers, B. D. Stone, W. A. Barnhardt and A. M. Gontz (2012). "Refining the model of barrier island formation along a paraglacial coast in the Gulf of Maine." Marine Geology **307-310**: 40-57.

Hiatt, M. and P. Passalacqua (2015). "Hydrological connectivity in river deltas: The first-order importance of channel-island exchange." Water Resources Research **51**(4): 2264-2282.

Hinkel, J. and R. J. T. Klein (2009). "Integrating knowledge to assess coastal vulnerability to sea-level rise: The development of the DIVA tool." Global Environmental Change **19**(3): 384-395.

Hoyal, D. C. J. D. and B. A. Sheets (2009). "Morphodynamic evolution of experimental cohesive deltas." Journal of Geophysical Research **114**(F2).

Isikdogan, F., A.C. Bovik, and P. Passalacqua (2015). "Automatic channel network extraction from remotely sensed images by singularity analysis." IEEE Geoscience and Remote Sensing Letters 12(11): 2218-2221.

Jalowska, A. M., A. B. Rodriguez and B. A. McKee (2015). "Responses of the Roanoke Bayhead Delta to variations in sea level rise and sediment supply during the Holocene and Anthropocene." Anthropocene **9**: 41-55.

James, C. S., A. L. Birkhead, A. A. Jordanova and J. J. O'Sullivan (2004). "Flow resistance of emergent vegetation." Journal of Hydraulic Research **42**(4): 390-398.

Jerolmack, D. J. (2009). "Conceptual framework for assessing the response of delta channel networks to Holocene sea level rise." Quaternary Science Reviews **28**(17-18): 1786-1800.

Kim, W. (2012). "Geomorphology: Flood-built land." Nature Geoscience **5**(8): 521-522.

Kim, W., D. Mohrig, R. Twilley, C. Paola and G. Parker (2009). "Is it feasible to build new land in the Mississippi River delta." EOS **90**(42): 373-374.

Kim, W., C. Paola, J. B. Swenson and V. R. Voller (2006). "Shoreline response to autogenic processes of sediment storage and release in the fluvial system." Journal of Geophysical Research **111**(F4).

Kirwan, M. L., G. R. Guntenspergen, A. D'Alpaos, J. T. Morris, S. M. Mudd and S. Temmerman (2010). "Limits on the adaptability of coastal marshes to rising sea level." Geophysical Research Letters **37**(23).

Kirwan, M. L. and J. P. Megonigal (2013). "Tidal wetland stability in the face of human impacts and sea-level rise." Nature **504**(7478): 53-60.

Kraus, N. C. (2007). Coastal Inlets of Texas. Coastal Sediments, ASCE Press.

Kraus, N. C. and W. G. McDougal (1996). "The effects of seawalls on the beach: Part I, and updated lliterature review." Journal of Coastal Research **12**(3): 691-701.

Lazarus, E., A. Ashton, A. B. Murray, S. Tebbens and S. Burroughs (2011). "Cumulative versus transient shoreline change: Dependencies on temporal and spatial scale." Journal of Geophysical Research **116**(F2).

Lazarus, E. D., A. D. Ashton and A. B. Murray (2012). Large-scale patterns in hurricane-driven shoreline change. Extreme events and natural hazards: the complexity perspective. Washington D.C., AGU**:** 127-138.

Lazarus, E. D. and A. B. Murray (2011). "An integrated hypothesis for regional patterns of shoreline change along the Northern North Carolina Outer Banks, USA." Marine Geology **281**(1-4): 85-90.

Leatherman, S. P., K. Zhang and B. C. Douglass (2000). "Sea level rise shown to drive coastal erosion." EOS **81**(6): 55-57.

Leonardi, N. and S. Fagherazzi (2014). "How waves shape salt marshes." Geology **42**(10): 887-890.

Leonardi, N., N. K. Ganju and S. Fagherazzi (2016). "A linear relationship between wave power and erosion determines salt-marsh resilience to violent storms and hurricanes." Proc Natl Acad Sci U S A **113**(1): 64-68.

Leonardi, N., A. S. Kolker and S. Fagherazzi (2015). "Interplay between river discharge and tides in a delta distributary." Advances in Water Resources **80**: 69-78.

Liang, M., N. Geleynse, D. A. Edmonds and P. Passalacqua (2015). "A reduced-complexity model for river delta formation; Part 2: Assessment of the flow routing scheme." Earth Surface Dynamics **3**(1): 87-104.

Liang, M., W. Kim and P. Passalacqua (2016). "How much subsidence is enough to change the morphology of river deltas?" Geophysical Research Letters **43**(19): 10,266-210,276.

Liang, M., C. Van Dyk and P. Passalacqua (2016). "Quantifying the patterns and dynamics of river deltas under conditions of steady forcing and relative sea level rise." Journal of Geophysical Research: Earth Surface **121**(2): 465-496.

Liang, M., V. R. Voller and C. Paola (2015). "A reduced-complexity model for river delta formation; Part 1: Modeling deltas with channel dynamics." Earth Surface Dynamics **3**(1): 67-86.

Lightbody, A. F. and H. M. Nepf (2006). "Prediction of Velocity Profiles and Longitudinal Dispersion in Emergent Salt Marsh Vegetation." Limnology and Oceanography **51**(1): 218-228.

List, J. H. and A. S. Farris (1999). Large-scale shoreline response to storms and fair weather. Coastal Sediments, Am. Soc. of Civ. Eng.

List, J. H., A. S. Farris and C. Sullivan (2006). "Reversing storm hotspots on sandy beaches: Spatial and temporal characteristics." Marine Geology **226**(3-4): 261-279.

Lorenzo-Trueba, J., V. R. Voller, C. Paola, R. R. Twilley and A. E. Bevington (2012). "Exploring the role of organic matter accumulation on delta evolution." Journal of Geophysical Research **117**.

Marani, M., A. D'Alpaos, S. Lanzoni, L. Carniello and A. Rinaldo (2007). "Biologically-controlled multiple equilibria of tidal landforms and the fate of the Venice lagoon." Geophysical Research Letters **34**(11).

Marani, M., A. D'Alpaos, S. Lanzoni, L. Carniello and A. Rinaldo (2010). "The importance of being coupled: Stable states and catastrophic shifts in tidal biomorphodynamics." Journal of Geophysical Research **115**(F4).

Mariotti, G. and J. Carr (2014). "Dual role of salt marsh retreat: Long-term loss and short-term resilience." Water Resources Research **50**(4): 2963-2974.

Mariotti, G. and S. Fagherazzi (2010). "A numerical model for the coupled long-term evolution of salt marshes and tidal flats." Journal of Geophysical Research **115**(F1).

Mariotti, G. and S. Fagherazzi (2013). "Critical width of tidal flats triggers marsh collapse in the absence of sea-level rise." Proc Natl Acad Sci U S A **110**(14): 5353-5356.

Martin, J., B. Sheets, C. Paola and D. Hoyal (2009). "Influence of steady base-level rise on channel mobility, shoreline migration, and scaling properties of a cohesive experimental delta." Journal of Geophysical Research **114**(F3).

Masetti, R., S. Fagherazzi and A. Montanari (2008). "Application of a barrier island translation model to the millennial-scale evolution of Sand Key, Florida." Continental Shelf Research **28**(9): 1116-1126.

McLoughlin, S. M., P. L. Wiberg, I. Safak and K. J. McGlathery (2014). "Rates and Forcing of Marsh Edge Erosion in a Shallow Coastal Bay." Estuaries and Coasts **38**(2): 620-638.

Millar, R. G. (2000). "Influence of bank vegetation on alluvial channel patterns." Water Resources Research **36**(4): 1109-1118.

Moore, L. J., J. H. List, S. J. Williams and D. Stolper (2010). "Complexities in barrier island response to sea level rise: Insights from numerical model experiments, North Carolina Outer Banks." Journal of Geophysical Research **115**(F3).

Moore, L. J., K. Patsch, J. H. List and S. J. Williams (2014). "The potential for sea-level-rise-induced barrier island loss: Insights from the Chandeleur Islands, Louisiana, USA." Marine Geology **355**: 244-259.

Morris, J. T., P. V. Sundareshwar, C. T. Nietch, B. Kjerfve and D. R. Cahoon (2002). "Responses of coastal wetlands to rising sea level." Ecology **83**(10): 2869-2877.

Morton, R. A. and T. L. Miller (2005). "National Assessment of Shoreline Change: Part 2. Historical Shoreline Changes And Associated Coastal Land Loss Along The U.S. Southeast Atlantic Coast." U.S. Geological Survey Open-file Report **2005-1401**.

Morton, R. A., T. L. Miller and L. J. Moore (2004). "National Assessment of Shoreline Change: Part 1, Historical Shoreline Change and Associated Coastal Land Loss along the U.S. Gulf of Mexico." U.S. Geological Survey Open-file Report **2004-1043**.

Morton, R. A., T. L. Miller and L. J. Moore (2005). "Historical shoreline changes along the US Gulf of Mexico: A summary of recent shoreline comparisons and analyses." journal of Coastal Research **21**(4): 704-709.

Morton, R. A., J. G. Paine and J. C. Gibeaut (1994). "Stages and durations of post-storm beach recovery, southeastern Texas coast, U.S.A." Journal of Coastal Research **10**(4): 884-908.

Mudd, S. M., A. D'Alpaos and J. T. Morris (2010). "How does vegetation affect sedimentation on tidal marshes? Investigating particle capture and hydrodynamic controls on biologically mediated sedimentation." Journal of Geophysical Research **115**(F3).

Murray, A. B. (2003). "Contrasting the goals, strategies, and predictions associated with simplified numerical models and detailed simulations." Prediction in Geomorphology.

Murray, A. B. and L. J. Moore (2018). Geometric constraints on long-term barrier migration: From simple to surprising. Barrier Dynamics and Response to Changing Climate. L. J. Moore and A. B. Murray. New York, Springer.

Murray, A. B. and C. Paola (1997). "Properties of a cellular braided-stream model." Earth Surface Processes and Landforms **22**: 1001-1025.

Murray, A. B. and C. Paola (2003). "Modelling the effect of vegetation on channel pattern in bedload rivers." Earth Surface Processes and Landforms **28**(2): 131-143.

Nardin, W. and D. A. Edmonds (2014). "Optimum vegetation height and density for inorganic sedimentation in deltaic marshes." Nature Geoscience **7**(10): 722-726.

Nardin, W., D. A. Edmonds and S. Fagherazzi (2016). "Influence of vegetation on spatial patterns of sediment deposition in deltaic islands during flood." Advances in Water Resources.

Nepf, H. M. (2012). "Flow and Transport in Regions with Aquatic Vegetation." Annual Review of Fluid Mechanics **44**(1): 123-142.

Nepf, H. M. (2012). "Hydrodynamics of vegetated channels." Journal of Hydraulic Research **50**(3): 262-279.

Nepf, H. M., J. A. Sullivan and R. A. Zavistoski (1997). "A model for diffusion with emergent vegetation." Limnology and Oceanography **48**(2): 1735-1745.

Nicholls, R. J. and A. C. Vega-Leinert (2008). "Implications of sea-level rise for Europe's coasts: An introduction." journal of Coastal Research **24**(2): 285-287.

Nienhuis, J. H., A. D. Ashton and L. Giosan (2015). "What makes a delta wave-dominated?" Geology **43**(6): 511-514.

Nyman, J. A., R. J. Walters, R. D. Delaune and W. H. Patrick (2006). "Marsh vertical accretion via vegetative growth." Estuarine, Coastal and Shelf Science **69**(3-4): 370-380.

Odezulu, C. I., J. Lorenzo-Trueba, W. D.J. and J. B. Anderson (2018). Follets Island: A case of unprecedented change and transition from rollover to subaqueous shoals. Barrier Dynamics and Responses to Changing Climate. L. J. Moore and A. B. Murray. New York, Springer.

Orton, G. J. and H. G. Reading (1993). "Variability of deltaic processes in terms of sediment supply with particular emphasis on grain size." Sedimentology **40**: 475-512.

Paola, C. and M. Leeder (2011). "Environmental dynamics: Simplicity versus complexity." Nature **469**(7328): 38-39.

Paola, C., R. R. Twilley, D. A. Edmonds, W. Kim, D. Mohrig, G. Parker, E. Viparelli and V. R. Voller (2011). "Natural processes in delta restoration: application to the Mississippi Delta." Ann Rev Mar Sci **3**: 67-91.

Pasquale, N., P. Perona, R. Francis and P. Burlando (2014). "Above-ground and below-groundSalixdynamics in response to river processes." Hydrological Processes **28**(20): 5189-5203.

Passalacqua, P. (2016). "The Delta Connectome: A network-based framework for studying connectivity in river deltas." Geomorphology **277**: 50-62.

Perona, P., P. Molnar, B. Crouzy, E. Perucca, Z. Jiang, S. McLelland, D. Wüthrich, K. Edmaier, R. Francis, C. Camporeale and A. Gurnell (2012). "Biomass selection by floods and related timescales: Part 1. Experimental observations." Advances in Water Resources **39**: 85-96.

Pilkey, O. H. and J. A. G. Cooper (2004). "Society and Sea Level Rise." Science **303**: 1781-1782.

Plant, N. G., E. Robert Thieler and D. L. Passeri (2016). "Coupling centennial-scale shoreline change to sea-level rise and coastal morphology in the Gulf of Mexico using a Bayesian network." Earth's Future **4**(5): 143-158.

Powell, E. J., W. Kim and T. Muto (2012). "Varying discharge controls on timescales of autogenic storage and release processes in fluvio-deltaic environments: Tank experiments." Journal of Geophysical Research **117**(F2).

Priestas, A., G. Mariotti, N. Leonardi and S. Fagherazzi (2015). "Coupled Wave Energy and Erosion Dynamics along a Salt Marsh Boundary, Hog Island Bay, Virginia, USA." Journal of Marine Science and Engineering **3**(3): 1041-1065.

Reed, D. J. (1995). "The response of coastal marshes to sea-level rise: Survival or submergence?" earth Surface Processes and Landforms **20**: 39-48.

Rodriguez, A. B., S. R. Fegley, J. T. Ridge, B. M. VanDusen and N. Anderson (2013). "Contribution of aeolian sand to backbarrier marsh sedimentation." Estuarine, Coastal and Shelf Science **117**: 248-259.

Rodriguez, A. B., W. Yu and E. J. Theuerkauf (2018). Abrupt increase in washover deposition along a transgressive barrier island during the late nineteenth century acceleration in sea-level rise. Barrier Dynamics and Response to Changing Climate. L. J. Moore and A. B. Murray. New York, Springer.

Rosati, J. D., R. G. Dean and T. L. Walton (2013). "The modified Bruun Rule extended for landward transport." Marine Geology **340**: 71-81.

Rosen, T. and Y. J. Xu (2013). "Recent decadal growth of the Atchafalaya River Delta complex: Effects of variable riverine sediment input and vegetation succession." Geomorphology **194**: 108-120.

Ruggiero, P., M. Buijsman, G. M. Kaminsky and G. Gelfenbaum (2010). "Modeling the effects of wave climate and sediment supply variability on large-scale shoreline change." Marine Geology **273**(1-4): 127-140.

Ruggiero, P., M. G. Kratzmann, E. A. Himmelstoss, D. Reid, J. Allan and G. M. Kaminsky (2013). "National Assessment of Shoreline Change: Historical Shoreline Change Along the Pacific Northwest Coast." U.S. Geological Survey Open-file Report **2012-1007**.

Safak, I., J. H. List, J. C. Warner and W. C. Schwab (2017). "Persistent Shoreline Shape Induced From Offshore Geologic Framework: Effects of Shoreface Connected Ridges." Journal of Geophysical Research: Oceans **122**(11): 8721-8738.

Schwarz, C., Q. H. Ye, D. van der Wal, L. Q. Zhang, T. Bouma, T. Ysebaert and P. M. J. Herman (2014). "Impacts of salt marsh plants on tidal channel initiation and inheritance." Journal of Geophysical Research: Earth Surface **119**(2): 385-400.

Schwimmer, R. A. (2001). "Rates and Processes of Marsh Shoreline Erosion in Rehoboth Bay, Delaware, U.S.A." Journal of Coastal Research **17**(3): 672-683.

Sendrowski, A. and P. Passalacqua (2017). "Process connectivity in a naturally prograding river delta." Water Resources Research **53**(3): 1841-1863.

Shaw, J., R. B. Taylor, S. Solomon, H. A. Christian and D. L. Forbes (1998). "Potential impacts of global sea-level rise on Canadian coasts." Canadian Geographer **42**(4): 365-379.

Shaw, J. B., M. A. Wolinsky, C. Paola and V. R. Voller (2008). "An image-based method for shoreline mapping on complex coasts." Geophysical Research Letters **35**(12): n/a-n/a.

Slott, J. M., A. B. Murray, A. D. Ashton and T. J. Crowley (2006). "Coastline responses to changing storm patterns." Geophysical Research Letters **33**(18).

Solari, L., M. Van Oorschot, B. Belletti, D. Hendriks, M. Rinaldi and A. Vargas-Luna (2016). "Advances on Modelling Riparian Vegetation-Hydromorphology Interactions." River Research and Applications **32**(2): 164-178.

Stolper, D., J. H. List and E. R. Thieler (2005). "Simulating the evolution of coastal morphology and stratigraphy with a new morphological-behaviour model (GEOMBEST)." Marine Geology **218**(1-4): 17-36.

Straub, K. M., Q. Li and W. M. Benson (2015). "Influence of sediment cohesion on deltaic shoreline dynamics and bulk sediment retention: A laboratory study." Geophysical Research Letters **42**(22): 9808-9815.

Stumpf, R. P. (1983). "The process of sedimentation on the surface of a salt marsh." Estuarine, Coastal and Shelf Science **17**: 495-508.

Syvitski, J. P. M., A. J. Kettner, I. Overeem, E. W. H. Hutton, M. T. Hannon, G. R. Brakenridge, J. Day, C. Vörösmarty, Y. Saito, L. Giosan and R. J. Nicholls (2009). "Sinking deltas due to human activities." Nature Geoscience **2**(10): 681-686.

Syvitski, J. P. M. and Y. Saito (2007). "Morphodynamics of deltas under the influence of humans." Global and Planetary Change **57**(3-4): 261-282.

Tal, M., K. Gran, A. B. Murray, C. Paola and D. M. Hicks (2004). Riparian vegetation as a primary control on channel characteristics in multi-thread rivers. Raparian Vegetation and Fluvial Geomorphology: Hydraulic, Hydrologic, and Geotechnical Interactions. S. J. Bennett and A. Simon. Washington, D.C., American Geophysical Union**:** 43-58.

Tal, M. and C. Paola (2010). "Effects of vegetation on channel morphodynamics: results and insights from laboratory experiments." Earth Surface Processes and Landforms **35**(9): 1014-1028.

Taylor, E. B., J. C. Gibeaut, D. W. Yoskowitz and M. J. Starek (2015). "Assessment and Monetary Valuation of the Storm Protection Function of Beaches and Foredunes on the Texas Coast." Journal of Coastal Research **315**: 1205-1216.

Tejedor, A., A. Longjas, R. Caldwell, D. A. Edmonds, I. Zaliapin and E. Foufoula-Georgiou (2016). "Quantifying the signature of sediment composition on the topologic and dynamic complexity of river delta channel networks and inferences toward delta classification." Geophysical Research Letters **43**(7): 3280-3287.

Temmerman, S., T. J. Bouma, G. Govers, Z. B. Wang, M. B. De Vries and P. M. J. Herman (2005). "Impact of vegetation on flow routing and sedimentation patterns: Three-dimensional modeling for a tidal marsh." Journal of Geophysical Research: Earth Surface **110**(F4): n/a-n/a.

Temmerman, S., T. J. Bouma, J. Van de Koppel, D. Van der Wal, M. B. De Vries and P. M. J. Herman (2007). "Vegetation causes channel erosion in a tidal landscape." Geology **35**(7).

Theuerkauf, E. J. and J. T. Ridge (2014). Researchers Bring Local Science Into Classrooms. EOS Trans., AGU. **95:** 41.

Valvo, L. M., A. B. Murray and A. Ashton (2006). "How does underlying geology affect coastline change? An initial modeling investigation." Journal of Geophysical Research **111**(F2).

Van Dijk, M., G. Postma and M. G. Kleinhans (2009). "Autocyclic behaviour of fan deltas: an analogue experimental study." Sedimentology **56**(5): 1569-1589.

Vargas-Luna, A., A. Crosato and W. S. J. Uijttewaal (2015). "Effects of vegetation on flow and sediment transport: comparative analyses and validation of predicting models." Earth Surface Processes and Landforms **40**(2): 157-176.

Vitousek, S., P. L. Barnard, P. Limber, L. Erikson and B. Cole (2017). "A model integrating longshore and cross-shore processes for predicting long-term shoreline response to climate change." Journal of Geophysical Research: Earth Surface **122**(4): 782-806.

Walters, D., L. J. Moore, O. Durán Vinent, S. Fagherazzi and G. Mariotti (2014). "Interactions between barrier islands and backbarrier marshes affect island system response to sea level rise: Insights from a coupled model." Journal of Geophysical Research: Earth Surface **119**: 2013-2031.

Walters, D. C. and M. L. Kirwan (2016). "Optimal hurricane overwash thickness for maximizing marsh resilience to sea level rise." Ecol Evol **6**(9): 2948-2956.

Wang, C. and S. Temmerman (2013). "Does biogeomorphic feedback lead to abrupt shifts between alternative landscape states?: An empirical study on intertidal flats and marshes." Journal of Geophysical Research: Earth Surface **118**(1): 229-240.

Wang, F. C., T. Lu and W. B. Sikora (1993). "Intertidal marsh suspended sediment transport processes, Terrebonne Bay, Louisiana, U.S.A." Journal of Coastal Research **9**(1): 209-220.

Wessel, P. and W. H. F. Smith (1996). "A global, self-consistent, hierarchical, high-resolution shoreline database." Journal of Geophysical Research: Solid Earth **101**(B4): 8741-8743.

Wickert, A. D., J. M. Martin, M. Tal, W. Kim, B. Sheets and C. Paola (2013). "River channel lateral mobility: metrics, time scales, and controls." Journal of Geophysical Research: Earth Surface **118**(2): 396-412.

Widdows, J., N. D. Pope and M. D. Brinsley (2008). "Effect of Spartina anglica stems on near-bed hydrodynamics, sediment erodability and morphological changes on an intertidal mudflat." Marine Ecology Progress Series **362**: 45-57.

Wikramanayake, P. N. and O. S. Madsen (1991). Calculation of movable bed friction factors. Vicksburg, Miss., U.S. Army Corps of Engineers, Coastal Engineering Research Center.

Wilson, C. A. and M. A. Allison (2008). "An equilibrium profile model for retreating marsh shorelines in southeast Louisiana." Estuarine, Coastal and Shelf Science **80**(4): 483-494.

Wolinsky, M. A., D. A. Edmonds, J. Martin and C. Paola (2010). "Delta allometry: Growth laws for river deltas." Geophysical Research Letters **37**(21): n/a-n/a.

Wolinsky, M. A. and A. B. Murray (2009). "A unifying framework for shoreline migration: 2. Application to wave-dominated coasts." Journal of Geophysical Research **114**(F1).

Yates, M. L. and G. Le Cozannet (2012). "Brief communication "Evaluating European Coastal Evolution using Bayesian Networks"." Natural Hazards and Earth System Science **12**(4): 1173-1177.

Young, I. R. and L. A. Verhagen (1996). "The growth of fetch limited waves in water of finite depth. Part 1. Total energy and peak frequency." Coastal Engineering **29**: 47-78.

Zhang, K., B. C. Douglass and S. P. Leatherman (2002). "Do storms cause long-term beach erosion along the U.S. east barrier coast?" The Journal of Geology **110**(4): 493-502.

Zong, L. and H. Nepf (2010). "Flow and deposition in and around a finite patch of vegetation." Geomorphology **116**(3-4): 363-372.

Biography

Rebecca Lauzon was born September 16th, 1991 in Martinez, California and grew up in Hampton, Virginia. She graduated from Boston University in 2013 with a B.A. in Marine Science and minors in Environmental Science and Italian. Since then, she has received the James B. Duke Fellowship, an honorable mention for the National Science Foundation Graduate Research Fellowship Program, and was awarded a Duke Support for Interdisciplinary Graduate Networks grant for the project: "A STEM researcher-educator network to improve K-12 science literacy". During her PhD she also completed the National Association for Interpretation's Certified Interpretive Guide program and the North Carolina Office of Environmental Education's Environmental Education Certification program.